DEVELOPING SYNTHESIS TECHNIQUES FOR ZEOLITIC-IMIDAZOLATE

FRAMEWORK MEMBRANES FOR HIGH RESOLUTION PROPYLENE/PROPANE

SEPARATION

A Dissertation

by

HYUK TAEK KWON

Submitted to the Office of Graduate and Professional Studies of
Texas A&M University
in partial fulfillment of the requirements for the degree of

DOCTOR OF PHILOSOPHY

Chair of Committee,	Hae-Kwon Jeong
Committee Members,	Hongcai Zhou
	Perla Balbuena
	Benjamin Wilhite
Head of Department,	M. Nazmul Karim

December 2015

Major Subject: Chemical Engineering

ABSTRACT

Propylene/propane separation is one of the most challenging separations, currently achieved by energy-intensive cryogenic distillation. Despite the great potentials for energy-efficient membrane-based propylene/propane separation processes, no commercial membranes are available due to the limitations (i.e., low selectivity) of current polymeric materials.

Zeolitic imidazolate frameworks (ZIFs) are promising membrane materials primarily due to their well-defined ultra-micropores with controllable surface chemistry along with their relatively high thermal/chemical stabilities. In particular, ZIF-8 with the effective aperture size of ~ 4.0 A has been shown very promising for propylene/propane separation. Despite the extensive research on ZIF-8 membranes, only a few of ZIF-8 membranes have displayed good propylene/propane separation performances presumably due to the challenges of controlling the microstructures of polycrystalline membranes. Since the membrane microstructures are greatly influenced by processing techniques, it is critically important to develop new techniques.

In this dissertation, three state-of-the-art ZIF membrane synthesis techniques are developed. The first is a one-step *in-situ* synthesis technique based on the concept of counter diffusion. The technique enabled us to obtain highly propylene selective ZIF-8 membranes in less than a couple of hours with exceptional mechanical strength. Most importantly, due to the nature of the counter-diffusion concept, the new method offered unique opportunities such as healing defective membranes (i.e., poorly-intergrown) as

well as significantly reducing the consumption of costly ligands and organic solvents. The second is a microwave-assisted seeding technique. Using this new seeding technique, we were able to prepare seeded supports with a high packing density in a couple of minutes, which subsequently grown into highly propylene-selective ZIF-8 membranes with an average propylene/propane selectivity of ~40. The last is a heteroepitaxial growth technique. The first well-intergrown membranes of ZIF-67 (Co-substituted ZIF-8) by heteroepitaxially growing ZIF-67 on ZIF-8 seed layers were reported. The ZIF-67 membranes exhibited impressively high propylene/propane separation capabilities. The presence of a methanol co-solvent in the growth solution was critically important to reproducibly prepare high quality ZIF-67 membranes. Furthermore, when the tertiary growth of ZIF-8 layers was applied to the ZIF-67 membranes, the membranes exhibited unprecedentedly high propylene/propane separation factors of ~ 200 possibly due to enhanced grain boundary structure.

ACKNOWLEDGEMENTS

I would like to thank the committee chair, Dr. Jeong and committee members, Dr. Zhou, Dr. Balbuena, and Dr. Wilhite for their guidance and support throughout the course of this research.

Thanks also go to my previous and current labmates, friends, department faculties, staffs, and collaborators for making my time a great experience.

Finally, special thanks to my father in heaven, mother and sisters for their ceaseless and unconditional support and love.

TABLE OF CONTENTS

LIST OF FIGURES

LIST OF TABLES

CHAPTER I

INTRODUCTION AND OVERVIEW

Propylene is one of the most highly demanded commodity chemicals in petrochemical industries. When produced by naphtha steam-cracking and/or heavy oil liquid Fluidized Catalytic Cracking (FCC) of heavy oil liquid, propylene needs to be separated from its paraffin counterpart, propane for further processing. Currently highly energy-intensive cryogenic distillation is employed due to the similar physical properties (e.g., volatility and size) between propane and propylene. Membranes-based separation has therefore gained tremendous interest as an efficient alternative technology. It has been proposed that in order for membranes to be commercially-viable a minimum propylene permeability of 1 Barrer and a propylene selectivity of 35 are required.[1] So far, there have been many different types of membranes studied including polymer,[2] zeolite,[3] carbon molecular sieve,[4-6] mixed matrix,[7] and facilitated transport membranes.[8] However, most of these membranes suffer from certain limitations one way or another. For example, most of polymeric membranes do not meet the selectivity/permeability threshold while suffering from low reliability and durability. The selectivity/permeability performance targets are met neither by more robust membranes such as zeolites and ceramics nor by mixed matrix membranes consisting of highly selective phases dispersed in polymer matrix until recently. Facilitated transport membranes can be easily poisoned by small amount of impurities, leading to irreversible degradation while carbon molecular sieve membranes are brittle and difficult to scale-up

1

the production. Moreover, most importantly, almost all of these membrane candidates do not meet performance requirements for commercial applications. Accordingly, it is evident that new material paradigms are essential to successfully address this energy-intensive yet industrially important separation.

Metal−organic frameworks (MOFs) are a new class of nanoporous organic−inorganic hybrid materials that exhibit regular crystalline lattices with rigid pore structures.[9-11] With unprecedented control over pore size and chemical/physical properties via a judicious choice of organic linkers, MOFs offer unique opportunities to overcome the limitations of not only current membrane materials but also conventional membrane system design/integration and operation.[12-14] An important subclass of MOFs, especially when considering gas separation applications, is zeolitic-imidazolate frameworks (ZIFs).[15-17] ZIFs consist of metal nodes (usually zinc or cobalt) connected to imidazole (or its derivative) linkers and exhibit zeolite-like structures due to the metal−linker−metal bond angle of ∼145° (close to the T−O−T angle found in zeolites).[15] ZIFs have been extensively investigated for gas separation membranes mainly due to their relatively high thermal/chemical stabilities as compared to other MOFs and molecular level pore aperture.[18-23]

To date, several ZIF materials such as ZIF-7,[24] ZIF-8,[18] ZIF-22,[21] ZIF-69,[20] ZIF-71,[25] ZIF-78,[26] ZIF-90,[27] ZIF-95,[28] and SIM-1[29] have been successfully processed into supported polycrystalline and/or mixed matrix membranes and tested for gas separations.[30] Due to the effective aperture of ∼ 4.0 Å,[31] ZIF-8 membranes showed a sharp propylene/propane separation based on size exclusion principle.[32-40] So far, well-

intergrown ZIF-8 membranes were prepared using either *in situ*[18,32,41] or secondary[22,34-36] growth. However, only a few ZIF-8 membranes[32-40] exhibited relatively high propylene/propane separation performances primarily because of the difficulty in controlling the microstructures of polycrystalline membranes (e.g., grain boundary structure, non-selective intercrystalline diffusional pathway): the poorer grain boundary structure is, the less selective membranes are. The microstructures of polycrystalline membranes are greatly affected by processing techniques. It is, therefore, imperative to develop simple and reproducible processing techniques that may result in the improved microstructures of polycrystalline membranes, thereby leading to the improved separation performances.

By recognizing the above-described issues in the field, this dissertation is principally dedicated to the development of new membrane processing techniques, yielding high-quality ZIF membranes with high resolution propylene/propane separation. Two of prototypical ZIFs, ZIF-8 and ZIF-67 (cobalt-substituted equivalent to ZIF-8) are selected to demonstrate the developed membrane processing techniques. ZIF-8 is known to have intrinsic capacity for keen propylene/propane kinetic separation.

The dissertation is composed of 7 chapters. The following chapter II provides general backgrounds on (1) propylene industry and propylene/propane separation, (2) ZIF chemistry and, (3) membrane transport through microporous membranes and membrane terminologies.

The research results are presented through Chapter III~VI in which the developed ZIF membrane processing techniques are elucidated. Specifically, Chapter III

is about the demonstration of a microwave-assisted seeding technique for the rapid synthesis of compact ZIF-8 seed layers. The densely-packed ZIF-8 seed layers were formed remarkably rapidly in a couple of minutes, leading to high quality continuous ZIF-8 membranes via a subsequent secondary growth. Chapter IV is dedicated to elucidate a counter-diffusion-based *in-situ* synthesis technique (hereafter, CD-based *in situ* method) for ZIF-8 membranes. A few novel concepts were demonstrated such as defect healing and ligand/solvent recycling, enabled by the nature of the counter-diffusion concept. In following chapter V, the microstructure optimization of ZIF-8 membranes prepared by the CD-based *in situ* method is attempted by controlling important synthesis parameters such as the nature of metal salts and catalyst to ligand ratios, leading to enhanced membrane performance. In chapter VI, the fabrication of ZIF-67 membranes is demonstrated via a heteroepitaxial growth approach. Unprecedented propylene/propane separation performances were observed and plausible membrane separation mechanism is proposed on the basis of IR and NMR spectroscopy data.

Lastly, the conclusions and suggested future works are presented in chapter VII.

CHAPTER II

BACKGROUNDS

2.1 Propylene Industry

2.1.1 Propylene market status
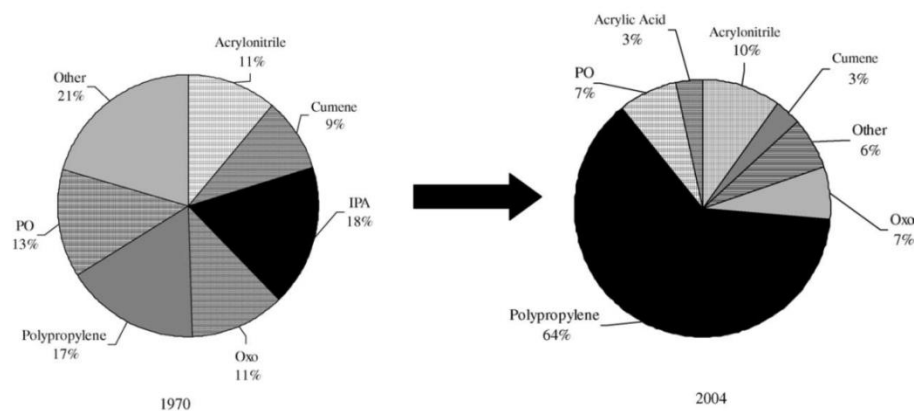
Figure 2.1 Global propylene consumption distribution on the basis of its intermediate derivative in 1970 and 2004, respectively. Reproduced with permission.[42] Copyright 2005, Elsevier.

The entire petrochemical industry principally relies on a few of essential key building blocks. One of which is propylene. By using it as a feedstock, a battery of derivatives can be produced such as polypropylene, oxo alcohol, cumene and propylene oxide, which are further utilized in a wide range of industrial sectors. Figure 2.1 displays global propylene consumption distribution on the basis of its intermediate derivatives in 1970 and 2004.[42] As shown, primarily due to the robust global demand increase of polypropylene, global propylene market has been substantially expanded, reaching to ca.

75 million tons in 2010 and is projected to continue to grow, driven by the emerging economies in developing countries in Asia such as China and India.[43]

Commonly, propylene was dominantly produced as a byproduct of ethylene and gasoline by steam cracking of naphtha or Fluidized Catalytic Cracking (FCC) of heavy oil liquids in refineries, together covering 90% of the current market. Recently, however, the propylene market, which was used to be fairly balanced in terms of supply and demand, fails to meet propylene's booming demand with the conventional propylene sources. As consequence, the historical price competitiveness of propylene over ethylene has not been maintained since 2007. Then, where does the propylene supply disruption come from? This is attributed to the global transition to cheap and easily accessible lighter feedstocks such as natural gas liquid (NGL) for cracking processes.[44] The lighter feedstocks prefer to produce less propylene-containing byproducts (majorly ethylene) than the cracking of naphtha or heavy liquids, leading to the unintentional decrease in propylene production. The feedstock transition was mainly driven by the consequence of the recent discovery of enormously large natural gas (shale gas) reserves in U.S.. The U.S. is one of the largest propylene consuming and producing countries in the worlds, in turn affecting global propylene market in a negative way. This feedstock transition trend, leading to propylene market tightening is expected to be more aggravated if China, where has the largest natural gas reserves in the world, starts to tab into the huge natural gas resources of their own.

Owing to observed supply/demand imbalance and resulted price distortion for propylene, now propylene producers are seeking for on-purpose propylene production

technologies to alleviate the current imbalanced market. Three representative on-purpose technologies[45] are now under operation such as propane dehydrogenation (PDH), methanol to propylene (MTP) and olefin methathesis processes. These techniques traditionally have been marginal, but current rising propylene price renders them to be economically viable. While PDH and MTP processes have produced a profit due to their low cost of raw materials (propane and methanol, respectively), olefin methathesis, which use 2-butene and ethylene as raw materials, still stays on the margin due to the rising price of 2-butene. It was forecasted that existing crackers in combination with on-purpose processes will meet global propylene demand projection of ca. 95 million tons by 2015, which might restore market stability.[44]

2.1.2   Propylene/propane separation

When propylene is produced from selected routes (e.g., steam cracking, FCC), it is mainly coexisted with its paraffin counterpart, propane. Since propylene need to have a certain degree of purities for further processing (chemical grade, 95%, polymer grade, 99.5%, and refinery grade, 70%), the separation of propylene from propane is essential. However, due to their similar physical properties (e.g., size and boiling point), the separation is still quite challenging, yet commercially very important. Conventionally, the separation is implemented by thermally-driven cryogenic distillation process which requires high capital cost and enormous energy consumption to operate. Distillation column with over 200 trays which operates with high reflux ratio of over 10 at 233~188 K under high pressure of 16~20 bar due to similar volatilities between propylene and
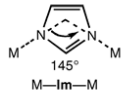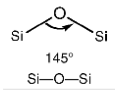
propane, and intrinsically involved gas-to-liquid phase change in the distillation process makes this process highly energy-intensive.[46] In fact, it was estimated by the US DOE in 1991 that 0.12 Quads/year (1 Quad = 10^{15} BTU) was spent only for olefin/paraffin separations.[47] To alleviate the high energy footprint of cryogenic distillation, A few technologies have been put to the test such as extractive distillation, adsorption, absorption, membrane technologies.[47] However, the majority of techniques still are neither technologically mature nor economically and energetically profitable, though potentially promising, to fully and even partially replace conventional workhorse, cryogenic distillation. For example, membrane-based separation has recently gained tremendous interest due to its high energy efficiency and structural and operational simplicity.[48] However, there still are no commercialized membranes due to certain limitations such as chemical and mechanical instability, and more importantly insufficient performance for commercial applications.[2,49] In case of extractive distillation,[50] no advantage over traditional distillation was concluded while adsorption technique,[51-54] though achieving high product purities, suffered from low olefin loadings and complicated regeneration processes. Therefore, further technological advancements are more than necessary with the alternatives.

2.2 Chemistry of Zeolitic Imidazolate Frameworks (ZIFs)

2.2.1 What are ZIFs?

Zeolitic imidazole frameworks (ZIFs)[15,17,55] are one of emerging branches of metal organic frameworks (MOFs) with zeolite topologies. ZIFs are constructed by

Table 2.1 Comparison between the properties of ZIFs and zeolites.

	ZIFs	Zeolites
Structure (bond angle)	M—Im—M, 145°	Si—O—Si, 145°
Components	• Metals (Zn or Co) • Imidazole or imidazole derivatives	• T=Si, (Al/Si), (Al/P), etc • Oxygen
Chemistry	• Coordination	• Covalent
Stability	• Moderate	• Highly stable
Flexibility	• Flexible: ligand flipping motion and/or framework breathing motion	• Relatively rigid
Activation	• Solvent exchange followed by drying	• Removal of structure directing agent (SDA) by calcination
Property control	• Theoretically unlimited metal/ligand combinations • Post-synthetic modification • Post-synthetic (ligand and/or metal) exchange	• Limited T/O combinations • Cation exchange
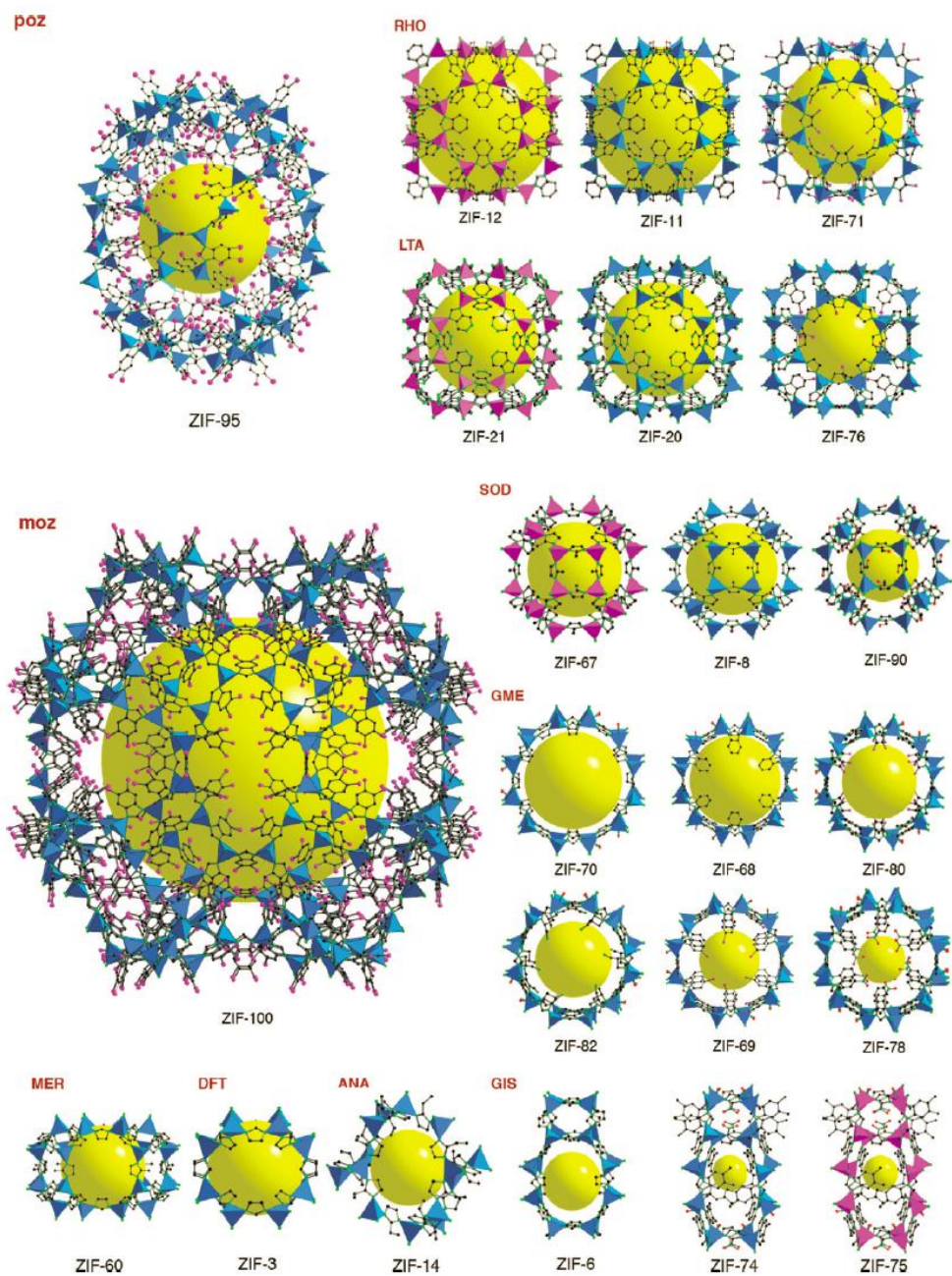
Figure 2.2 Representative crystal structures of ZIFs. Reproduced with permission.[55] Copyright 2010, American Chemical Society.

bridging metal nodes (usually, zinc or cobalt) with imidazole or its substituted derivatives whose theoretically unlimited combinations have yielded ZIF structures with various topologies. So far, over 150 ZIF structures were discovered. ZIFs have zeolite topologies owing to the fact that the metal−imidazole−metal bond angle of ∼145° resembles the T−O−T angle found in zeolites, which gives its naming convention. For reader's understanding, basic features of zeolites and ZIFs are compared in Table 2.1 and representative ZIF and zeolite structures are displayed in Figure 2.2.

Historically, the study of crystalline structures constructed from imidazole and transition metal combinations dates back to 1960. However, it is rather recent events for ZIFs to get tremendous research attention, initiated by the discovery of their exceptional thermal/chemical stabilities.[15] In conjunction with the exceptional stabilities, remarkable framework tunability (de novo or in post-synthetic ways), ultramicroporosity (e.g. molecular level pore aperture), and unusual framework flexibility (e.g., ligand flipping motions) added value to ZIFs, leading to numerous applications.[56] In particular, the unique features of ZIFs have offered unprecedented opportunities in gas storage and separation applications.

2.2.2 Chemistry

The construction of ZIF structures is superficially simple. Deprotonating imidazole ligand allows bidentate coordination sites and the sites are continuously coordinated with metal nodes, forming three dimensional supramolecular structure. However, it is not simple at all inside the system. Multiple variables interplay to yield a

final product in which only the right combination of variables allows a small window to synthesize a structure with intended topology, composition and morphology. The variables can be, for example, solvent, metal source, ligand substitution, precursor molar ratio, synthesis time and temperature. Since the physicochemical properties of crystalline materials like ZIFs depend on topology, morphology, and composition, it is critically important to understand the complex interplay between variables to have precise control over properties of ZIFs. In following sections, we will look into how synthesis variables influence on framework topology and morphology via reported examples. In addition, general strategies in ZIF chemistry to control framework composition de novo or in post-synthetic ways will be briefly discussed.

2.2.2.1   Topology control

The physical properties of frameworks such as pore volume, surface area, and pore aperture are mainly direct products of frameworks' topology control. Since those physical properties have dramatic influence on framework performances, especially in gas storage and separation,[57,58] it is imperative to have an understanding of how framework topology can be controlled. Although there is no the theory to offer crystal clear guidelines for topology control, major parameters were clarified via case studies. The parameters are primarily ligand substitution, solvent, metal source (counter anion), and synthesis time, which have structure directing roles. However, their interplay is not yet clear.

2.2.2.1.1   Via ligand substitution
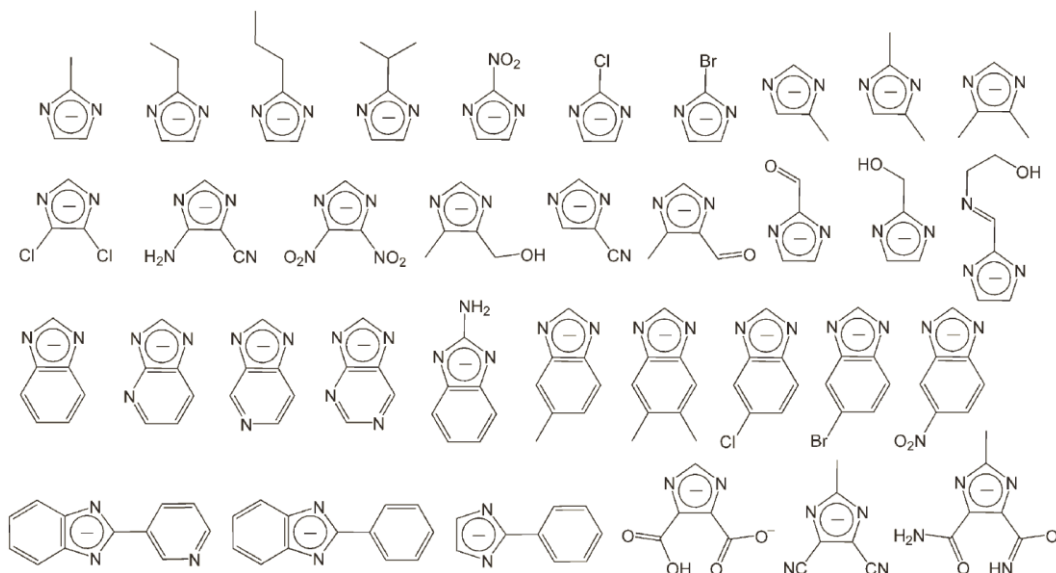
Figure 2.3 Various substituted imidazolates. Reproduced with permission.[59] Copyright 2012, American Chemical Society.

Due to the ability to substitute functional groups at 2, 4, and 5 positions of imidazole ligand (Figure 2.3), an unlimited variety of ZIF structures was created. Depending on the type and position of substitutes, resulted ZIF structures (produced under similar conditions) possess various topologies, indicating a structure directing role of substitutes on imidazole ligand. It has been proposed that different substitution environments on imidazole ligand induce different ligand-ligand interaction and steric effect during ZIF crystallization and their relative contribution leads to a variety of framework topologies. For example, while the frameworks from unsubstituted imidazole (*im*) (so far 17 $Zn(im)_2$ polymorphs were discovered) are either too dense or unstable,[60] imidazoles substituted at 2 position such as 2-methyimidazole and 2-ethylimidazole led

to SOD and ANA topologies with exceptional stability.[61] In addition, imidazoles substituted at 4 and 5 positions generally produced ZIFs with RHO topology.[62] This simple but powerful ligand-directed framework strategy expanded further. Benzimidazole ligand typically forms either SOD or RHO topologies depending on solvent systems.[63] The Yahgi's group introduced nitrogen substitution on benzimidazole ligand at 5 position or 5&7 positions, which led to the discovery of ZIF structures with LTA topology for the first time.[16] They hypothesized that it is attributed to electrostatic and dipole-dipole interactions between CH-N----N-CH pair at 5 and 6 positions of adjacent two linkers. The group continued to explore the same strategy and discovered ZIF structures with poz and moz topologies using 5-chlorobenzimidazole, which are predicted but undiscovered in zeolites.[64]

Considering the fact that zeolite structures are determined by structure directing agents, the ligand-directed framework strategy offers remarkable design flexibility on ZIF structures as evidenced. Obtaining an in-depth understanding of ligand-ligand interactions will pave the way to predict and design ZIFs with desired structures.

2.2.2.1.2 Via solvent, synthesis parameters, metal precursors and additives

In addition to the ligand substitution, there are generally-known other variables to affect final ZIF topologies such as solvent, synthesis parameters (e.g. time), metal source (especially counter anion), additive (some amines as a structure directing agent).

Solvent is known to play a role in directing ZIF structures by either occupying open space or altering ligand-ligand interactions during ZIF crystallization. One of

representative examples is benzimidazole-based frameworks. Under identical synthesis conditions, the same ligand ended up with structures with different topologies depending on the type of solvents. Dimethylformamide (DMF) yielded ZIF-7 with SOD topology while the bulkier solvent, diethylformamide (DEF) led to the formation of more open ZIF-11 with RHO topology.[57] When an ethanol/ammonium hydroxide mixture was used instead of dialkylformamides, the addition of toluene to the solvent system was essential to form ZIF-11; otherwise it led to small-cage ZIF-7.[65] Author proposed that the structure directing role of toluene is originated from aromatic-aromatic interactions between toluene and benzimidazole ligands. A similar trend was also observed on 2-nitroimidazole-based frameworks (CoNIm) in which SOD and RHO topologies were produced from DMF and DEF, respectively.[66] Interestingly, the CoNIm with RHO topology evolved to SOD topology by extending synthesis time (aging) when DEF is used as a solvent while DMF only produced SOD topology. It implies that the CoNIm crystallization takes different reaction pathways depending on solvents and the RHO topology is one of kinetically-trapped metastable intermediates encountered during the CoNIm crystallization in DEF. This aging-driven topology change in the synthesis solution was also observed with ZIF-71 crystals. When aged in the mother solutions, the topologies of ZIF-71 crystals (RHO) were transformed from RHO to SOD to lcs.[67] The significant reduction in framework porosity was accompanied, showing a natural structure evolution tendency toward thermodynamically stable dense structures.

It has been rarely observed that the type of metal precursors (especially counter anions) affects final ZIF topologies. Generally, the type of metal precursors plays a role

in modulating ZIF crystallization kinetic, thus mainly affecting ZIF morphologies (e.g., size, shapes). It is, however, recently reported that 4-methylimidazole-5-carbaldehyde-based ZIF frameworks can have different final topologies (SOD vs. RHO) depending on starting zinc precursors (zinc nitrate vs. acetate) under identical synthesis conditions.[57] Unfortunately, the study only put emphasis on showing the topology effect on CO_2 adsorption capacity and the detailed structure directing roles of counter anions were omitted.

Lastly, adding additives (structure directing agents, SDAs), similar with zeolite synthesis, is another option to control ZIF topologies. Reactive organic amines have been typically used as SDAs. For instance, cobalt and imidazole-based zeolite-like MOF, $[Co_5(im)_{10} \cdot 2MB]\infty$ was constructed by using piperazine (PZ) as a SDA.[68] The PZ was confirmed not to be present in the final structure and using other types of SDA led to the formation of different topologies, indirectly demonstrating a specific structure directing role of the PZ. Eddaoudi and coworkers also used organic amine additives to construct anionic ZMOFs with RHO and SOD topologies using Indium and 4, 5-imidazoledicarboxylic acid.[69] In the resulted anionic frameworks, protonated amine species acted as charge-balancing templates which easily could be exchanged after the framework constructions with other cations such as Na^+ and Cs^+. This was a first case of indium-based anionic ZMOFs which has ionic exchange capacity like zeolites.

2.2.2.2   Morphology control

Controlling the morphologies (size, shape) of ZIF particles has a great impact on their performances as well as fundamental studies. For instance, while the ZIF particles with smaller size is beneficial to diffusion-limited adsorption processes or membrane synthesis (e.g. compact seed layer), hundred micron-sized single crystals are required for crystal structure determination or diffusion kinetic studies.

Similar with the topology control, the ZIF morphologies are greatly influenced by synthesis variables. The known critical variables are precursor composition, nature of metal sources, additives, and synthesis routes. For size control, these parameters are used to control the deprotonation equilibria of imidazole ligands and/or to modulate crystal growth, affecting the relative rates of crystal nucleation and growth. The more rapid nucleation is, the smaller particle size is. For shape control, it is usually accomplished by inserting additives (e.g., counter anion of metal precursors, amines, and surfactants) which function as crystal shape modulators possibly via selective binding to crystal facets (e.g., inhibitor or promotor).

Please note that all reviewed studies in this section used a prototypical ZIF, ZIF-8 (2-methylimidazole-based ZIF with SOD topology) as a material platform, unless otherwise noted.

2.2.2.2.1   Size control

Two major processes of crystallization, nucleation and crystal growth are what determine the size of ZIF crystals. If nucleation is favored over crystal growth, the system yields many small crystals, while the formation of large crystals is dominant if growth is favored. Manipulating the relative rates of ZIF crystal nucleation and growth can be achieved by controlling coordination equilibria. The coordination equilibria in ZIF chemistry is representatively a function of (1) ligand deprotonation, (2) crystallization modulators, and. In addition, the size of ZIF crystals can be adjusted by synthesis routes with unconventional energy sources such as microwave and ultrasonication. It should be noted that the reviews on the effect of solvent on the size of ZIF crystals are not included here, though it is highly likely, due to a lack of reported systematic studies.

2.2.2.2.1.1   Via controlling coordination equilibria

2.2.2.2.1.1.1 Ligand deprotonation

Since ZIF crystallization is initiated by deprotonating imidazole ligand, controlling ligand deprotonation equilibria is one of the keys to adjust ZIF crystal size: the more deprotonated ligands are present in the system, more nuclei are formed and therefore ZIF crystals become smaller.

By selecting high ligand to metal ratio, one can increase nucleation to obtain smaller crystals. The excessive amount of ligand augments the relative amount of deprotonated ligand and therefore induces rapid nucleation rate. For example, Cravillon

and coworkers could produce ZIF-8 nanoparticles with a diameter of ~50 nm by augmenting ligand to metal ratio from 2:1 (large microcrystals) to 8:1 in methanol.[70] Their hypothesized formation mechanism was (1) the excessive amount of ligand increases nucleation rate due to the large amount of deprotonated ligands and (2) remaining protonated neural ligand caps uncoordinated surface zincs to terminate further crystal growth. Later, Lai[71] and Miyake[72] groups also separately observed the same trend of crystal size variation depending on ligand to metal ratio in the synthesis of ZIF-8 crystals in an aqueous system. This approach also applied to other ZIF kinds. Caro and coworkers reduced the size of ZIF-7 crystals from micron to nano scales (~30 nm) at room temperature by increasing ligand to metal ratio from 0.74:1 to 6.5:1.[73] In addition, it was also observed in ZIF-90 crystallization in that the size can be adjusted in the range of 450~2500 nm in an aqueous system by altering ligand to metal ratio (4~60:1).[74]

Another option to control deprotonation equilibria is to add base to synthesis mixtures. Increasing the basicity of the synthesis mixtures enhances the rate of ligand deprotonation and hence nucleation becomes favored, yielding smaller particle. The presence of base in the mixtures not only enables the fast formation of nanocrystals due to enhanced nucleation rate but also simultaneously reduces the amount of ligand required to trigger rapid crystallization. Wiebcke and coworkers first adapted this approach in ZIF crystallization.[75] They selected n-butylamine as a base which enables to instantaneously form 18 nm ZIF-8 nanocrystals with ligand to metal ratio of 4:1 at room temperature in methanol. In the absence of the base, 65 nm ZIF-8 crystals were produced under the identical synthesis conditions. Regardless of solvent, the same approach

worked. Gross and coworkers successfully synthesized ZIF-8 and ZIF-67 (cobalt-substituted equivalent to ZIF-8) with ligand to metal ratio of 4~16:1 at room temperature in 10 min by adding triethylamine.[76] Considering a typical ligand to metal ratio of reported aqueous ZIF-8 syntheses (40~70:1) without inserted base,[71,72,77] it is significant reduction in ligand consumption. It is noteworthy that in a typical aqueous synthesis of ZIF-8, phase-pure ZIF-8 cannot be obtained if ligand to metal ratio is below 40~70:1.[72,77]

2.2.2.2.1.1.2 Crystallization modulators

In MOF chemistry, modulators are chemical species can adjust crystal nucleation or growth and hence ZIF crystal size via a process of competing for coordination sites with uncoordinated bidentate ligands.

Auxiliary monodentate ligands are one of kinds. Since the monodentate ligands have only one coordination site available, they ideally cannot be a part of ZIF structures. Instead, they compete with bidentate bridging ligands for undercoordinated metal sites, and therefore slow down crystal nucleation, causing conditions favoring crystal growth. Kitagawa and coworker first used this strategy (coordination modulation method) in controlling the size of carboxylate-based MOF, HKUST-1[78] and later, Wiebcke and coworkers adapted the strategy to produce ZIF-8 microcrystals (~1 μm) at room temperature using sodium formate and 1-methylimidazole as monodentate modulating ligands.[75] In the absence of the modulators, the size of ZIF-8 crystals was about ~65 nm due to excessive ligand-induced rapid nucleation. In the study, using *ex-situ* SEM and *in-*

situ static light scattering, the trajectory of ZIF-8 crystallization were followed in the presence of the modulators with great detail. In their follow-up study,[79] the different roles of sodium formate in ZIF-8 crystallization depending on synthesis temperature were discovered using *in situ* EDXRD: While the sodium formate functions as a coordination modulator at room temperature as reported, it acts rather as a base for ligand deprotonation at elevated temperature (120~140 ^{o}C).

Counter anions introduced together with metal precursors also are known to have the capability to modulate ZIF crystallization. Schneider and coworkers conducted through investigation on the effect of the counter anions of zinc sources on the size of ZIF-8 crystals in methanol and observed a trend in crystal size variation.[80] Their explanation is on the basis of the hard soft acid base (HSAB) theory. If zinc/anion pairs are in hard-hard or soft-soft relations, not much free zinc ion to coordinate with ligand are available due to their strong pair interaction, favoring crystal growth rather than nucleation. In contrast, if they are in a soft-hard relation, the situation is the other way round, leading to the formation of smaller crystals due to rapid nucleation. Indeed, soft-soft pairs like $Zn(Cl)_2$ and $Zn(Br)_2$ formed relatively large crystals (~1050 nm) while soft-hard pairs like $Zn(NO_3)_2$ and $Zn(ClO_4)_2$ produced smaller crystals (140~230 nm). Recently, the similar study was implemented by Zhang and coworkers, but water was used as a solvent instead of methanol.[77] Unexpectedly, the opposite trend was observed and explanation was not supplied in the study.

Lastly, although it is rare, there was an attempt to use surfactants as a crystallization modulator for controlling the size of ZIF crystals. Lai and coworkers

introduced surfactants (e.g., CTAB, CTAC, and STAC) into an aqueous ZIF-8 crystallization system and the sizes of ZIF-8 crystals were adjusted in the range of 100 nm ~ 4 μm by precisely controlling surfactant concentration under the critical micelle concentration (CMC).[81] On the basis of controlled experiments in combination with simulation results, they proposed that the long hydrocarbon tail of the surfactants selectively adsorbs to a specific crystal facet and the adsorbed surfactants cap and prevent ingredients from approaching to the surface. Thus it decreases the crystal growth rate of the facet and put constraints on crystal shape development simultaneously.

2.2.2.2.1.2 Via using unconventional energy sources

Unconventional energy sources such as ultrasonication and microwave are advantageous for triggering rapid nucleation over conventional heating owing to the ability to cause instantaneous and localized heating through their own unique principles: ultrasonication can produce the localized high temperature by transient cavitation and oscillating microwave is selectively adsorbed by charged species (e.g., ions, polar molecules) whose flipping motions in medium induce frictional heat enabling rapid volumetric heating. A few groups employed the untrasonication and microwave to synthesize ZIF crystals.[34,82-84] The instantaneous and localized heating increases the rate of nucleation significantly, leading to the rapid formation of smaller crystals than ones with conventional heating. Coronas and coworkers successfully prepared a series of ZIFs such as ZIF-7, ZIF-8, ZIF-11, and ZIF-20 using ultrasonication.[82] The crystals were featured by the smaller sizes, narrow size distributions, more short synthesis time than

counterparts from conventional heating. Later, the sonochemical route was also adapted by Ahn and coworkers to scale up the synthesis of ZIF-8 in substantially reduced time.[83] Using microwave heating, Jeong's group formed densely-packed ZIF-8 seed layers on ceramic substrates. The seed crystals of ~100 nm were formed in a couple of minutes and covered the substrate uniformly, leading to the formation of continuous ZIF-8 membranes after a subsequent secondary growth.[34] The effectiveness of microwave heating on producing smaller and uniform ZIF-8 crystals was also observed by Chen and coworkers.[84]

2.2.2.2.2   Shape control

The shape of ZIF crystals is usually manipulated by growth modulators. The growth modulators either retard or facilitate the growth of specific crystal planes and consequently lead to the formation of thermodynamically unexpected crystal shapes. Although they are not universally applicable, a few growth modulators have been known in ZIF chemistry such as amine, counter anions of metal salts, and surfactants.

A first reported example is the formation of rod-shaped ZIF-7 crystals by Li and coworkers.[85] In the study, by simply replacing a metal source from zinc nitrate to zinc chloride, dramatic crystal shape change was observed from isotropic hexagon to prismatic hexagon (rod). It was hypothesized that relatively strong interaction of a zinc/chloride pair over a zinc/nitrate pair (HSAB theory) might bring about the growth rate changes on the specific planes of ZIF-7 crystals, leading to the shape transformation. In addition, further shape controls of the rod-shaped ZIF-7 crystals (size, aspect ratio)

23

was accomplished by inserting diethylamine (DEA), but detailed mechanism was absent. Similarly, Lai and coworkers observed the size and aspect ratio of ZIF-69 microrods are significantly reduced by using zinc acetate instead of zinc nitrate.[86] The smaller and squat ZIF-69 microrods were used as seeds for synthesizing oriented ZIF-69 membranes.

Amines also have been used as a growth modulator of ZIF crystals. Yang and coworkers conducted a systematic study on controlling the size and shape of ZIF-78 (one of mixed ligand ZIF crystals).[87] The essence of forming rod-shape ZIF-78 crystals instead of hexagonal disks was to use trimethylamine (TEA) as a growth modulator. In combination with the modulator, precursor concentration and ligand molar ratio turned out to be important parameters for precise control on the shape and size of the ZIF-78 crystals.

Lastly, there was a case where surfactants are used as a growth modulator. Lai and coworkers introduced surfactants (e.g., CTAB, CTAC, and STAC) into an aqueous ZIF-8 crystallization system and the shapes of ZIF-8 crystals were adjusted from rhombic dodecahedron to truncated rhombic dodecahedron to truncated cubic by precisely controlling surfactant concentration below the critical micelle concentration (CMC).[81] On the basis of controlled experiments in combination with simulation results, they proposed that the long hydrocarbon tail of the surfactants selectively adsorbs to specific crystal facets and the adsorbed surfactants cap and prevent ingredients from approaching to the surface. Thus it put constraints on crystal shape development.

2.2.2.2.3 Composition control

To see compositional effects on the properties of ZIFs, it is critically important to construct ZIFs with different metal/ligand combinations while keeping their topology identical. The composition control of ZIFs can be achieved by either direct synthesis or post-synthetic modifications (PSMs). The direct synthesis, though appears superficially to be simple, requires a time-consuming trial and error process for the optimization of synthesis variables before obtaining intended ZIF structures. This is because a final ZIF product is a consequence of the complex interplay of synthesis variables as briefly reviewed in the previous sections. It is sometimes more than true that one cannot directly synthesize intended stable porous structures with selected metal and ligand combinations (e.g., $Zn(im)_2$).[60] Furthermore, although intended ZIF structures are predicted to be obtainable, the variable optimization should be exhaustively implemented individually on every ZIF. Therefore, there is a clear limitation on the composition control through the direct synthesis. This limitation can be mitigated by the PSMs to a certain extent. The PSMs are chemical modification processes conducted in post-synthetic ways, enabled by the labile nature of coordination chemistry of MOFs/ZIFs. The PSMs are broadly classified into ligand/metal exchange and ligand augmentation (covalent chemistry on ligand functional groups). If successful, the PSMs can produce a framework with continuously modifiable properties that possesses the topology of a patent MOF.

2.2.2.2.3.1 Via direct synthesis

The imidazole ligands can expand their library by virtue of theoretically unlimited combination of substitutes on 2, 4, and 5 positions on an imidazole ligand.[59] This wide range of ligand derivatives is principally what enables the compositional diversity of ZIFs. However, since the final topologies of ZIFs are greatly affected by the type and position of substitutes together with other synthesis variables, it is not trivial to build ZIFs with the same topology from different ligand struts to see the sole compositional effect on ZIF properties. Although various isoreticular ZIFs have been reported,[55] the synthesis of intended ZIF structures still occurs through serendipity.

In spite of this synthetic limitation, there were original direct synthesis approaches such as mixed ligand and mixed metal approaches which deserve attention.

2.2.2.2.3.1.1 Via mixed ligand approach

Compositional and structural monotony of single ligand-based ZIFs can be overcome by constructing ZIFs with two different ligands. If the relative composition ratio between two ligands in a single framework can be varied in a wide range without topology change, the framework's physicochemical properties such as framework polarity and pore aperture/volume/surface area can continuously be fine-tuned, which is very important from application point of view. The potential of mixed ligand ZIFs was first demonstrated by Yaghi and coworkers in 2008[17] and followed by many research groups later.[88-91] Yaghi and coworkers discovered 10 of new ZIFs from different ligand combinations via a high-throughput method and some of them such as ZIF-68, -69, and -

26

70 (GME topology) showed impressive adsorption selectivities for a CO_2/CO mixture.[17] Unfortunately, however, only a single ligand composition on each mixed ligand ZIF was studied. Chen and coworkers reported a first case of mixed ligand ZIFs with a continuous composition spectrum between two ligands without altering the structure.[88] They used 2-methlyimidazole (2-HmIm) and 3-methyl-1,2,4-triazole (Hmtz), which individually form MAF-4 (ZIF-8, $Zn(2\text{-}mIm)_2$) and MAF-7 ($Zn(mtz)_2$) with a SOD topology, and constructed a series of MAF-47s ($Zn(2\text{-}mim)_{2x}(mtz)_{2\text{-}2x}$, $0<x<1$). Depending on the fraction of mtz in the frameworks, the gate opening pressures (inflection points in isotherms) for water and hydrophilicity/hydrophobicity were continuously fine-tuned. The MAF-47s with greater mtz fractions showed lower gate opening pressures and higher hydrophilicity due to higher content of unbound polar N atom belonging to mtz. Other comprehensive examples are two of mixed ligand ZIFs, ZIF-8-90 and ZIF-7-8 reported by Nair and coworkers.[89,90] In case of ZIF-8-90, it is constructed by combining 2-methylimidazle (2-HmIm, ZIF-8 ligand) and 2-imidazolecarboxaldehyde (2-ohcHIm, ZIF-90 ligand), and due to the similarity in size between 2-mIm and 2-ohcIm (negligible steric disturbance), the full range of 2-mIm/2-ohcIm ratio was achieved in a single crystalline phase. As the content of 2-ohcIm increases, the physicochemical properties of the ZIF-8-90 (e.g. gate opening pressure, surface area, pore volume, thermal stability, effective pore size, hydrophilicity and organophilicity) were continuously shifted from ones of pure ZIF-8 to ones of pure ZIF-90. In case of ZIF-7-8 which contains relatively bulky benzimidazole (bIm, ZIF-7 ligand) instead of 2-ohcHIm, there existed a gradual crystal structure transition from

ZIF-8 phase to ZIF-7 phase when the composition of bIm exceeds 35 %. Based on XRD patterns combined with exhaustive TEM investigation and nitrogen adsorption data, it was presumed that the ZIF-7-8s with mixed crystal phases stems from an intergrowth of ZIF-7 and ZIF-8, not from mixed ligand frameworks. When a substituted bIm, 2-aminobenzimidazole (2-ambIm) was used instead of bIm, the crystal phase transition was absent and maintained the ZIF-8 crystal structure even nearly at 47 % 2-ambIm loading, implying it is thermodynamically more favorable to form the ZIF-7 crystal structure with bIm than with 2-ambIm.[91] However, regardless of being either bIm or 2-ambIm, as increasing the content of them, the surface area and pore volume of the ZIF-7-8 and ZIF-8-ambIm were significantly reduced and became more rigid, evidenced by the fact that they gradually lost the gate opening nature.

2.2.2.2.3.1.2   Via mixed metal approach

Typical metal nodes for known ZIFs are divalent transition metal ions such as Zn^{2+}, Co^{2+}, and Cd^{2+}. Similar with zeolite-like aluminophosphates, $AlPO_4$ series in which Al^{3+} and P^{5+} replace Si^{4+} in silicalites,[92] the divalent metal nodes (M^{2+}) in ZIF structures theoretically can be replaced by M^+/M^{3+} combinations.[93-97] The demonstration of this concept with a couple of lightweight cation pairs (e.g., Li^{1+}/B^{3+} , Cu^{1+}/B^{3+}) and various imidazole ligands led to the discovery of a new family of ZIFs, boron imidazolate frameworks (BIFs). So far more than 20 different BIF structures were discovered and they all have the combined nature of coordination (M^{1+}-N bond) and covalent (B-N bond) bonds. Originated by the shorter bond distance of B-N (~1.5Å) as

compared to typical Zn-N distance (~2 Å) in typical ZIFs, BIFs generally have smaller pore aperture and surface area/volume as compared to ZIFs. The smaller pore aperture together with their lightweight framework would be advantageous for kinetic-based adsorption and membrane separations. However, so far BIFs are relatively rarely explored from application point of view and therefore, deserve more attention considering their potential in gas storage and separation applications.

2.2.2.2.3.2   Via postsynthetic modification

Due to the presence of convolutedly interplayed structure directing parameters on the formation of ZIFs, constructing designed ZIFs de novo is not trivial, thereby making the structure-property studies of ZIFs difficult. Fortunately, this synthetic limitation can be alleviated by post synthetic modifications (PSMs) such as ligand exchange (PSLE) or ligand augmentation (PSLA).

A typical way of implementing the PSLE is to incubate a mother ZIF in a solution containing a ligand to be introduced. The PSLE is controlled by less variables (e.g., solvent, ligand concentration, and temperature) than the direct synthesis and implemented under rather mild conditions. If successful, the resulted framework can contain the controllable amount of a new ligand in the structure without topology alteration.

The PSLA is about adding new functional groups on parent ZIFs via covalent chemistry. Therefore, the presence of modifiable pendant groups (e.g., aldehyde group) on parent ZIFs is a prerequisite for the PSLA.

2.2.2.2.3.2.1   Via postsynthetic ligand exchange (PSLE)

Initially, it was presumed that ZIFs are not susceptible to the PSLE due to their chemical robustness. However, it turned out that the PSLE can be applicable to some of the most stable MOFs such as UIO series without destroying mother frameworks, indicating small energy difference between analogues with different ligands is large enough to drive the PSLE.[98]   Since then, ZIFs were considered to be the viable object of the PSLE.

The first attempt of the PSLE on ZIFs was reported by Hupp and coworkers.[99] They exchanged 2-ethylimidazole (2-HeIm) in CdIF-4 (one of cadmium-based ZIFs with a RHO topology) with 2-nitroimidazole (2-HnIm) and 2-methylimidazole (2-HmIm), leading to the formation of CdIF-9 and SALEM-1, respectively. For both cases, full ligand exchanges were achieved after 48h under the same exchange conditions while showing negligible dependence on solvents (e.g., DMF, DMA, and n-butanol) and the RHO topology was maintained. Although CdIF-9 can be obtained by direct synthesis, the yield is typically low (below 14%) and an amorphous phase is simultaneously formed, which requires an additional separation process. In case of SALEM-1, it is a first case of new ZIFs obtained through the PSLE. While the exchange between 2-eIm and 2-nIm was fully reversible, the exchanges of 2-nIm to 2-eIm and to 2-mIn ended up with the dissolution of the parent frameworks. Authors reasoned that due to the presence of the electron withdrawing nitro functional groups, the 2-nIm-based framework (CdIF-9) possesses relatively weak framework stability as compared to CdIF-4 and SALEM-1, leading to the framework dissolutions when exposed to 2-mIm or 2-eIm. According to

30

the reasoning, ZIFs with ligands substituted with electron-donating substituents, thereby having better framework stability are ideal parent frameworks for the successful PSLE, which needs further experimental corroborations.

With unsubstituted imidazole (Im), the produced ZIFs ($Zn(Im)_2$) are usually dense or unstable, negating their effective functions as a porous material.[60] The elusive formation of $Zn(Im)_2$ with an open architecture was proven to be achievable by the PSLE.[60] A sod-type ZIF-8 ($Zn(2\text{-}mIm)_2$) was used as a parent ZIF and the PSLE between 2-mIm and Im was implemented solvothermally in n-butanol (SALEM-2). 85% of 2-mIM in the parent ZIF-8 could maximally be exchanged with Im and the reaction was reversible. The exchange reaction turned out to be very sensitive to the nature of solvent and the ratio of Im to parent ZIF-8. Using DMF or DMA led to negligible ligand exchange and if the ratios of Im to ZIF-8 are higher than 6.7:1, the SALEM-2 lost its framework integrity and if less than that, the parent ZIF-8 remained intact without ligand composition change. As consequences of the PLSE, the SALEM-2 could accommodate large guest molecules, which the parent ZIF-8 cannot uptake, due to enlarged pore aperture and when modified with n-butyllithium, it showed impressive catalytic reactivity on conjugate-addition reactions which the parent ZIF-8 cannot catalyze.

The PLSE was also used to enhance the stability and chemical affinity of parent ZIFs.[100] Considering the ubiquitous presence of water in the majority of separation applications, it is critically important for potential adsorbent/membrane materials like ZIFs to possess high hydrothermal stability. By introducing a hydrophobic ligand, 5,6-dimethylbenzimidazole (HdmbIm) to parent ZIF-8, Yang and coworkers significantly

improved the hydrothermal stability of ZIF-8.[100,101] Interestingly, due to the bulky size of dmbIm, the PLSE occurred selectively on the surface of the parent ZIF-8. As an application, the ZIF-8-dmbIm was employed as a filler material for mixed matrix membranes which showed improved selectivity for isobutanol/water separation primarily owing to the increased hydrophobicity.

Recently, the PLSE concept was further demonstrated on other ZIFs such as ZIF-7, -69, -71, -76, and -78,[101-103] leading to the discovery of new ZIFs which have not been accessible via direct synthesis before. Readers can visit elsewhere for more comprehensive reviews on the PLSE of MOFs.[104]

2.2.2.2.3.2.2 Via post synthetic ligand augmentation (PSLA)

Post synthetic ligand augmentation (PSLA) is a way to decorate MOFs by implementing covalent chemistry on modifiable functional groups in organic ligand struts. Therefore, the presence of one or more tunable pendant groups on ligands is an indispensable prerequisite for the PSLA. In addition, parent MOFs should be chemically robust enough to survive under strong reaction conditions. In this regard, chemically stable ZIFs with modifiable pendant groups are a suitable platform for the PSLA.

It was Yaghi and coworkers reported a first case of the PSLA on ZIFs.[105] By covalently modifying ZIF-90 containing imidazolate-2-carboxyaldehyde (ICA) via reduction reaction with $NaBH_4$ and imine condensation reaction with ethanolamine, they constructed two of new ZIFs, ZIF-91 and ZIF-92 without altering the structural integrity. After this initial demonstration, the concept has been effectively used to improve the

32

performances of ZIFs in multiple applications by tuning their chemical/physical properties such as membrane/adsorption-based separations,[106,107] catalysis,[108-111] and sensing[112]. For example, Caro and coworkers modified polycrystalline ZIF-90 membranes with 3-aminopropyltriethoxysilane (APTES)[107] or ethanolamine[106], enhancing H_2 separation performance of the membranes. They reasoned that the covalent modifications enable the sealing of nonselective transport path way (e.g., grain boundary), thereby causing the improvement. In addition, Wang and coworker modified ZIF-90 with malonitrile (MN-ZIF-90), enhancing hydrogen sulfide detection and selective amino acid recognition[112] while Farrusseng and coworkers attached long hydrocarbon tails on SIM-1, improving framework hydrophobicity as well as catalytic activity on Knoevenagel condensation[108,109]. Please note that the SIM-1 is a SOD-type ZIF constructed with zinc ions and 4-methyl-5-imidazolecarboxaldehyde ligands.

However, in spite of the promising potential of the PSLA and the presence of numerous ZIFs available to be covalently modified, only a couple of ZIFs such as ZIF-90 and SIM-1 have only been explored for the PSLA so far to the best of my knowledge and therefore more ZIFs needs to be investigated for the PSLA.

2.3 Membrane Transport Through Microporous Membranes

2.3.1 Qualitative description

According to the Barrer's description on gas transport through microporous membranes (pore diameter $\approx$ kinetic diameter of gas molecules),[113,114] it consists of successive activated steps in which sorption and diffusion processes are involved as
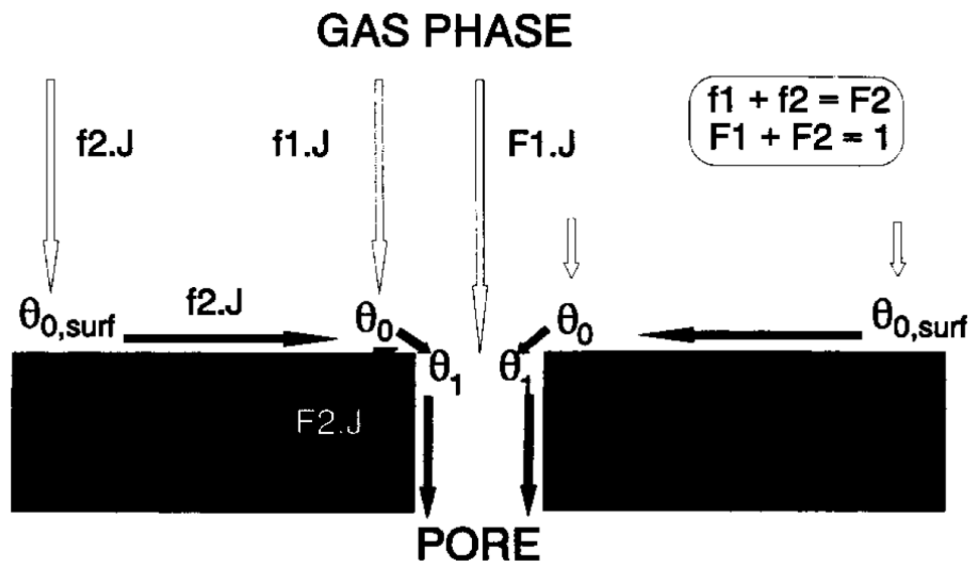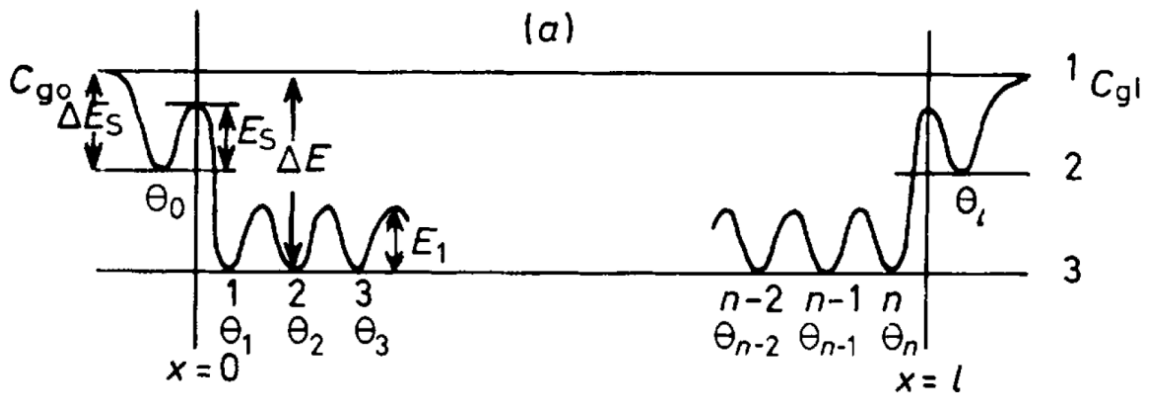
Figure 2.4 Potential energy curve of gas molecules diffusing through microporous crystal membranes (a), reproduced with permission [113], Copyright 1990, Royal Society of Chemistry and detailed description on the movement of gas molecules on the membrane surface (b), reproduced with permission[114], Copyright 1995, Elsevier.

illustrated in Figure 2.4(a). Each activated step uses up a part of a driving force (e.g., chemical potential) to complete the transport process.

(1) Gas adsorption to membrane surface (x = 0) and transport to pore entrances; ΔE_s is the energy difference between the molecules adsorbed on the external surface and in the free gas phase, which is a heat of adsorption. As depicted in Figure 2.4(b), the gas molecules can adsorb on surface adsorption sites either relatively far from ($\theta_{0,surf}$) or near pore entrances (θ_0). If the former is a case, the molecules needs to further surface-diffuse to the sites near pore entrances (θ_0) before entering into the micropores. In addition, It is worthy of noting that there are possibly gas molecules which directly enter into pore entrances without adsorbing on the surface. However, this is usually dominant when pore aperture is relatively bigger than the size of gas molecules (e.g., mesoporous or macroporous materials) and/or sorption energies are below RT.

(2) Entrance of the adsorbed molecules to the first sites (θ_1) in the micropores; E_s is the activation barrier to be overcome for the adsorbed molecules to enter into the micropores. The magnitude of the activation barrier is principally influenced by the geometry and chemistry of pore entrances (e.g., partial pore blockage, functional group).

(3) Micropore diffusion in the pores; once gas molecules pass through pore entrances, they will adsorb on energy minimum sites and moving through the sites by hopping. The E_1 is the activation energy for micropore diffusion.

(4) Desorption from the inner pores to the external surface (x = l) or directly go the gas phase; it is a reverse process of step (2). To move from θ_n to θ_1, $E_s + \Delta E - \Delta E_s$ needs to be overcome. θ_n and θ_1 is last energy minimum sites before pore exits and pore

exits (x = l), respectively. ΔE is the energy difference between the molecules in the micropores and in the free gas phase.

(5) Desorption from the external surface to the gas phase.

2.3.2 Mathematical (theoretical) description[115,116]

In general, Fick's first law is employed to describe diffusion of matters at steady state from macroscopic point of view:

$$J = -D(c)\frac{dc}{dz} \tag{1}$$

where J is the flux, $D(c)$ is the concentration dependent transport diffusivity, and $\frac{dc}{dz}$ is the concentration gradient across diffusional pathway. This equation implies that the driving force for diffusion of matters is the concentration gradient. However, since diffusion is nothing but an equilibrium process for composition homogenization, the gradient of chemical potential (μ) should be the true driving force. When diffusion occurs, diffusing species are opposed by frictional drag (fu) and therefore a steady state energy balance can be constructed as:

$$fu = -\frac{d\mu}{dz}; \quad u = -\frac{1}{f}\frac{d\mu}{dz} \tag{2}$$

where f is a friction coefficient and u is the flow velocity of diffusing species. By assuming the molecules behave ideally, the chemical potential can be expressed in terms of the partial pressure of the diffusing species;

$$\mu = \mu^o + RT \ln p \tag{3}$$

In addition, the flux (J) also can be defined as:

$$J = uc \tag{4}$$

where c is the concentration of adsorbed diffusing species on porous adsorbents. By inserting eq. (2) and eq. (3) into eq. (4), the expression for the diffusive flux is obtained as;

$$J = -\frac{RT}{f}\frac{d \ln p}{d \ln c}\frac{dc}{dz} = -D_c(c)\frac{d \ln p}{d \ln c}\frac{dc}{dz} \tag{5}$$

By comparing eq. (5) with eq. (1), one can express the transport diffusivity (D) as;

$$D(c) = D_c(c)\frac{d \ln p}{d \ln c} \tag{6}$$

where $D_c(c)$ is the corrected diffusivity (or mobility coefficient) and $\frac{d \ln p}{d \ln c}$ is the thermodynamic correction factor (Γ) which is the gradient of equilibrium isotherm, containing the information on the degree of system's thermodynamic non-ideality. Under Henry's adsorption regime ($c \propto p$), Γ reaches ~1 and therefore, eq. (5) reduces to the simple Fick's first law.

By integrating eq. 5 over membrane thickness (L), one can obtain the flux expression for supported membranes.

$$\int_0^L J \, dz = -\mu^* \int_0^L D_c(c) \frac{d \ln p}{d \ln c} \frac{dc}{dz} dz = -\mu^* \int_{c_s, \, x=0}^{c_p, \, x=L} D_c(c) \frac{d \ln p}{d \ln c} dc \tag{7}$$

where c_s and c_p are the concentrations of adsorbed diffusing species at z = 0 and z = L, respectively. μ^* is the geometrical correction factor added to count the presence of permeation area blocked by the solid surface area of supports. To integrate Eq. (7), we need a mathematical relation between p and c, which is an adsorption isotherm. In membrane-based gas separations, adsorption is normally not multilayer, and on and off less than a monolayer, which is well delineated by the simple Langmuir model.

$$\frac{q}{q_s} = \theta = \frac{Kp}{1 + Kp}; \quad \Gamma = \frac{d \ln p}{d \ln q} = \frac{1}{1 - q/q_s} = \frac{1}{1 - \theta} \tag{8}$$

$$K = K_0 \exp(\frac{\Delta H_{ad}}{RT}) \tag{9}$$

38

where q $(= c)$ is the amount of gas adsorbed per unit mass of adsorbent (mol/kg), q_s is

the saturated amount of adsorbed gas molecules, θ is the surface coverage by adsorbates,

K is the equilibrium constant which is a ratio of adsorption (k_{ad}) and desorption (k_d)

rate constants, p is the partial pressure of adsorbates over the adsorbent surface and

ΔH_{ad} is the heat of adsorption. Eq. (9) is an expression for the temperature dependence

of the equilibrium constant. Using Eq. (8) and assuming $D_c(c)$ is constant for simplicity

(which is not always the case), one can integrate Eq. (7) and obtain the flux expression

for supported membranes:

$$J = \mu^* q_s \frac{D_c}{L} \ln\left(\frac{1 + Kp_s}{1 + Kp_p}\right) = \mu^* q_s \frac{D_c}{L} \ln\left(\frac{1 - \theta_p}{1 - \theta_s}\right) \tag{10}$$

By inserting Eq. (9) and the temperature dependence of D where E_d is the activation

energy for diffusion:

$$D = D_0 \exp\left(-\frac{E_d}{RT}\right) \tag{11}$$

into Eq. 10, the temperature dependence of the flux can be obtained:

$$J = \mu^* q_s \frac{D_c}{L} \ln\left(\frac{1 + Kp_s}{1 + Kp_p}\right)$$

$$= \frac{\mu^* q_s}{L} D_{c,0} \exp\left(-\frac{E_d}{RT}\right) \ln\left(\frac{1 + p_s K_0 \, exp\left(\frac{\Delta H_{ad}}{RT}\right)}{1 + p_p K_0 \, exp\left(\frac{\Delta H_{ad}}{RT}\right)}\right) \tag{12}$$

Under Henry's adsorption regime ($Kp_p < Kp_s \ll 1$), Eq. (12) are approximated based on the Tayler series as:

$$J = \mu^* q_s \frac{D_c}{L} Kp_s = \frac{\mu^* q_s}{L} D_{c,0} \exp\left(-\frac{E_d}{RT}\right) p_s K_0 \, exp\left(\frac{\Delta H_{ad}}{RT}\right)$$

$$= \frac{\mu^* q_s}{L} D_{c,0} p_s K_0 \exp\left(\frac{\Delta H_{ad} - E_d}{RT}\right) \tag{13}$$

Therefore, under Henry's adsorption regime, the temperature dependence of the flux depends on the sign (+ or -) of ($\Delta H_{ad} - E_d$) and there are neither maxima nor minima.

2.3.3 Diffusion mechanisms

2.3.3.1 Through mesopore

Knudsen diffusion is the dominant diffusion mechanism occurred in the mesopore regime (2 nm $< d_p <$ 50 nm) in which the mean free path of diffusing gas molecules (λ) is larger than the pore diameter ($\lambda > d_p$).[117] Therefore, in this regime, the gas molecules diffuse under more frequent collisions with pore wall than other gas molecules. The Knudsen diffusivity (D_{kn}) can be estimated by:

$$D_{kn} = \frac{\varepsilon d_p}{3\tau} u = \frac{\varepsilon d_p}{3\tau} \left(\frac{8RT}{\pi M}\right)^{1/2} \qquad (14)$$

where ε is the porosity, d_p is the pore diameter, τ is the tortuosity, u is the gas kinetic velocity, R is the gas constant, T is the temperature, and M is the molecular weight of the diffusing gas molecules.[117] Since there is no adsorption involved in the Knudsen diffusion-based gas transport, the Knudsen permeance simply is calculated by using the Knudsen diffusivity and the Fick's first law as:

$$Q = \frac{\varepsilon d_p}{\tau L} \left(\frac{8}{9\pi MRT}\right)^{1/2} \qquad (15)$$

where L is the membrane thickness. As being noticed, the permeance decreases by increasing temperature, indicating the Knudsen diffusion is not an activated process. In microporous polycrystalline membranes, the Knudsen diffusion is usually responsible for diffusions through non-selective pathways such as pinhole, cracks and grain boundary defects.

2.3.3.2 Through micropore

In micropore regime, since the size of diffusing molecules starts to approach the pore diameter of a diffusing medium, they cannot be free from the potential of pore wall. Depending on the ratio between pore diameter / the kinetic diameter of diffusing molecules (d_p/d_m), the different relative potentials $(U_{z,A})$ of the diffusing molecules
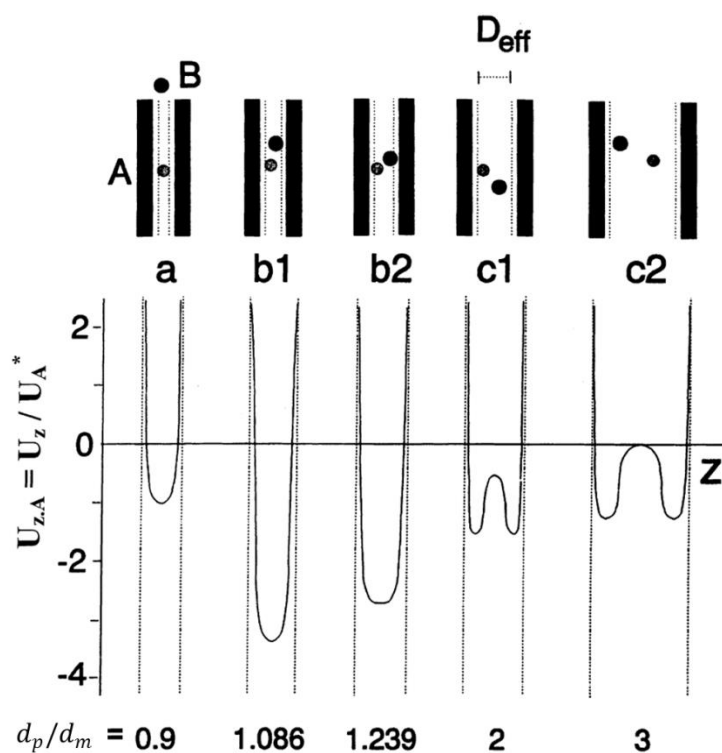
Figure 2.5 Relative potential ($U_{z,A}$) of a molecule A as a function of the distance z from the center of the pore with diameter. Reproduced with permission.[116] Copyright 1999, Elsevier.

inside pores can be expected as shown in Figure 2.5. Relying on the d_p/d_m values, the diffusion through micropores can be described as gas translational diffusion (activated Knudsen diffusion), or surface diffusion, or configurational diffusion or their combinations.[114] For example, if the b2 or C in Figure 2.5 is the case, the diffusion mechanism is the combination of gas translational diffusion and surface diffusion while

the configurational diffusion is a dominant mechanism for b1 and a. More detailed discussion on this matter can be found elsewhere.[114,118]

The general equation of all type of diffusivity can be expressed as:

$$D = guLexp\left(-\frac{\Delta E_d}{RT}\right) \tag{16}$$

where g is the geometrical factor, u is the velocity, L is the average distance between collisions or jumps, ΔE_d is the activation energy for diffusion.[119]

In case of the gas translational (GT) diffusion (activated Knudsen diffusion), gas molecules propagate through energy minimum sites on the surface by jumping via overcoming the diffusion activation barrier. Between the jumping, the molecules are still in a gaseous phase and move in a transitional mode (considered as a Knudsen gas).[116,119] Therefore we can insert the gas kinetic velocity used in the Knudsen expression, Eq (14) to Eq. (16) and obtain the GT diffusivity:

$$D_{GT} = g\left(\frac{8RT}{\pi M}\right)^{\frac{1}{2}} Lexp\left(-\frac{\Delta E_{GT}}{RT}\right) \tag{17}$$

In case of the surface diffusion, owing to the strong interaction between the diffusing molecules and the pore wall, the molecules lose their gaseous characteristics. Once adsorbed on one sorption site, the diffusing molecule vibrates together with its host site until it charges enough energy to hop to the next sorption sites.[116,119] Therefore, the

diffusing molecules move through the sorption sites in a vibrational mode rather than in a transitional mode and Eq. (16) becomes:

$$D_s = gvL^2 exp\left(-\frac{\Delta E_{sf}}{RT}\right) \tag{18}$$

where v is the vibrational frequency.

Lastly, when the d_p/d_m value becomes close to 1, the configurational diffusion occurs. The diffusivity has the same form with the Eq. (18) and this is where we can observe true molecular sieving effect. The molecules with d_m, bigger than d_p, are excluded from pore entrances, leading to theoretically an infinite separation factor.

2.4 Membrane Terminologies

The steady state diffusive flux (J) can be calculated by the Fick' first law:

$$J = -D\frac{dc}{dz} \approx -D\frac{\Delta c}{l} \tag{19}$$

where D is the diffusion constant, c is the gas concentration on the external surface of membranes and l is the membrane thickness. If the gas adsorption on the membrane surface ideally occurs under the Henry's regime, Eq. (19) can be approximated as:

$$J = -D\frac{dc}{dz} \approx -D\frac{\Delta c}{l} = -DK\frac{\Delta p}{l} \tag{20}$$

where K is the Henry constant (solubility constant (K)) and Δp the pressure gradient across the membrane.

The permeability (P), which is one of the intrinsic material properties, is defined as:

$$P = J\frac{l}{\Delta p} \tag{21}$$

The common permeability unit is the Barrer. 1 Barrer is 10^{-10} cc·(STP)/(cm^2·sec·cmHg) which is approximately equal to 3.348×10^{-16} mol·m^{-1}·s^{-1}·pa^{-1} in the S.I units. The permeability has two components:

$$P = J\frac{l}{\Delta p} = DK \tag{22}$$

where D is the diffusion coefficient and K is the solubility constant.

The permeance (Q) can be obtained by dividing the permeability (P) with the membrane thickness (l):

$$Q = \frac{P}{l} \tag{23}$$

The membrane ideal selectivity for a two component system (A and B) is the ratio of their permeability:

$$\alpha_{aB} = \frac{P_A}{P_B} = \frac{K_A}{K_B} \frac{D_A}{D_B} \tag{24}$$

which is also separated into two components of the solubility selectivity (K_A/K_B) and the diffusion selectivity (D_A/D_B). It should be noted that the ideal selectivity is obtained from the ratio of pure gas permeabilities.

For a two component mixture system (A and B), the membrane separation factor is defined as:

$$\alpha_{aB} = \frac{(y_A/y_B)}{(x_A/x_B)} \tag{25}$$

where x and y are the mole fraction of the gas components in the feed side and permeate side, respectively.

CHAPTER III

HIGHLY PROPYLENE-SELECTIVE SUPPORTED ZEOLITIC-IMIDAZOLATE

FRAMEWORK ZIF-8 MEMBRANES BY RAPID MICROWAVE-ASSISTED

SEEDING AND SECONDARY GROWTH[*]

3.1 Introduction

Zeolitic-imidazolate frameworks (ZIFs) are a sub-class of metal-organic frameworks (MOFs), comprising hybrid organic-inorganic moieties and exhibiting regular crystalline lattices with well-defined pore structures.[9,13,15,120-125] ZIFs consist of metal nodes coordinated to imidazolate-based ligands. The metal-linker-metal bond angle (~145°) in ZIFs is comparable to the T-O-T bond angle in zeolites, thereby resulting in zeolite topologies. Their exceptional thermal and chemical stabilities coupled with ultra-microporosity[15] make them desirable candidates for gas sensors,[126] catalytic membrane reactors,[108,127] and gas separation membranes.[18,20-24,27,73] As a result, the synthesis of ZIF films and membranes has attracted a great deal of research interest in recent years.[14]

ZIF-8 is of particular interest due to its robust synthesis protocol as well as its potential in industrially important propylene/propane separation.[128] ZIF-8 is composed of Zn atoms interconnected with 2-methylimidazolate (m-Im) ligand molecules, forming

the sodalite (SOD) zeolite-like structure with large cavities (11.6 Å) and small pore apertures (3.4 Å).[15]

So far, diverse synthesis routes for ZIF films and membranes have been reported[14] and can be broadly classified into two categories: *in situ* growth[18] and secondary (seeded) growth.[35,129,130] Given the importance of microstructure (particularly grain boundary structure) of polycrystalline membranes, though more complicated as compared to *in situ* method, secondary growth is preferred in which preformed seed crystals are anchored on porous supports followed by the growth of the seed crystals. Indeed, ZIF-8 membranes synthesized by Pan et al.[35] using secondary growth method showed unprecedented propylene/propane gas separation performance. In secondary growth method, strong attachment of seed crystals on porous supports is the key step for the successful preparation of well-intergrown polycrystalline membranes. However, conventional seeding methods such as dip-coating, slip-coating, and manual rubbing often lead to poor reproducibility mainly due to the weak attachment of seed crystals and the inconsistency in obtaining uniform distribution of seed crystals.

Here, we report a new strategy to rapidly prepare supports strongly attached with seed crystals under microwave irradiation. Using this new seeding technique, we were able to prepare seeded supports with a high packing density in a couple of minutes, which subsequently grown into continuous well-intergrown ZIF-8 membranes. The ZIF-8 membranes are highly propylene-selective with an average propylene/propane selectivity of ~ 40. Microwave-assisted seeding was also used to prepare well-

intergrown films of other ZIFs including ZIF-7[15] and SIM-1,[127] suggesting the possibility of its general applicability.

3.2   Experimental Section

3.2.1   Chemicals

Chemicals were used as purchased without further purification. Zinc nitrate hexahydrate ($Zn(NO_3)_2 6H_2O$, 98%, Sigma-Aldrich,)) were used as metal sources. 2-methylimidazole ($C_4H_5N_2$, 97%, Sigma-Aldrich, hereafter m-Im), benzimidazole ($C_7H_6N_2$, 98%, Sigma-Aldrich, hereafter b-Im), and 4-methyl-5-imidazolecarboxaldehyde ($C_5H_6N_2O$, 95%, Santa Cruz Biotechnology, hereafter m-Imca) were used as ligand sources. Sodium formate (HCOONa, 99%, Sigma-Aldrich, denoted as S.F.) was used as a deprotonating agent. Graphite powder (-300 mesh, 99%, Alfa Aesar) was used for coating a conductive layer on a support for MITD seeding. Methanol (99.8%, Alfa Aesar), ethanol (99.5%, Sigma-aldrich), and dimethylformamide (99.88%, Alfa Aesar, hereafter DMF) were used as solvents for membrane synthesis.

3.2.2   Preparation of α-Al_2O_3 supports

First, 1.9 g of alumina powder (CR6, Baikowski) was mixed with 8 mg of D.I. water (binder) and grinded in mortar to eliminate aggregated powder. Then the powder was injected into a die and compressed uniaxially with 10 ton for 1 min. The molded disks were dried at room temperature for 4 days and subsequently sintered at $1100^{o}C$ for 2 hr. The disks were polished with a sand paper (grid #1200) and washed with methanol

under sonication for 1min. Finally, the disks were dried at 120$^{\text{o}}$C in an oven before usage. The prepared disks have a dimension of 22 mm in diameter and 2 mm in thickness with 46% of porosity.

3.2.3 Formation of ZIF-8 seed layer and secondary growth

A metal precursor solution was prepared by dissolving 2.43 g of zinc nitrate hexahydrate in 40 ml of methanol while a ligand precursor solution was prepared by dissolving 2.59 g of m-Im and 0.125 g of S.F. in 30 ml of methanol. After a support was soaked in the metal precursor solution for 1 hr, it was placed vertically using a Teflon holder in the ligand solution contained in microwave-inert glass tube and immediately followed by the microwave radiation with the power of 100 W for 1.5 min. The seeded support was then thoroughly washed in fresh methanol under stirring for 4 hr followed by drying at 60$^{\text{o}}$C for 4 hr. The secondary growth of the ZIF-8 seed layer was done using the recipe reported by Pan et al.[35] Briefly, an aqueous precursor solution was prepared by dissolving 0.11 g of zinc nitrate hexahydrate and 2.27 g of m-Im in 40 ml of DI water. The seeded support was immersed vertically in the aqueous precursor solution and kept in an oven at 8$^{\text{o}}$C and 30$^{\text{o}}$C for 6 hr, respectively. The membrane was washed in fresh methanol under stirring for 5 days. Finally the sample was dried at 60$^{\text{o}}$C for 6 hr before further characterization.

3.2.4 Formation of ZIF-7 seed layer and secondary growth

Similarly, the seed layer was prepared by irradiating the microwave with the power of 100 W for 3 min onto the disk saturated with a metal precursor solution (3.06 g of zinc nitrate hexahydrate in 40 ml of DMF) positioned vertically inside of a ligand solution (1.62 g of b-Im and 0.01 g of S.F. in 40 ml of DMF). The seeded disk was thoroughly washed in ethanol under stirring for 4 hr and consecutively dried at 60°C for 4 hr. Then the seeded disk was placed in an autoclave containing precursor solution (0.57 g of zinc nitrate hexahydrate and 0.31 g of b-Im in 40 ml of DMF) and kept at 100°C for 6 hr in a convective oven. The membrane was rinsed in ethanol under stirring for 5 days. Lastly the sample was dried at 60°C for 6 hr before further characterization.

3.2.5 Formation of SIM-1 seed layer and secondary growth

The disk soaked in metal solution (2.5 g of zinc nitrate hexahydrate in 30 ml of ethanol) for 1 hr was injected into ligand solution (0.35g of m-Imca in 30 ml ethanol). Then the microwave with a power of 100 W was irradiated on the system for 3 min. Then the seeded disk was thoroughly washed in ethanol under stirring for 4 hr and consecutively dried at 60°C for 4 hr. Afterward the seeded layer was solvothermally treated at 85°C for 4 hr in an autoclave containing a precursor solution (0.1 g of zinc nitrate hexahydrate and 0.1 g of m-Imca in 40 ml of ethanol). Then, the membrane was rinsed in ethanol under stirring for 5 days. Lastly the sample was dried at 60°C for 6 hr before further characterization.

3.2.6 Binding strength of ZIF-8 seed layers

The binding strength of seed layers were tested by sonication method.[131] Briefly, the seed layers were sonicated with a power of 90 W (RF frequency, 35 kHz) in methanol as a function of time (20 min, 1 hr, 1.5hr, and 2 hr). XRD diffraction patterns were collected at each time intervals and (110) diffraction peaks were normalized by the (110) peak intensity obtained from the initial seed layers. Then the tendencies of variation in the normalized intensities as a function of sonication time were compared to judge the binding strength to supports between the seed layers prepared in different ways such as dip-coating,[35] MITD,[132] and microwave-assisted seeding. The dip-coated seed layers were prepared by following the recipe reported by Pan et al. In case of MITD seeding, first, the conductive graphite layer was coated on a support by manually rubbing graphite powder. Then the graphite coated supports were placed in the solution, a mixture of 0.04 ml of metal solution (2.43 g of zinc nitrate hexahydrate in 40 ml methanol) and 30 ml of ligand solution (2.59 g of m-Im and 0.125 g of S.F. in 30 ml of methanol). Subsequently, the system was exposed to the microwave with the power of 100 W for 1.5 min. The seeded support was then thoroughly washed in fresh methanol under stirring for 4 hr followed by drying at 60°C for 4 hr.

3.2.7 Characterization

Crystal phases of the seed layers and membranes were identified by a Rigaku Miniflex II powder X-ray diffractometer using Cu-Kα radiation (λ = 1.5406 Å) which were scanned with a step size of 0.02^{0}. Scanning electron micrographs were collected

using a JEOL JSM-7500F operating at 5 keV acceleration voltage and 15 mm working distance. The gas separation performance of ZIF-8 membranes was tested using the Wicke-Kallenbach technique under atmospheric pressure. The 50:50 mixture of propylene and propane was supplied to a feed side while a permeate side was swept by argon with the total flow rates of both sides maintained at 100 ml/min. The gas composition of the permeate side was analyzed using a gas chromatography (Agilent GC 7890A equipped with HP-PLOT/Q column).

3.3 Results and Discussion

A densely-packed ZIF-8 seed layer can be rapidly formed on porous alumina supports under microwave irradiation as illustrated in Figure 3.1. The microwave seeding process involves three steps: 1) saturation of a porous support with a metal precursor solution, 2) exposure of the support soaked with metal ions to a ligand precursor solution, and 3) rapid crystal formation under microwave irradiation. It is critically important to maintain relatively high concentration of both metal ions and ligand molecules in the vicinity of the support ("reaction zone") by soaking the support with metal ions prior to the microwave irradiation. The formation of the reaction zone near the support surface maximizes the heterogeneous crystal formation while minimizing the undesirable homogeneous crystal formation. Furthermore, microwave energy is rapidly absorbed by metal ions inside supports, resulting in the rapid rise of the local temperature inside the support. This sharp temperature rise leads to the rapid
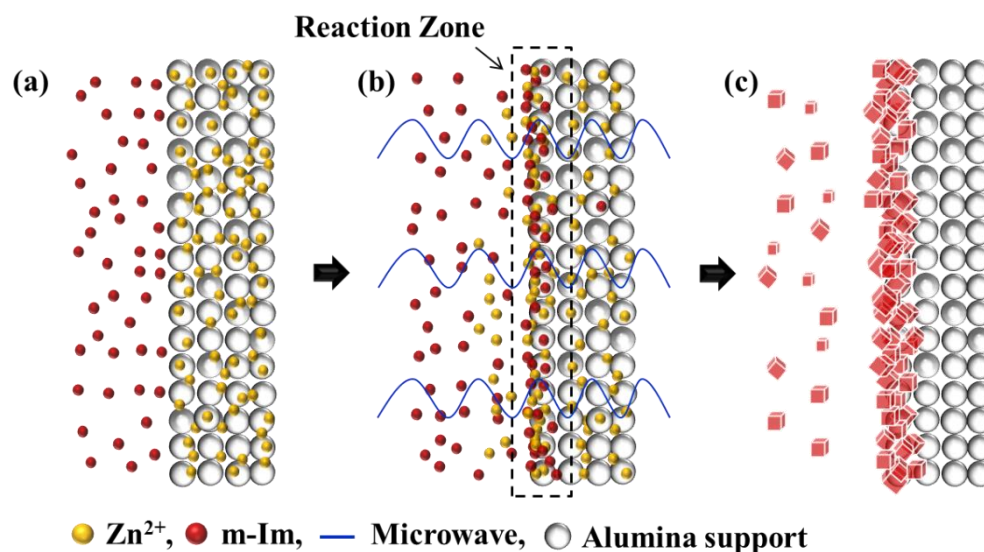
Figure 3.1 Schematic illustration of rapid microwave-assisted seeding process; (a) a support saturated with a metal solution in a ligand solution, (b) formation of a reaction zone at the interface and microwave irradiation, and (c) preferential heterogeneous nucleation near the support surface.

formation (in less than a couple of minutes) of ZIF-8 nanocrystals inside as well as on the surface of the supports.

The X-ray diffraction (XRD) pattern of a seeded support (Figure 3.2) confirms phase-pure ZIF-8 crystals formed on the support and the crystals are nano-sized as evidenced by the substantial broadening of the diffraction peaks. The presence of the nano-sized ZIF-8 crystals was further corroborated by the electron micrographs of a seeded support (Figure 3. 3(a) and (b)). As can be seen, the support surface was uniformly and densely covered with ZIF-8 nanocrystals of about 100 nm displaying well-defined rhombic dodecahedral facets. Besides, ZIF-8 nanocrystals formed inside
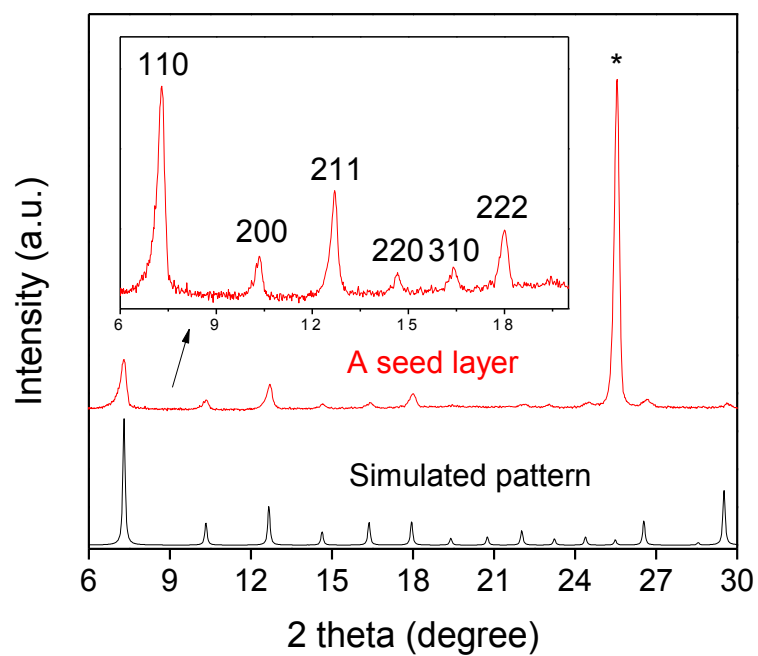
Figure 3.2 X-ray diffraction pattern of a ZIF-8 seed layer on an α-Al₂O₃ support prepared under microwaves in comparison with a simulated pattern. The characteristic peak of α-Al₂O₃ support is marked with an asterisk.
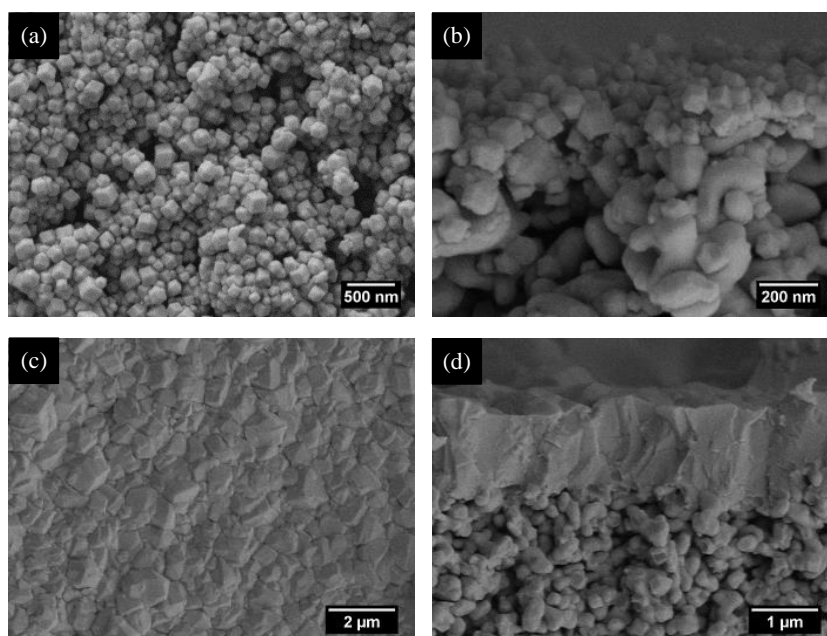
Figure 3.3 SEM images of a ZIF-8 seed layer: (a) top-view and (b) cross-section and a membrane grown at 8 $^{\circ}$C for 6 hr: (c) top-view and (d) cross-section.

the support as well, which is expected to enhance the mechanical stability of seed layers, ultimately ZIF-8 membranes.

Previously we have shown the rapid formation of MOF-5 (also known as IRMOF-1) films on the porous supports coated with thin conductive layers such as graphite under microwave irradiation, which we called microwave-induced thermal deposition (MITD).[132] The important step for the MITD process is to have an electrically conductive layer on the surface of supports. Under microwave irradiation, the strong interaction of the conductive layer with microwave energy (i.e., Joule heating) gives rise to rapid temperature increase at the coated support surface, thereby leading to fast

heterogeneous nucleation. The MITD-prepared MOF-5 films were subsequently grown into continuous membranes by secondary growth.[133] However, MITD-based seeding has drawbacks, including the necessity of conductive surface layers, a limited number of MOF structures that can be deposited, and the mechanical stability of subsequently grown membranes. The microwave-assisted seeding approach reported here is fundamentally different from the MITD seeding in that the temperature rise results primarily from the interactions of metal ions inside supports with microwave, therefore not necessary to have conductive coatings. In addition, the subsequent heterogeneous nucleation and crystal growth is limited mostly in the reaction zone (Figure 3.1) near the support surface. Furthermore, the seeding process is much simpler and more reproducible as compared to conventional seeding methods in which nano-sized seed crystals are to be synthesized (which often is not straightforward) and to be deposited on supports.

To achieve well-intergrown MOF membranes using secondary growth method, it is essential to have strong adhesion of seed crystals onto supports. Different strategies have been employed to ensure strong adhesion of seed crystals, including the incorporation of polymer binder[134] or usage of smaller seed crystals than the support pores.[130] The binding strength of the ZIF-8 seed layers prepared by microwave seeding was examined by sonication method,[131] showing strong adhesion of the seed crystals onto the supports (Figure 3.4). Even with extensive sonication for up to 2 hr, the majority of seed crystals remained intact. In contrast, most of the seed crystals deposited using conventional methods such as dip-coating and MITD were detached from the
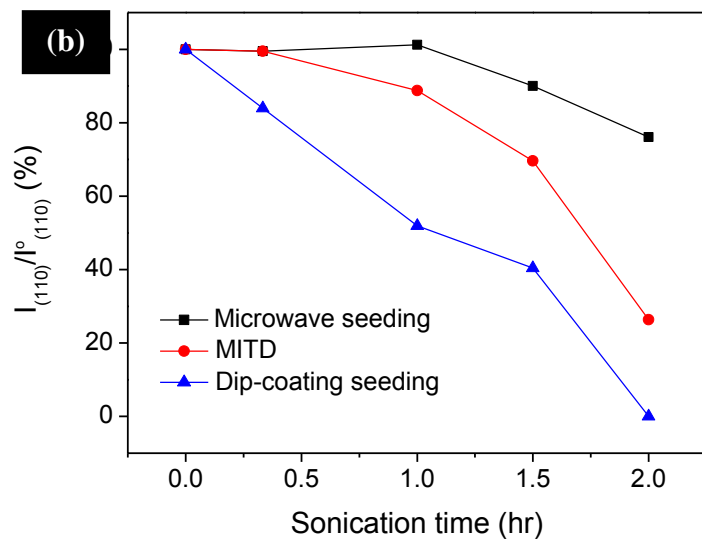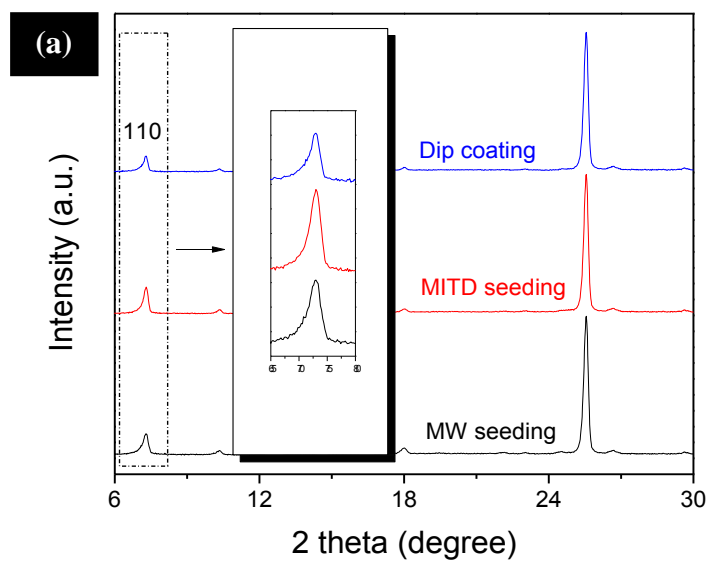
Figure 3.4 (a) XRD patterns of initial seed layers prepared by various method and (b)

binding strength of the ZIF-8 seed crystals on α-Al_2O_3 supports.

supports. This remarkably strong attachment of seed crystals on the support is attributed to the possible presence of chemical bonds formed between the seed crystals and the support. As reported previously,[23] one plausible scenario might be the formation of covalent bond (Al-N) between the support and ligand molecules by the condensation reaction between the surface hydroxyl group of the supports and the nitrogen of m-Im triggered by intensive microwave heating.

Subsequently, the ZIF-8 seeded supports were subjected to secondary growth to form continuous ZIF-8 membranes using the aqueous recipe[130] reported elsewhere with a slight modification in growth temperature as described in the experimental section. Figure 3.5 displays X-ray diffraction (XRD) patterns of ZIF-8 membranes synthesized as a function of growth time. Well-intergrown ZIF-8 membranes with the thickness of about 1.5 μm were obtained after 6 hr of growth (Figure 3.3(c) and (d)).

The gas separation performance of the ZIF-8 membranes was examined by performing binary gas permeation measurements with a propylene/propane mixture (50/50) using a Wicke-Kallenbach technique (Figure 3.6). Table 3.1 indicates the separation performance of the membranes prepared at different growth temperature, 8°C and 30°C, in comparison with the one of a bare α-Al_2O_3 support. The membranes grown at 8°C showed an average propylene permeance of about 208 mol Pa^{-1} m^{-2} s^{-1} with an average propylene/propane separation factor of ~ 40, similar to the values reported by Pan et al.[35] Intriguingly, the separation performances (propylene permeance and separation factor) are enhanced as the growth temperature decreases. Our reasoning is that slow crystal growth at lower temperature results in membranes with thinner
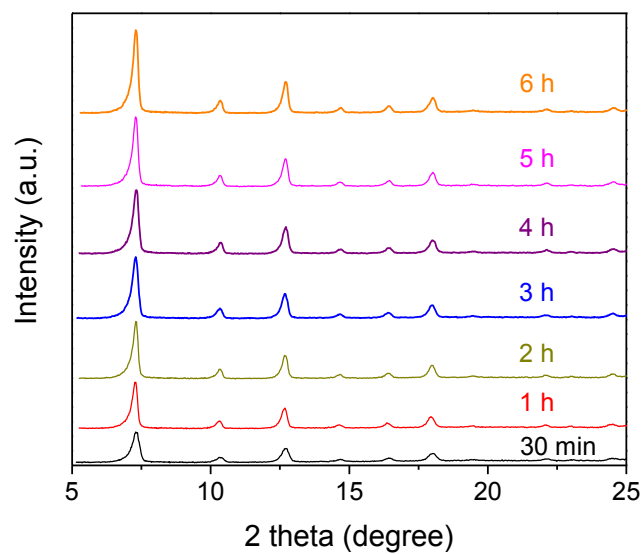
Figure 3.5 XRD patterns of ZIF-8 membranes as a function of growth time.
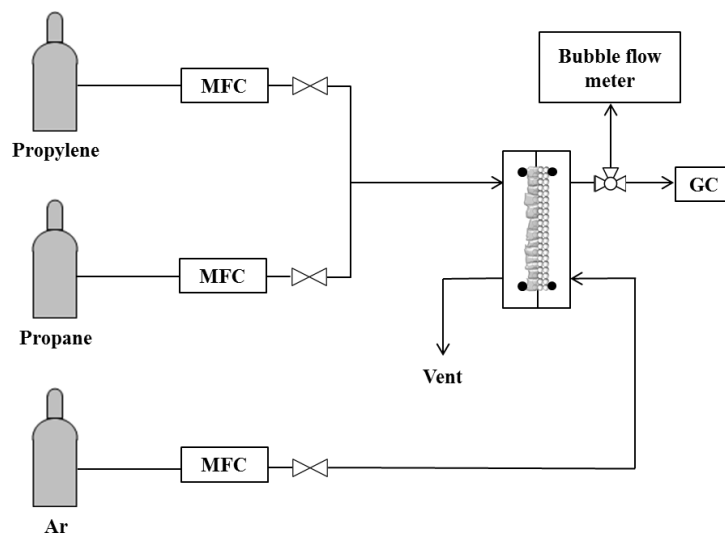
Figure 3.6 Schematic diagram of a Wicke-Kallenbach gas permeation test setup.

Table 3.1 Propylene/propane separation performance of ZIF-8 membranes synthesized at different secondary growth temperature for 6 hr. Three membranes at each condition were tested to obtain standard deviation.

Growth temperature (^{o}C)	Permeance (x 10^{-10} mol Pa^{-1} m^{-2} s^{-1})		C_3H_6/ C_3H_8 Sparation factor
	C_3H_6	C_3H_8	
8	207.88 ± 6.54	5.46 ± 1.45	40.43 ± 8.45
30	143.62 ± 6.46	4.82 ± 0.64	30.77 ± 2.92

thickness given the same growth time, and better grain boundary structure as compared to the ones formed at higher temperature (Figure 3.7 and 3.8). When compared with other membranes (Figure 3.9), our ZIF-8 membranes have outstanding performance, meeting the proposed separation property requirement[1] for commercial applications (a minimum permeability of 1 Barrer and selectivity of 35). It is worthwhile to note that the flexibility of ligands enables ZIF-8 to accommodate molecules much bigger than its pore aperture (3.4 Å).[18,128] Peralta et al[135] recently showed that ZIF-8 framework can adsorb the molecules with the size up to 6.4 Å through the transitory deformation of the pore aperture.

Finally, to show its general applicability, the microwave-assisted seeding technique was applied to synthesize membranes of other MOFs such as ZIF-7 and SIM-1 (Figure 3.10 and 3.11). After secondary growth, well-intergrown ZIF-7 and SIM-1 membranes were successfully prepared. In case of SIM-1 membranes, synthesis time was drastically reduced (4 hr vs. 72 hr) as compared to the *in situ* synthesis reported by
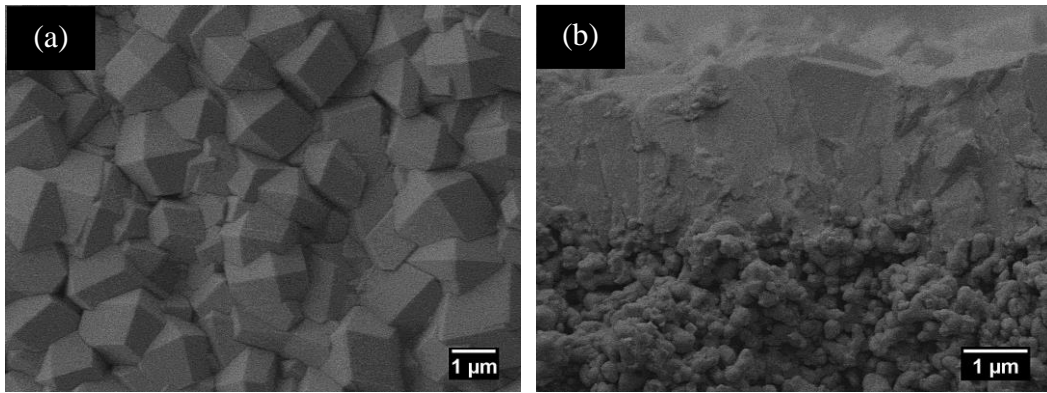
Figure 3.7 SEM images of ZIF-8 memrbanes grown: at 30 ^{o}C (a) top view and (b) cross-section.
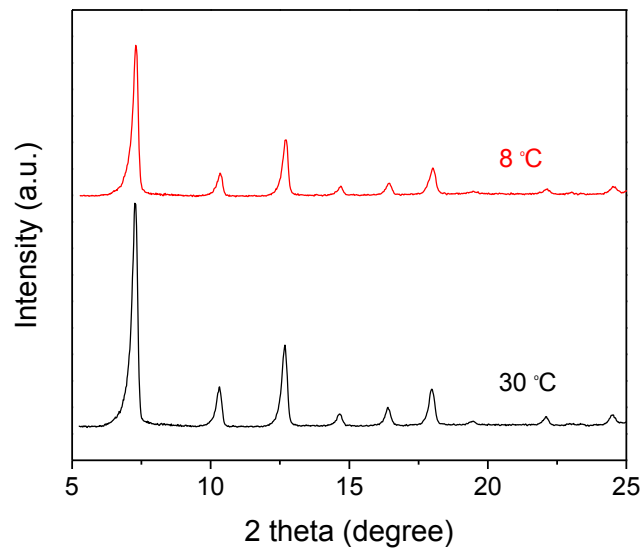
Figure 3.8 XRD patterns of ZIF-8 membranes prepared at 8°C and 30°C.
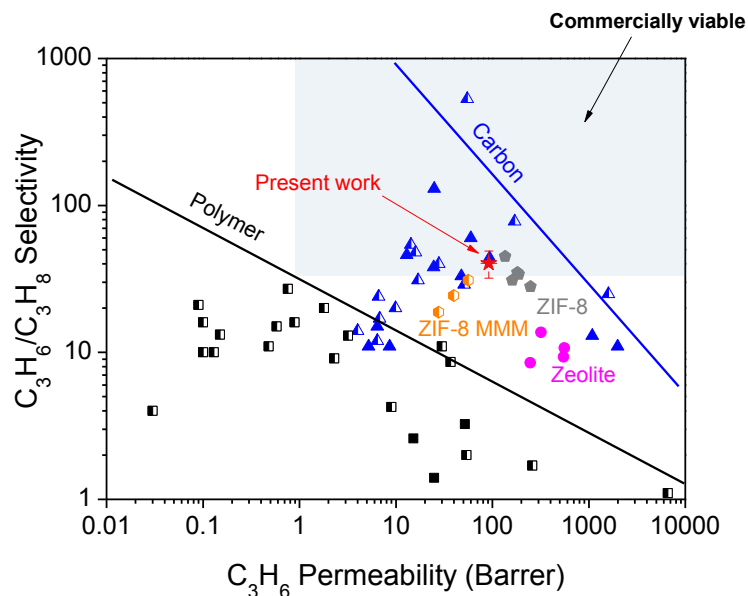
Figure 3.9 Comparison of ZIF-8 membrane performances for propylene/propane separation with other literature data. Half-filled and full-filled symbols indicate separation data from singles gas permeation and binary gas permeation test, respectively. The shaded area in the graph implies the performance requirement of a membrane (a minimum permeability of 1barrer and selectivity of 35) for commercial application.[1] (triangle : Carbon membrane,[4-6,136] circle : zeolite membrane,[3] rectangle : polymer membrane,[2] pentagon : ZIF-8 membrane,[35] hexagon : ZIF-8 mixed matrix membrane,[7] star : ZIF-8 membrane in this work).
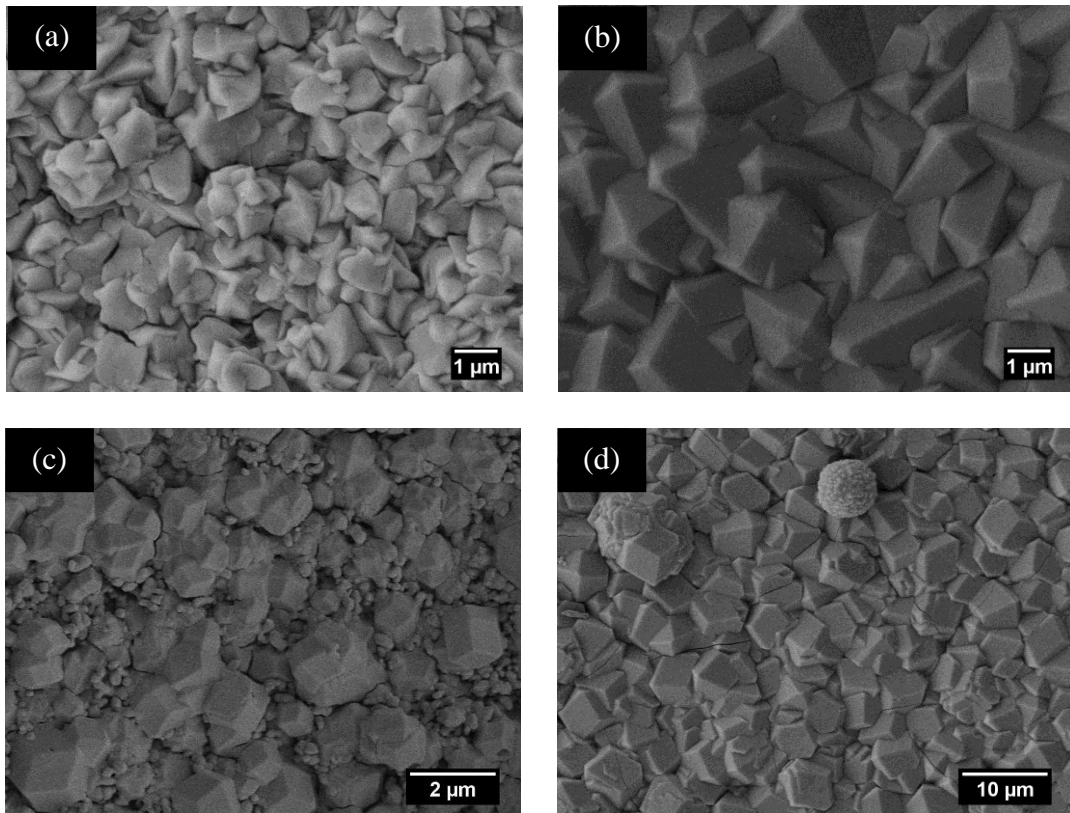
Figure 3.10 SEM images of (a) a ZIF-7 seed layer, (b) a ZIF-7 membrane, (c) a SIM-1 seed layer, and (d) a SIM-1 membrane prepared by rapid microwave-assisted seeding and secondary growth.
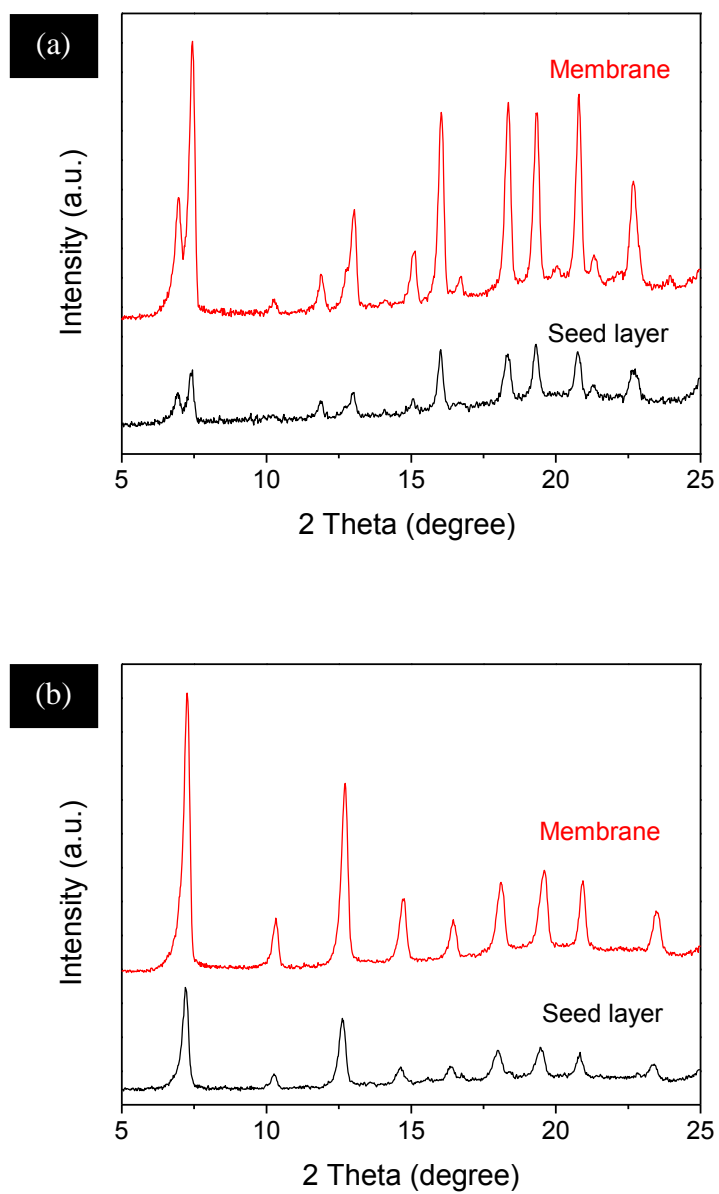
Figure 3.11 XRD patterns of (a) a ZIF-7 seed layer and a ZIF-7 membrane and (b) a SIM seed layer and a SIM-1 membrane.

Aguado et al.[29] This reduction in the synthesis time is ascribed to two factors: secondary growth approach and use of ethanol as solvent instead of dimethylformamide. We will test gas separation performances of these membranes and report later.

3.4 Conclusions

In conclusion, we have developed a new microwave-assisted rapid seeding method that enables rapid formation of nanosized seed crystals on porous supports with uniform and high surface coverage. The key step in this method is to saturate porous supports with metal ions prior to the microwave irradiation in a ligand solution. The strong absorption of microwave energy by metal ions inside support along with the concentration of microwave energy on the support surface rapidly increase the local temperature of the supports, resulting in the rapid heterogeneous nucleation and growth of ZIF-8 nanocrystals. Subsequent secondary growth of these ZIF-8 seed layers led to well-intergrown ZIF-8 membranes, which have shown an excellent propylene/propane separation performance. Our rapid microwave-assisted seeding in combination with secondary growth led to the successful synthesis of well-intergrown membranes of other ZIFs including ZIF-7 and SIM-1, suggesting the feasibility of its potentially general applicability.

CHAPTER IV

IN SITU SYNTHESIS OF THIN ZEOLITIC-IMIDAZOLATE FRAMEWORK ZIF-8

MEMBRANES EXHIBITING EXCEPTIONALLY HIGH PROPYLENE/PROPANE

SEPARATION[*]

4.1 Introduction

Due to the close physical properties, olefin/paraffin separation (such as propylene/propane) is quite challenging, yet commercially very important.[2,47,48] Separation of olefin/paraffin mixtures is traditionally performed using highly energy intensive cryogenic distillation.[2,48] Membranes have therefore gained tremendous interest as an energy-efficient alternative technology. It has been proposed that in order for membranes to be commercially viable a minimum propylene permeability of 1 Barrer and a propylene selectivity of 35 are required.[1] So far, there have been many different types of membranes studied including polymer,[2] zeolite,[3] carbon molecular sieve,[4-6] mixed matrix,[7] and facilitated transport membranes.[8] However, most of these membranes suffer from certain limitations one way or another. For example, most of polymeric membranes do not meet the selectivity/permeability threshold while suffering from low reliability and durability.[2] The selectivity/permeability performance targets are met neither by more robust membranes, such as zeolites and ceramics, nor by mixed

matrix membranes consisting of highly selective phases dispersed in polymer matrix until recently. Facilitated transport membranes can be easily poisoned by small amount of impurities, while carbon molecular sieve membranes are brittle and difficult to scale-up the production. Accordingly, it is evident that new material paradigms are essential to successfully address this energy-intensive yet industrially important separation.

Metal−organic frameworks (MOFs) are a new class of nanoporous organic−inorganic hybrid materials that exhibit regular crystalline lattices with rigid pore structures.[9-11] With unprecedented control over pore size and chemical/physical properties via a judicious choice of organic linkers, MOFs offer unique opportunities to overcome the limitations of not only current membrane materials but also conventional membrane system design/integration and operation.[12-14] An important subclass of MOFs, especially when considering gas separation applications, is zeolitic-imidazolate frameworks (ZIFs).[15-17] ZIFs consist of metal nodes (usually zinc or cobalt) connected to imidazole (or its derivative) linkers and exhibit zeolite-like structures due to the metal−linker−metal bond angle of ~145° (close to the T−O−T angle found in zeolites).[15] ZIFs have been extensively investigated for gas separation membranes mainly due to their exceptional stability and ultramicropores.[18,21-23,85,86] Of particular interest is ZIF-8 composed of Zn and 2-methylimidazole ligands, forming the sodalite (SOD) zeolite structure with large cavities (11.6 Å) and small pore apertures (3.4 Å).[15] Recently Li et al.[128] have reported that propylene (~4 Å) diffuses in ZIF-8 2 orders of magnitude faster than propane (~4.3 Å),[137] suggesting that high-quality ZIF-8 membranes could effectively distinguish propylene from propane based on size.

So far, several research groups have reported diverse synthesis protocols for ZIF films and membranes.[14,121] In order to achieve well-intergrown ZIF membranes, it is critical to favor the heterogeneous nucleation and crystal growth of ZIFs on porous supports over the homogeneous nucleation and crystal growth in solutions. To promote the heterogeneous nucleation and crystal growth, a number of different strategies have been devised including the chemical modification of support surfaces[18,23] and the anchoring of seed crystals on supports,[35,129,130] making ZIF membrane synthesis complicated. The added complexity not only increases the cost of membrane manufacturing but also often leads to poor membrane microstructure (i.e., grain boundary structure). Indeed, none of ZIF membranes reported so far has shown any impressive gas separation performance.[14] The only exception is the ZIF-8 membranes reported by Lai and co-workers,[35] showing excellent propylene/propane separation performance. The membranes were synthesized using a secondary (or seeded) growth method in which preformed seed crystals are deposited on supports followed by subsequent growth of the seed crystals into well-intergrown films. However, an increased number of steps involved in secondary growth can add to the complexity of the synthesis process, thereby potentially causing reproducibility issues.[35] In contrast, though conceptually simpler and less complicated than secondary growth, an in situ method has failed to yield ZIF membranes with high gas separation performance.

Reaction systems where reacting species are physically separated and brought into contact by diffusion (such as interfacial and counter-diffusion synthesis) have been used to create MOF films and membranes.[138,139] Self-supporting HKUST-1 hollow shell-

membranes were synthesized at the interface between two immiscible liquids in which metal ions and ligand molecules meet and react.[139] These HKUST-1 membranes were found to be selective toward small molecules.[139] ZIF-8 membranes were prepared on porous polymer supports using a counter-diffusion concept in which the supports physically separate metal ions and ligand molecules.[138] However, These ZIF-8 membranes have not shown any good gas separation performance, likely due to their poor grain boundary structure.[138]

Here we report a new in situ approach for the synthesis of well-intergrown ZIF-8 membranes with significantly enhanced microstructure. Our synthesis method is based on a counter-diffusion concept in which a metal precursor solution is soaked in porous α-alumina supports followed by rapid solvothermal reaction in a ligand solution. Due to the nature of the counter-diffusion concept, the new method offers unique opportunities, such as healing defective membranes (i.e., poorly intergrown) as well as significantly reducing the consumption of costly ligands and organic solvents. The ZIF-8 membranes show excellent propylene/propane separation performance and exhibit exceptional mechanical strength. The technique appears to be potentially general evidenced by the successful synthesis of well-intergrown membranes of prototypical ZIFs, such as ZIF-7 and SIM-1.

4.2 Experimental Section

4.2.1 Chemicals

Zinc chloride ($ZnCl_2$, 99.99%, Alfa Aesar), 2- methylimidazole ($C_4H_6N_2$, 99%, Sigma-Aldrich), sodium formate (NaCOOH, > 95%, Sigma-Aldrich), and methanol (CH_3OH, > 99%, Alfa Aesar) were used as a metal source, a ligand, a deprotonating agent, and a solvent for the synthesis of ZIF-8 membranes, respectively. All of the chemicals were used as purchased without further purification.

4.2.2 Preparation of ZIF-8 membranes

In a typical synthesis, 0.98 g of zinc chloride was dissolved in 40 mL of methanol (solution A), and 5.19 g of 2-methylimidazole (hereafter mIm) and 0.5 g of sodium formate was dissolved in 40 mL of methanol (solution B). A homemade α-Al_2O_3 disk (porosity = 46%, diameter = 22 mm, and thickness = 2 mm) was soaked in the solution A for 1 h. The disk saturated with the zinc salt solution was positioned vertically in a Teflon-lined autoclave containing the solution B. Then, the autoclave was subjected to solvothermal synthesis for 4 h at 120 °C. After synthesis, the membrane sample was rinsed with methanol several times and immersed in methanol under stirring for 1 day. Afterward, one side of the supported membranes was polished with sand paper manually since films are formed on both sides of supports. Additional washing of 4 days was conducted before drying in an oven at 60 °C for 12 h for further characterizations.

4.2.3 Preparation of SIM-1 membranes

In a typical synthesis, 5 g of zinc nitrate hexahydrate ($Zn(NO_3)_2 \cdot 6H_2O$, 98%, Sigma-Aldrich) was dissolved in 40 mL of ethanol (99.88%, Sigma-Aldrish), and 1 g of 4-methyl-5-imidazolecarboxaldehyde ($C_5H_6N_2O$, 95%, Santa Cruz Biotechnology) and 0.05 g of sodium formate (HCOONa, 99%, Sigma-Aldrich) was dissolved in 40 mL of ethanol (solution B). A home-made α-Al_2O_3 disk was soaked in the solution A for 1 hr. The disk saturated with the zinc salt solution was positioned vertically in a Teflon-lined autoclave containing the solution B. Then, the autoclave was subjected to solvothermal synthesis for 4 h at $85^{\circ}C$. After synthesis, the membrane sample was rinsed with ethanol several times and immersed in ethanol for washing under stirring for 1 day. Afterward, one side of the supported membranes was polished with sand paper manually since films are formed on both sides of supports. Additional washing of 4 days was conducted before drying at room temperature for 48 h.

4.2.4 Preparation of ZIF-7 membranes

In a typical synthesis, 3.06 g of zinc nitrate hexahydrate ($Zn(NO_3)_2 \cdot 6H_2O$, 98%, Sigma-Aldrich) was dissolved in 40 mL of dimethylformamide (99.88%, Alfa Aesar, hereafter DMF), and 1.62 g of benzimidazole ($C_7H_6N_2$, 98%, Sigma-Aldrich, hereafter b-Im) and 0.01 g of sodium formate (HCOONa, 99%, Sigma-Aldrich) was dissolved in 40 mL of DMF (solution B). A home-made α-Al_2O_3 disk was soaked in the solution A for 1 hr. The disk saturated with the zinc salt solution was positioned vertically in a Teflon-lined autoclave containing the solution B. Then, the autoclave was subjected to

solvothermal synthesis for 4 h at 85°C. After synthesis, the membrane sample was rinsed with DMF and ethanol several times and immersed in ethanol for solvent exchange under stirring for 1 day. Afterward, one side of the supported membranes was polished with sand paper manually since films are formed on both sides of supports. Additional solvent exchange of 4 days was conducted before drying at room temperature for 48 h.

4.2.5   Healing of defective membranes

Defective membranes were synthesized in a similar manner described above but using recycled precursor solutions (details explained in Results and Discussion section below). A poorly intergrown ZIF-8 membrane was loaded into a homemade diffusion cell. A ligand solution (2.27 g of 2-methyimidazole in 20 mL of D.I. water) was poured into the support side of the diffusion cell and kept for 1 h in order to saturate the support. A metal solution (0.11 g of zinc nitrate hexahydrate in 20 mL of D.I. water) was supplied into the membrane side of the diffusion cell. Finally, the diffusion cell is kept in an oven at 30 °C for 6 h for the healing process. The healed membrane is washed in methanol for 5 days under stirring followed by drying at 60 °C for 6 h.

4.2.6   Propylene/propane gas permeation test

Propylene/propane single and binary gas permeation measurements were carried out at various temperatures under atmospheric pressure by the Wicke−Kallenbach technique. The feed and argon sweeping gases were supplied to the feed and permeate sides at a flow rate of 100 cc/ min, respectively. For a binary measurement, an equimolar

propylene/ propane mixture was used as a feed. The composition of the permeate side stream was analyzed using a gas chromatography (Agilent GC 7890A equipped with a column of HP-PLOT/Q).

4.2.7   Characterization

X-ray diffraction (XRD) patterns were collected using a Rigaku Miniflex II powder X-ray diffractometer with Cu−Kα radiation (λ = 1.5406 Å). Electron micrographs were taken using a JEOL JSM-7500F operating with 5 keV acceleration voltage and 15 mm working distance.

4.3   Results and Discussion

Figure 4.1 illustrates the synthesis of continuous and defect-free supported ZIF-8 membranes using one step in situ growth based on counter-diffusion concept. As illustrated in the figure, porous α-Al_2O_3 supports are soaked with a metal ion solution, and the supports containing metal ions are then subjected to solvothermal growth in a ligand solution. Upon contact, the concentration gradients enable metal ions and ligand molecules to diffuse from the support into the solution and from the solution into the support, respectively. Therefore, relatively high concentrations of both metal ions and ligand molecules are maintained in the vicinity of the support ("reaction zone") during the solvothermal treatment. It should be noted that in a typical counter-diffusion concept,[138] two solutions (i.e., metal ions and ligand molecules) are provided from the opposite sides of the supports, resulting in much longer diffusion length as compared to
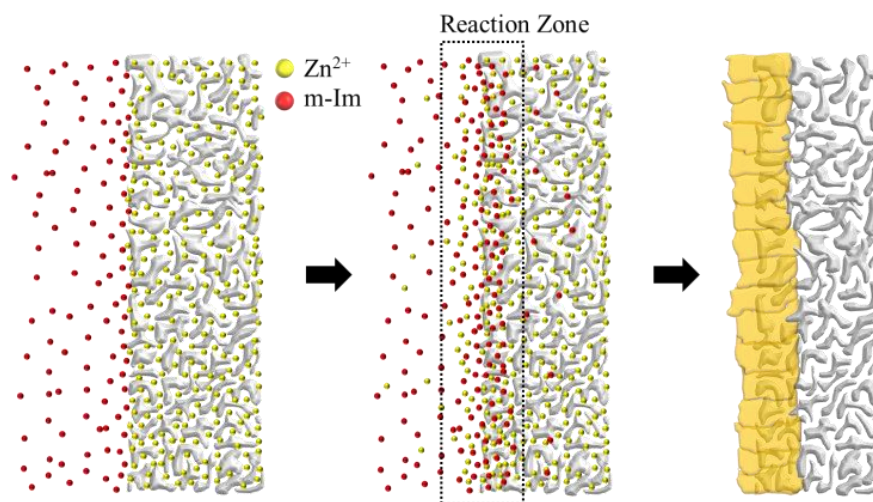
Figure 4.1 Schematic illustration of the membrane synthesis using the counter-diffusion-based *in situ* method: 1) a porous alumina support saturated with a metal precursor solution is placed in a ligand solution containing sodium formate, 2) the diffusion of metal ions and ligand molecules cause the formation of "reaction zone" at the interface, and 3) rapid heterogeneous nucleation/crystal growth in the vicinity at the interface leads to the continuous well-intergrown ZIF-8 membranes.

our case. Since reaction (crystallization) and diffusion occur simultaneously, it is critically important to consider both of these competing kinetic processes. For example, if the reaction rate is too slow as compared to the diffusion rate (i.e., low Thiele modulus which is the ratio of diffusion and reaction time constants), most of the metal ions will completely diffuse from the support to the solution, favoring the homogeneous nucleation and crystal growth. Ideally, the reaction should be faster than the diffusion (i.e., high Thiele modulus) so that the heterogeneous nucleation and growth can happen before metal ions are depleted from the support. One can increase the Thiele modulus by

raising the reaction rate by increasing temperature and/or by adding catalysts. In this study, sodium formate was added as a deprotonator to the ligand solution to increase the reaction rate,[23] maintaining relatively high Thiele modulus.

Figure 4.2 presents the XRD patterns and SEM images of the films grown for various growth times (see Figure 4.3 for the complete set). As can be seen in the figure, a substantial heterogeneous formation of phase-pure ZIF-8 crystals can be observed even after 2 min of the solvothermal growth, strongly suggesting the relatively high precursor concentrations at the support surface (i.e., reaction zone). After 30 min, the crystal growth appears to be completed so that the grain size and the film thickness of ca. 1.5 µm do not change even with further growth. In general, forming well-intergrown polycrystalline framework membranes with a thickness of ca. 1.5 µm is not straightforward using in situ methods. In a typical in situ method, heterogeneous nucleation and crystal growth are in competition with homogeneous nucleation and crystal growth. To prevent excessive homogeneous crystal formation, it is often necessary to maintain precursor concentrations low. This results in a much smaller number of nuclei and their growth into bigger crystals in a longer time scale as compared to the case with high precursor concentrations. Indeed, MOF membranes synthesized by in situ method have thicknesses in the rage of tens of micrometers,[18,20,21,41] compromising gas permeances through the membranes (i.e., low flux). However, in our method, throughout the crystallization, relatively high precursor concentrations are maintained near the supports. This high precursor concentration, combined with the presence of the catalyst, leads to the fast formation of a large number of nuclei and their

76
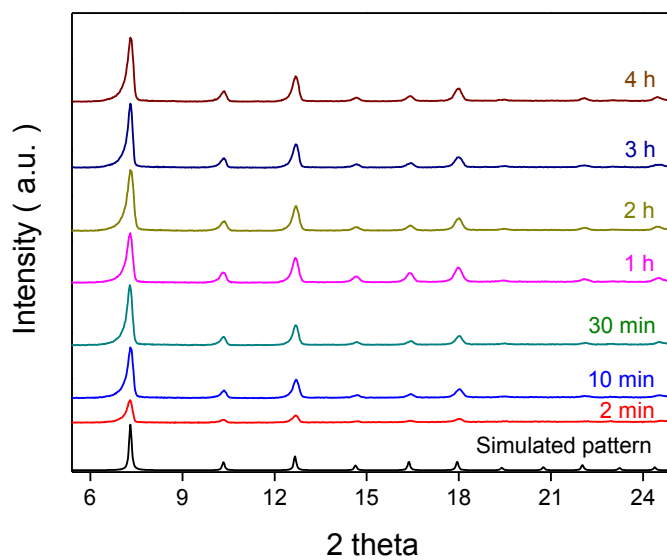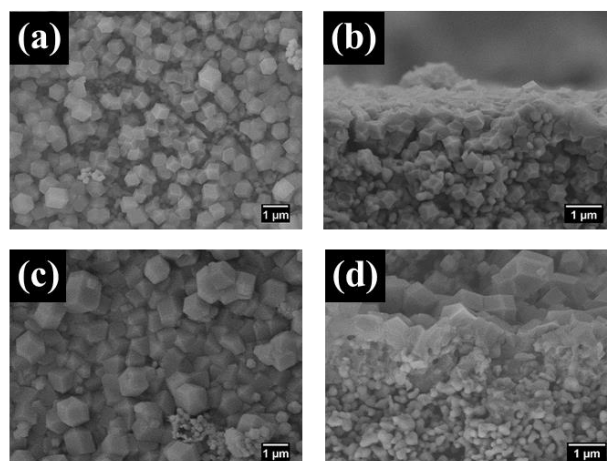
Figure 4.2 SEM images of ZIF-8 membranes grown for 2min (a, b) and for 30 min (c, d), and XRD patterns of ZIF-8 membranes as a function of growth time (e). Fast heterogeneous nucleation/crystal growth is due to the presence of a catalyst (i.e., sodium formate) and the relatively high concentration of both metal ions and ligand molecules in the vicinity of the interface.
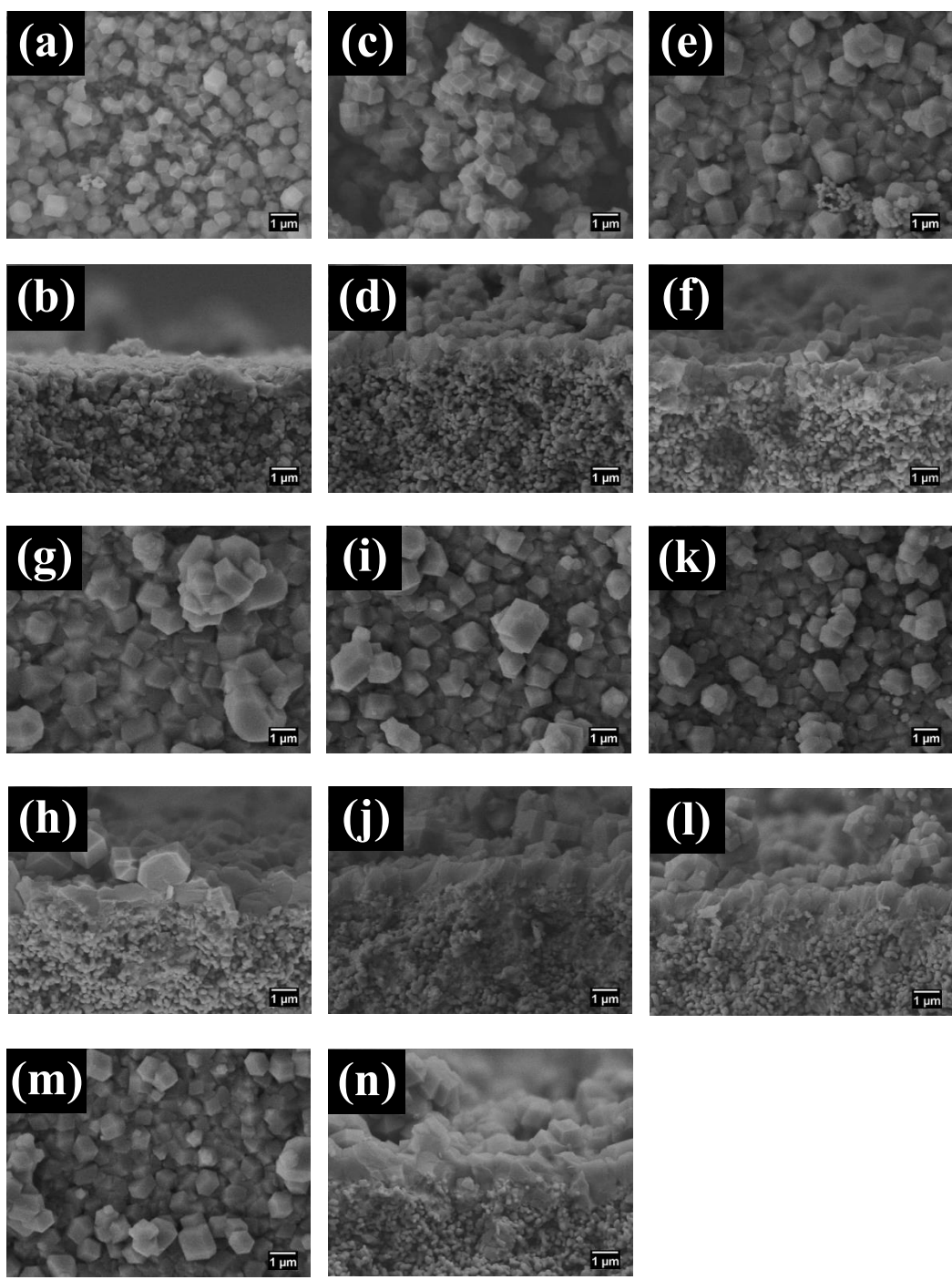
Figure 4.3 SEM images of ZIF-8 membranes grown for 2 min (a, b), 10 min (c, d), 30 min (e, f), 1 h (g, h), 2 h (i, j), 3 h (k, l), and 4 h (m, n).

78

subsequent crystal growth in the vicinity of the support surfaces, resulting in the formation of substantially thinner ZIF-8 membranes (ca. 1.5 μm) than typical in situ grown membranes. Furthermore, the self-limiting crystal growth, in which the crystals can grow only where the ligand molecules and metal ions are in contact, significantly limits further crystal growth. Another important observation is that a fraction of ZIF-8 crystals are formed inside the support (Figure 4.2(d)), which potentially enhances the mechanical stability of the membranes (more discussion follows).

In order to synthesize continuous well-intergrown ZIF-8 membranes using the counter-diffusion-based in situ method (hereafter, CD-based in situ method), it was found necessary to have metal ions inside supports as well as the presence of sodium formate in the ligand solution. When supports were soaked with ligand molecules along with sodium formate or when sodium formate was absent in the ligand solution even with metal ions inside the supports, no substantial heterogeneous crystal growth was observed (Figure 4.4). It is our hypothesis that unfavorable heterogeneous crystal growth in both of these cases is primarily due to the relatively low Thiele modulus (i.e., slow reaction as compared to diffusion). If ligand and sodium formate molecules are contained in supports prior to the solvothermal treatment in a metal solution, it is expected that the chemical potential gradient of the solvent (methanol) causes the solvent to diffuse from the ligand side (inside the supports) to the metal ion side (outside the supports). The diffusion of the solvent further promotes the diffusion of ligand molecules, leading to the quick depletion of ligand molecules inside the supports, thereby limiting heterogeneous crystal formation. On the other hand, without sodium
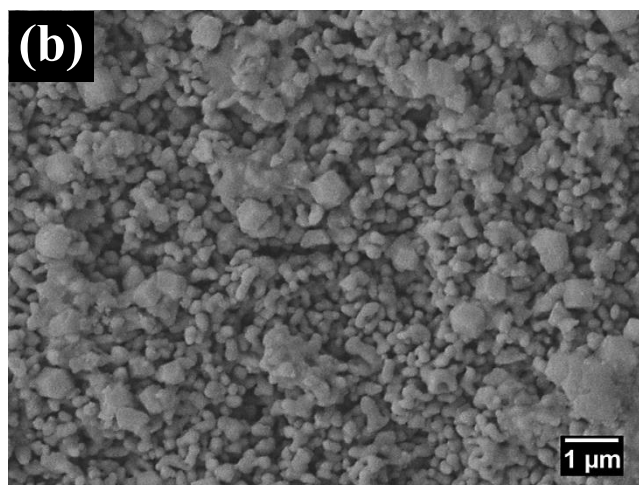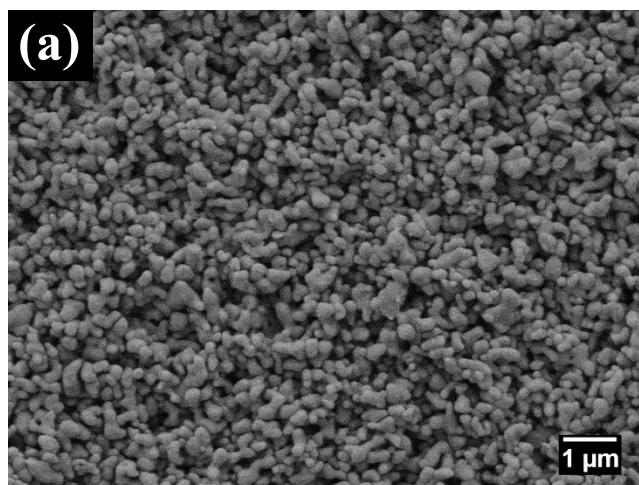
Figure 4.4 SEM images of ZIF-8 films synthesized by solvothermally treating a support soaked with a ligand solution containing sodium formate in a metal solution (a) and by solvothermally treating a support soaked with a metal solution in a ligand solution without sodium formate (b). Both films were prepared at 120ºC.

formate, which deprotonates ligand molecules, the reaction rate is relatively low as compared to the diffusion rate, favoring homogeneous nucleation and crystal growth. If our hypothesis is true, one can expect significantly enhanced heterogeneous crystal growth even with supports soaked with ligand molecules when the Thiele modulus is increased by increasing reaction rate. Indeed, this was the case when the excess amount of sodium formate was added either in the ligand solution alone or in both the metal ion and ligand solutions. Though not well-intergrown, continuous ZIF-8 films with high surface coverage were observed (Figure 4.5 and 4.6). In addition to enhancing the reaction rate by deprotonating ligand molecules, sodium formate is expected to play an important role in facilitating the crystal intergrowth[23,75,79] as well as the heterogeneous crystal growth.[23]

The separation performance of ZIF-8 membranes was evaluated by performing 50/50 propylene/propane binary gas permeation measurements in a Wicke−Kallenbach setup (Figure 4.7). Figure 4.8 displays the room-temperature propylene/propane separation performance of ZIF-8 membranes prepared for varying membrane growth times. Membranes grown even for 10 min started to show a moderate separation factor (∼ 3). As membranes were grown for longer times, the separation factor increases and then reaches at a plateau (∼50). ZIF-8 membranes prepared by the CD-based in situ method are in stark contrast with those synthesized by conventional in situ method[41] showing no separation toward the mixture (Figure 4.9). In fact, none of ZIF-8 membranes reported so far[18,22,23,129,140] have shown any good propylene/ propane selectivity. The only exception is the ZIF-8 membranes reported by Pan et al.[35] that
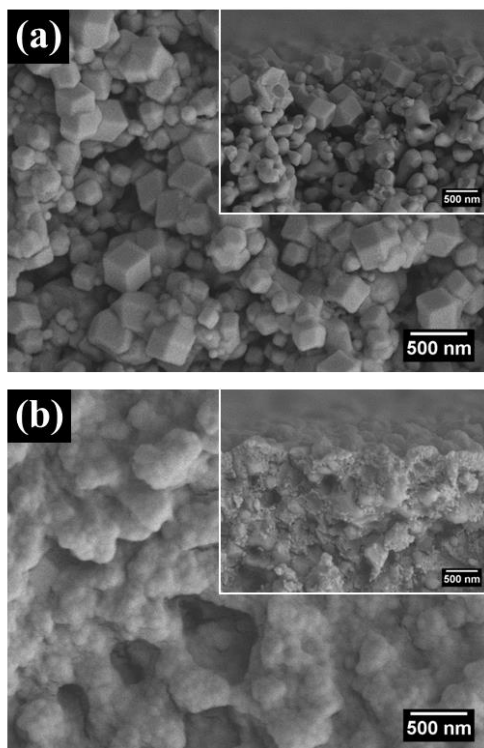
Figure 4.5 SEM images of ZIF-8 films synthesized when a ligand solution is saturated inside of a support and solvothermally treated in a metal solution; the addition of extra sodium formate of 0.35g in a metal solution (a), and the addition of extra sodium formate of 0.35g and 0.5g in both of a metal solution and a ligand solution, respectively (b). In a original recipe, a support saturated with a metal solution (0.98g of $ZnCl_2$ in 40 ml of methanol) is solvothermally treated in a ligand solution (5.19 g of 2-methylimidazole + 0.5g of sodium formate in 40 ml of methanol).
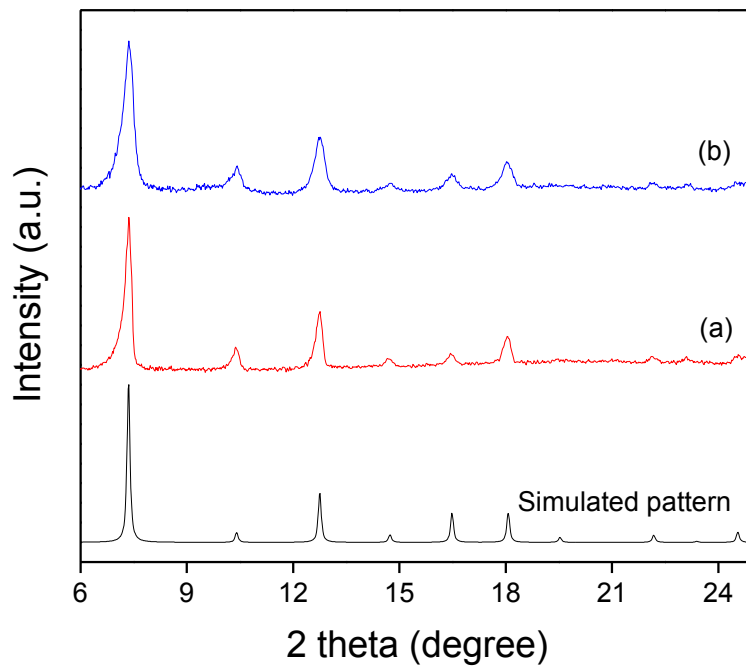
Figure 4.6 XRD patterns of of ZIF-8 films synthesized when a ligand solution is saturated inside of a support and solvothermally treated in a metal solution; the addition of extra sodium formate of 0.35g in a metal solution (a), and the addition of extra sodium formate of 0.35g and 0.5g in both of a metal solution and a ligand solution, respectively (b). In an original recipe, a support saturated with a metal solution (0.98g of $ZnCl_2$ in 40 ml of methanol) is solvothermally treated in a ligand solution (5.19 g of 2-methylimidazole + 0.5g of sodium formate in 40 ml of methanol).
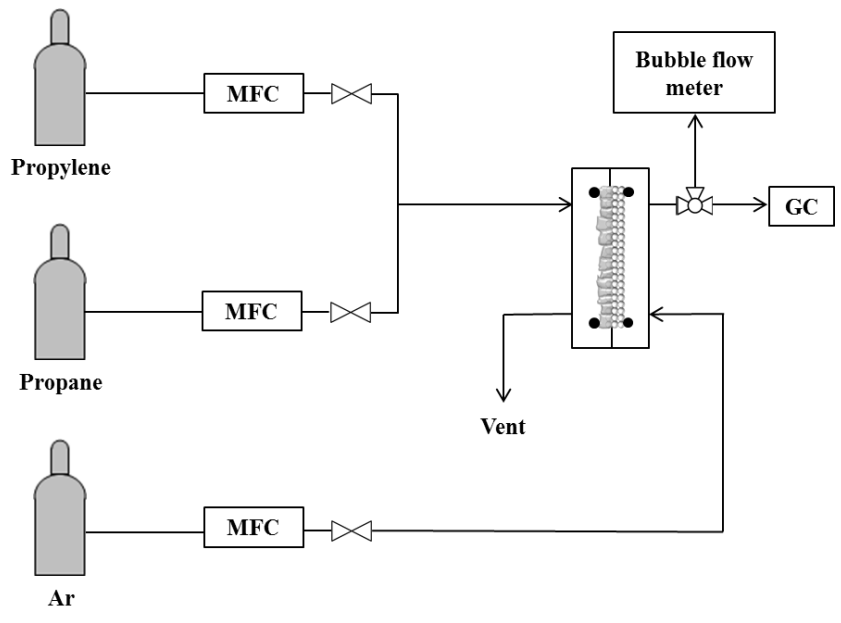
Figure 4.7 Schematic diagram of gas permeation set-up (Wicke-Kallenbach technique).
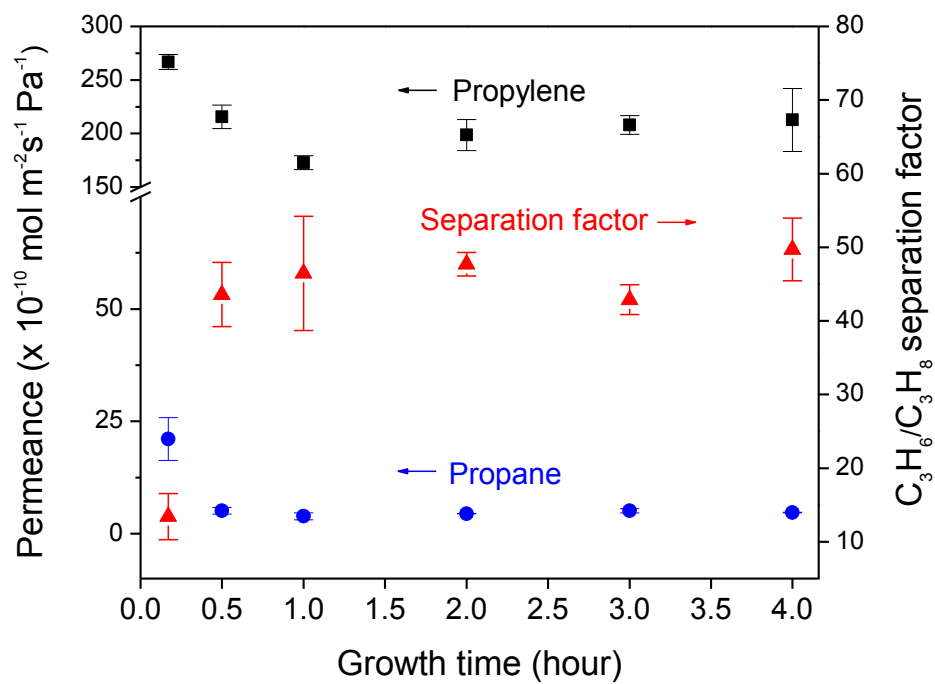
Figure 4.8 Propylene / Propane separation performance of ZIF-8 membranes ; as a function of growth time at room temperature. ZIF-8 membranes show excellent proplylene/propane separation factor (~ 50) even after growing for 30 min.
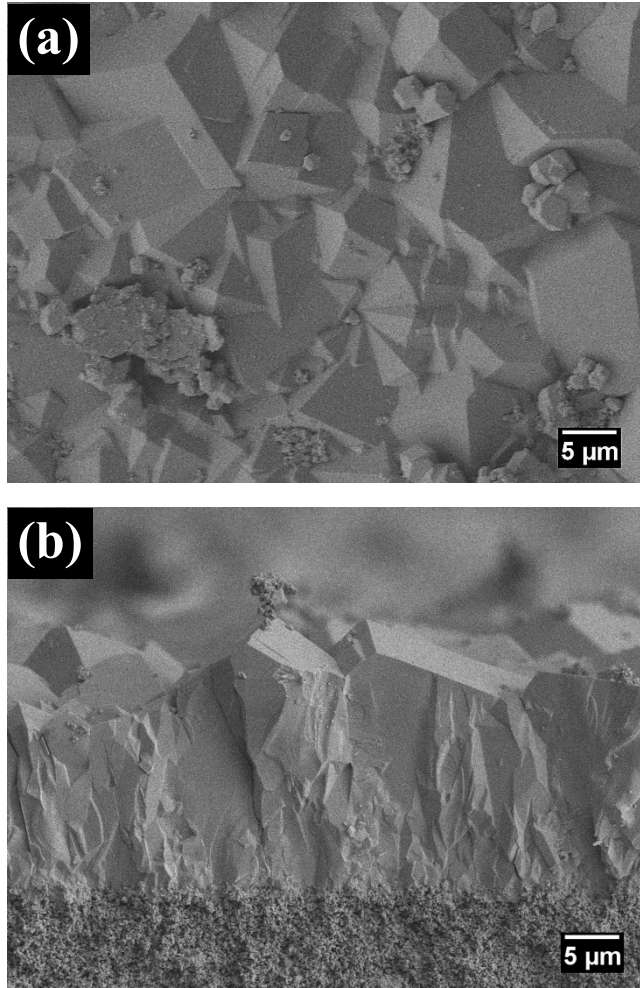
Figure 4.9 SEM images of ZIF-8 membranes synthesized by conventional *in-situ* method[41]; top view (a) and cross-section (b).

showed excellent propylene/ propane separation factors (average 35) similar to that of the current membranes. The drastically enhanced separation performance strongly suggests that the ZIF-8 membranes prepared via CD-based in situ method possess much better grain boundary structure as compared to those synthesized by other methods. When compared with other membranes reported in literature (Figure 4.10), our ZIF-8 membranes notably outperform both polymeric and zeolite membranes with respect to the separation factor and the propylene permeability. Furthermore, our membranes are close to the upper bound of carbon membranes while meeting the proposed requirement[1] (a minimum permeability of 1 Barrer and selectivity of 35) for commercial application.

The temperature dependences of both single and binary propylene/propane separation performance of the membranes (grown for 4 h) are presented in Figure 4.11. In both cases, the permeances of propylene decrease, while those of propane increase slightly as temperature rises, which is consistent with the previous report.[35] This leads to a decrease in propylene/ propane separation factor and ideal selectivity as the temperature increases. These trends can be explained by the surface diffusion model[141,142] in which the diffusion through microporous materials is described as an activation process composed of adsorption and subsequent diffusion of molecules by hopping along adsorbent surface. Therefore, the permeance of gas molecules depends on both the heat of adsorption and the activation energy for gas diffusion (i.e., $P \sim \exp((\Delta H_{ads} - E_a)/RT)$). The heats of adsorption of propylene and propane on ZIF-8 are 30 and 34 kJ/mol, respectively, while the diffusional activation energies for propylene and
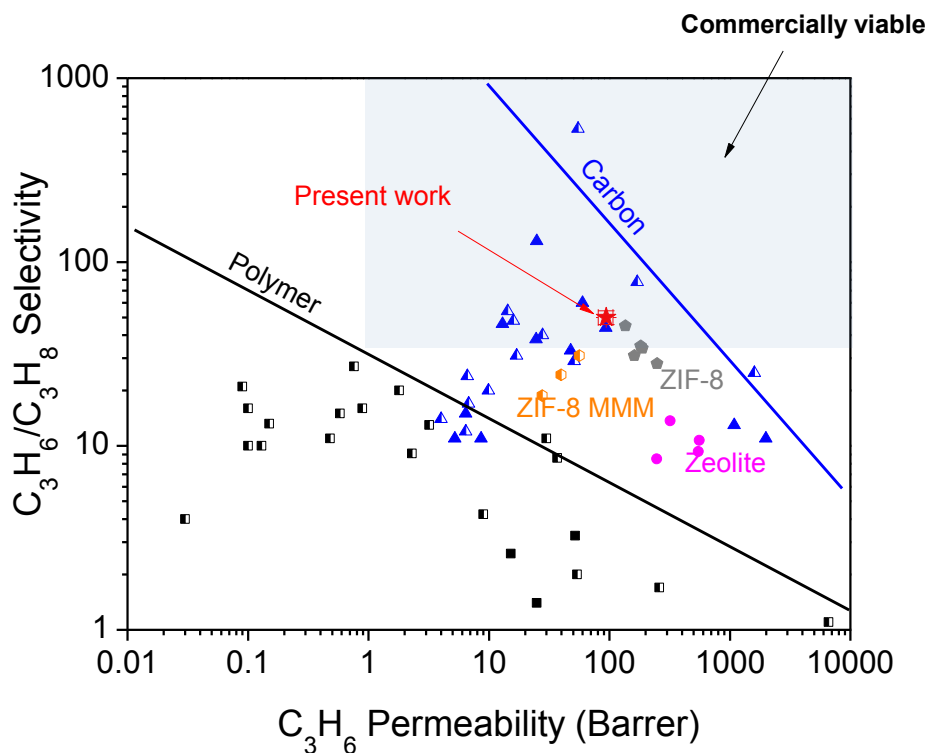
Figure 4.10 Comparison of the propylene/propane separation performance of our ZIF-8 membranes with those of other membranes reported in the literatures. Half-filled and full-filled symbols indicate separation data from single- and binary-gas permeation measurements, respectively. The shaded area in the graph implies the performance requirement of a membrane (a minimum permeability of 1 Barrer and selectivity of 35) for commercial application. The solid lines are the so-called Robison upper bound. Triangle: Carbon membrane,[4-6] circle: zeolite membrane,[3] rectangle: polymer membrane,[2] pentagon: ZIF-8 membrane,[35] hexagon: ZIF-8 mixed matrix membrane,[7] star: ZIF-8 membrane in this work.
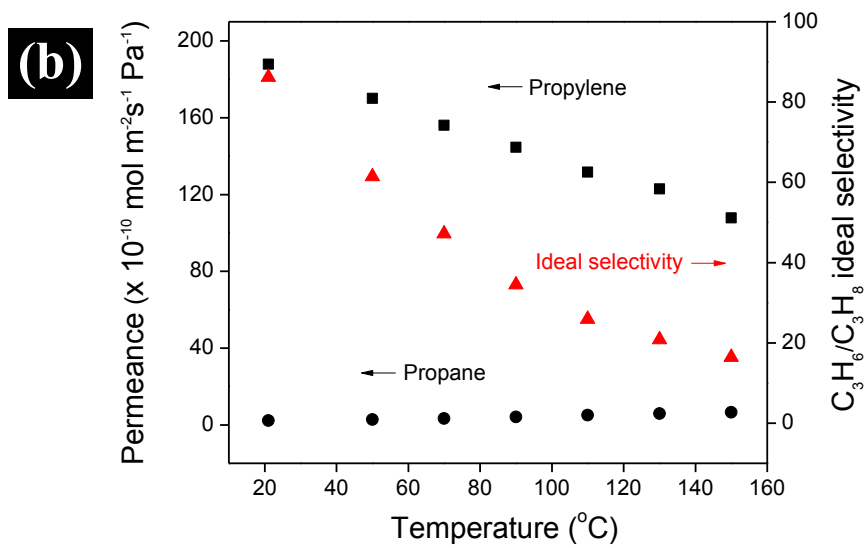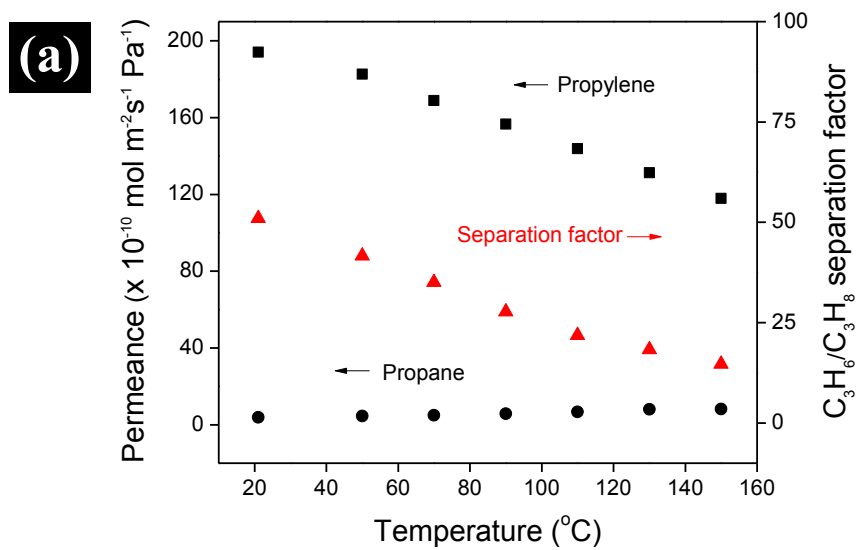
Figure 4.11 Propylene/propane separation performances of ZIF-8 membranes grown for

4 h as a function of temperature; binary (a) and single gas (b).

propane are 9.7 and 74 kJ/mol.26 As such, as the temperature increases, the permeance of proplyene decreases, while that of propylene increases.

When ZIF-8 membranes are applied in a large commercial scale, we envision membrane modules (similar to commercial polymer or ceramic membrane modules) with each module packed with a number of cylindrical membranes. As is often the case for commercial ceramic membrane modules, one has no choice but to discard the expensive membrane modules when there form defects in the individual membrane in the modules because it is often too costly to disassemble the modules and to identify and replace the defective membranes. Given the fact that membranes will develop defects and cracks, it is highly desirable if defective membranes can be healed in situ without disassembling and discarding the expensive membrane modules. As illustrated in Figure 4.12, the self-limiting nature of the counter-diffusion concept enables the defective membranes to be identified (since crystals grow preferentially from defects or cracks where the separated metal ions and ligand molecules are in contact) and to be healed readily without completely disassembling the membrane modules. To prove the concept of this unique defect-healing capability, a poorly intergrown ZIF-8 membrane was subjected to a custommade diffusion cell where metal ions are provided from the membrane side, while ligand molecules are supplied from the support side (Figure 4.13). Figure 4.14 shows the micrographs of the ZIF-8 membrane before and after the healing process. As can be seen in Figure 4.14 (c) and (d), the intercrystal gaps were completely filled with newly grown crystals (see the red arrows). The newly grown crystals have distinctive morphology possibly due to the difference in recipe (water vs methanol) and
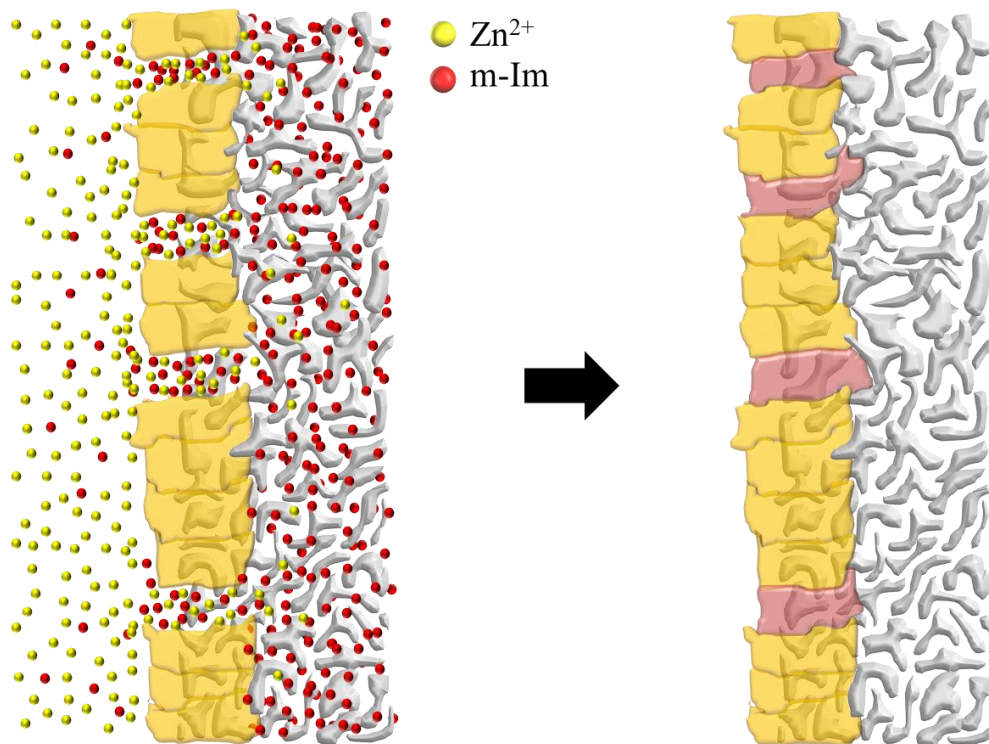
Figure 4.12 Schematic illustration of the defect healing process via the CD-based *in situ* method. The self-limiting nature of the counter-diffusion concept enables the defective membranes to be identified since crystals grow preferentially from defects or cracks where the separated metal ions and ligand molecules are in contact.
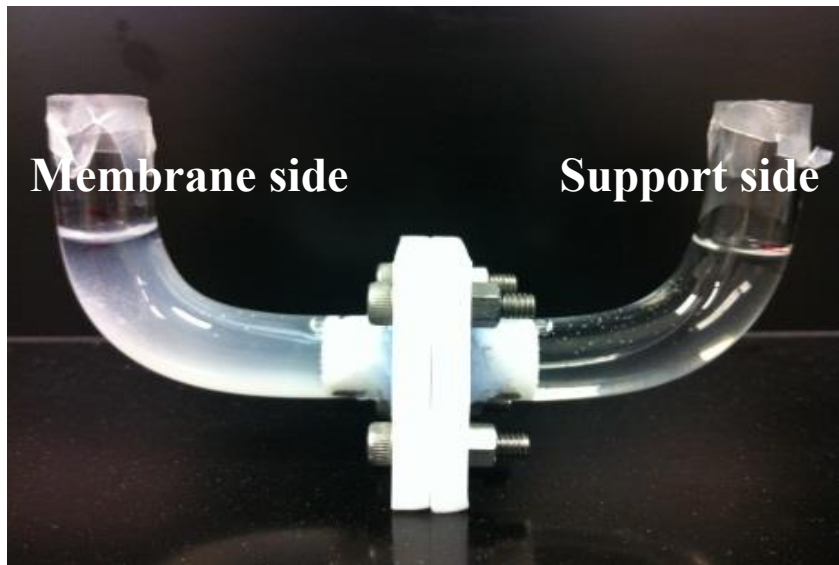
Figure 4.13 Digital photograph of a home-made counter diffusion cell. Note that the picture was taken after the healing process was completed.
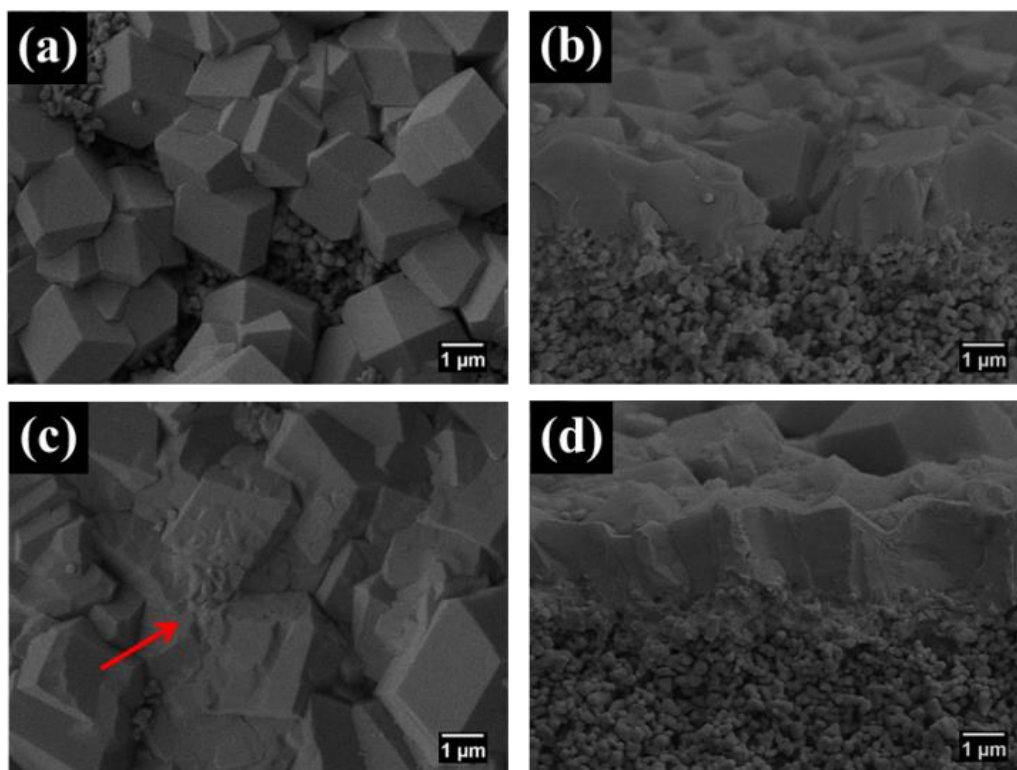
Figure 4.14 SEM images of ZIF-8 membranes before the healing process (a, b) and after the healing process (c, d). Red arrow indicates newly-grown crystals that have distinctive morphology possibly due to 1) the difference in recipe (water vs. methanol) and 2) the confined crystal growth in the inter-crystal spaces.

the confined crystal growth in the intercrystal spaces. It is important to note that the thickness of the membrane did not change after the healing process, not compromising the flux owing to the self-limiting feature of the counter-diffusion concept (Figure 4.15). The separation performance of the healed membranes is presented in Table 4.1. After healing, the permeance was dramatically reduced as the propylene/propane selectivity decreased to ~10. This reduced performance after healing is possibly due to the
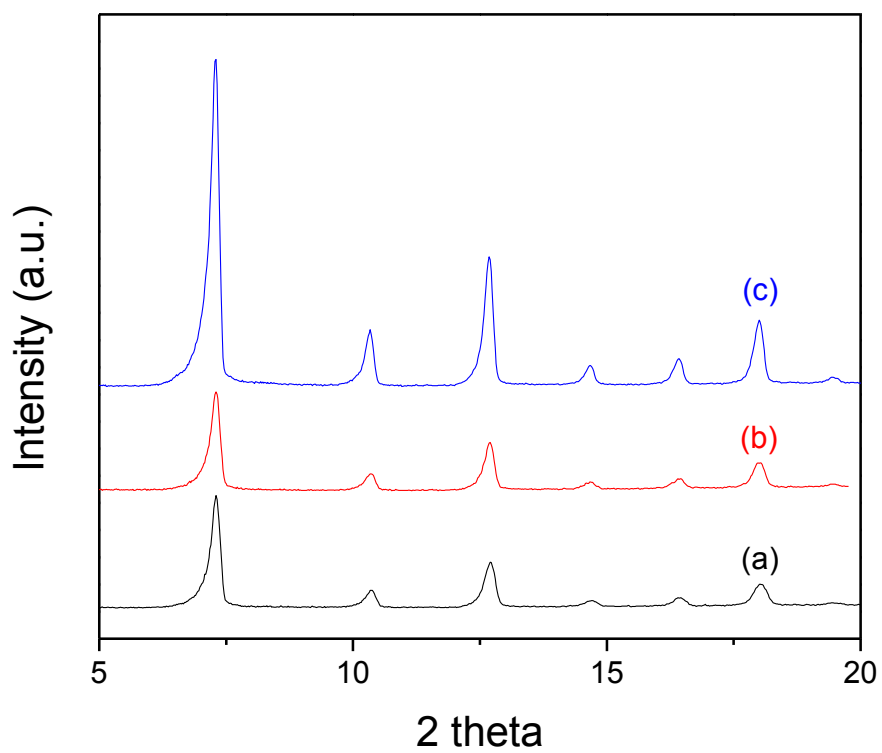
Figure 4.15 XRD patterns of ZIF-8 membranes; synthesized with a ligand solution recycled four times (a), healed by a counter-diffusion-based *in situ* growth (b), and healed by a secondary growth (c).

Table 4.1 Room-temperature propylene/propane separation performance of the ZIF-8 membranes after being healed in a diffusion cell. The defective membranes showed no separation performance.

Membrane	Permeance of propylene $(10^{-10} \text{ mol/m}^2 \cdot \text{s} \cdot \text{pa})$		Selectivity (After healing)
	Before healing	After healing	
M1	2496.94	406.35	8.77
M2	2139.47	392.02	9.43
M3	2385.11	407.75	9.78

insufficient healing and/or compromised grain boundary defects upon healing. Further investigation is currently under way.

Organic ligands and solvents (mostly organic) used for the typical synthesis of MOFs are costly and environmentally harmful. It is, therefore, very attractive if the consumption of organic ligands and solvents can be drastically reduced. Conceptually, the CD-based in situ method requires a significantly less amount of precursor solutions than conventional methods since the precursor solutions can be recycled. As a proof-of-concept, the ligand solution was recycled to grow ZIF-8 membranes multiple times (Figure 4.16 and 4.17). As can be seen in the figures, well-intergrown continuous ZIF-8 membranes were formed even after the ligand solution was recycled three times. The more the solution is recycled, the bigger the grains become, which can be explained by
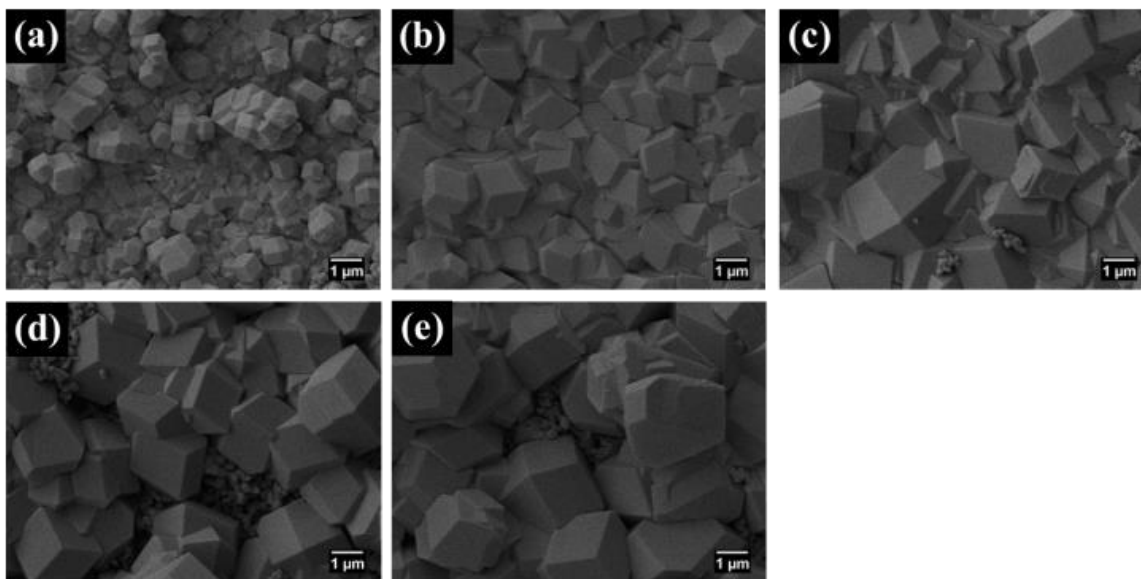
Figure 4.16 SEM images of ZIF-8 membranes synthesized with a ligand solution recycled; once (a), twice (b), three times (c), four times (d), and five times (e). Well-intergrown continuous ZIF-8 membranes were formed even after the ligand solution was recycled three times.
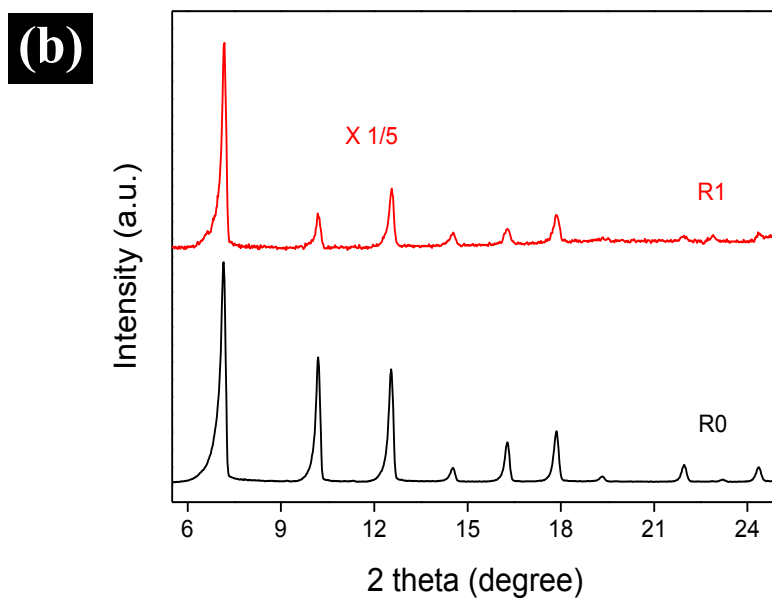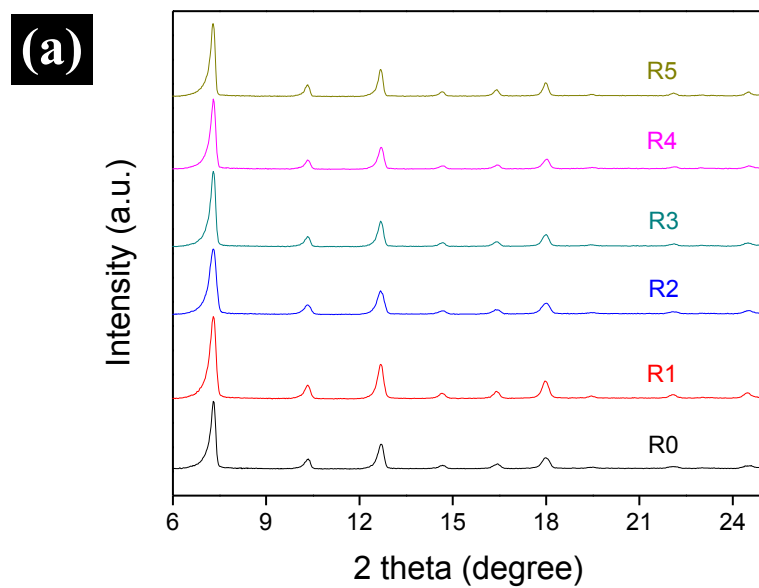
 Figure 4.17 XRD patterns of ZIF-8 membranes synthesized in recycled solutions obtained after; counter-diffusion-based in situ growth (a) and conventional *in-situ* method[41] (b). R0 and R1 denote the membranes prepared in a fresh precursor solution and in a solution recycled once, respectively.

the formation of a smaller number of nuclei as the ligand concentration drops due to the increased number of recycling. ZIF-8 membranes grown from the ligand solutions after recycled four times are not well-intergrown though continuous, mainly owing to the depletion of ligand molecules. These poorly intergrown membranes can be made into well intergrown membranes by healing the membranes using the CD-based in situ method. The separation performance of the membranes synthesized in a recycled ligand solution was tested and showed good separation performance (Table 4.2).

The mechanical stability of polycrystalline ZIF-8 membranes is also an important issue for their practical applications. The mechanical stability of ZIF-8 membranes was tested using a sonication method.[131] No substantial degradation of the films was observed even after subjected to intensive sonication for 2 h (Figure 4.18), strongly suggesting the excellent mechanical stability of ZIF-8 membranes. The gas separation properties of the membranes were also tested (Table 4.3). The membranes maintained excellent propylene/propane separation performance, though the separation factor was slightly dropped as the sonication time increases. This slight drop in the selectivity is likely due to the fact that the grain boundary structure of the membranes was somewhat compromised upon the sonication process.

Finally, ZIF-7 and SIM-1 membranes were synthesized using our CD-based in situ method to demonstrate its potentially general applicability (Figure 4.19 and 4.20). Even though these membranes show some cracks, given the fact that ZIFs are quite robust as compared to other MOFs (such as IRMOFs), chances are likely that the cracks formed during activation process. For example, it is well-known that rather bulky

Table 4.2 Room-temperature propylene/propane separation performance of the ZIF-8 membranes synthesized with recycled ligand solutions.

# of recycling	Permeance of propylene $(10^{-10}\ \mathrm{mol\ m^{-2}\ s^{-1}\ Pa^{-1}})$	Separation factor
1st	231.87 ± 39.55	34.48 ± 5.25
2nd	200.40 ± 18.98	26.99 ± 4.70
3rd	285.50 ± 23.12	31.06 ± 4.87
4th	Defective	-
5th	Defective	-
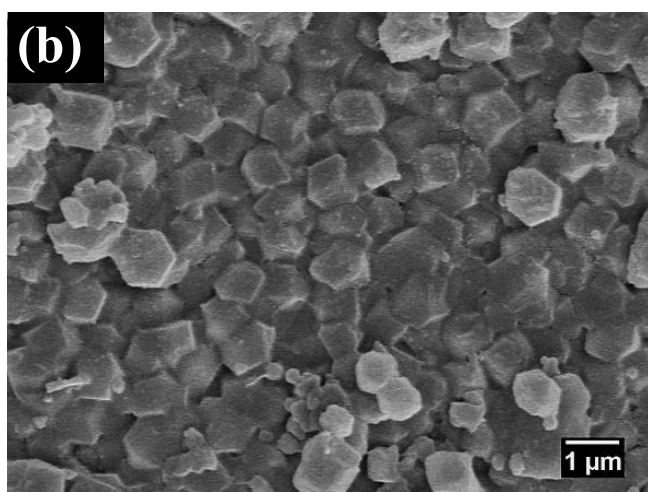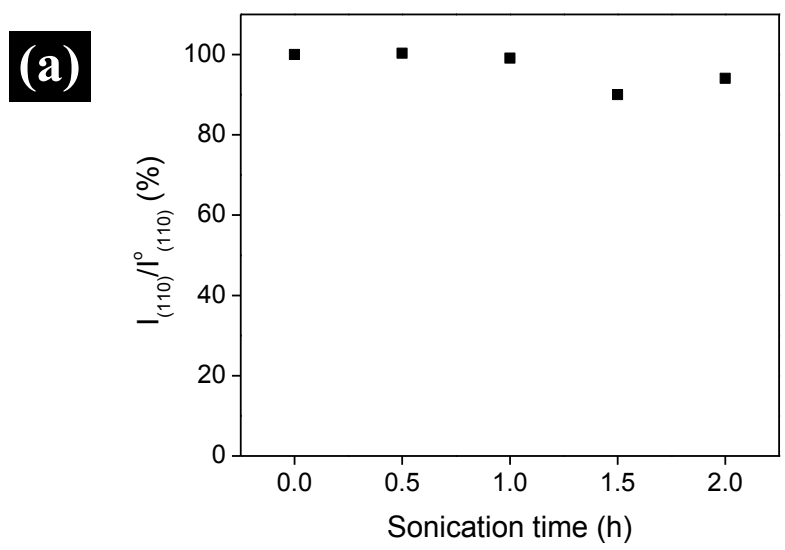
Figure 4.18 Binding strength of ZIF-8 membranes on a support measured by normalized (110) peak intensity as a function of sonication time (a) and a SEM image of the ZIF-8 membrane after sonication for 2 h (b).

Table 4.3   Propylene/propane separation performance of ZIF-8 membranes before and after 2 h of sonication

Sonication time (h)	Permeance (x 10^{-10} mol m^{-2} s^{-1} Pa^{-1})		Separation factor (C_3H_6/C_3H_8)
	C_3H_6	C_3H_8	
0	192.88 ± 2.32	4.61 ± 0.63	43.25 ± 5.82
2	277.99 ± 12.19	7.67 ± 0.41	37.09 ± 2.66
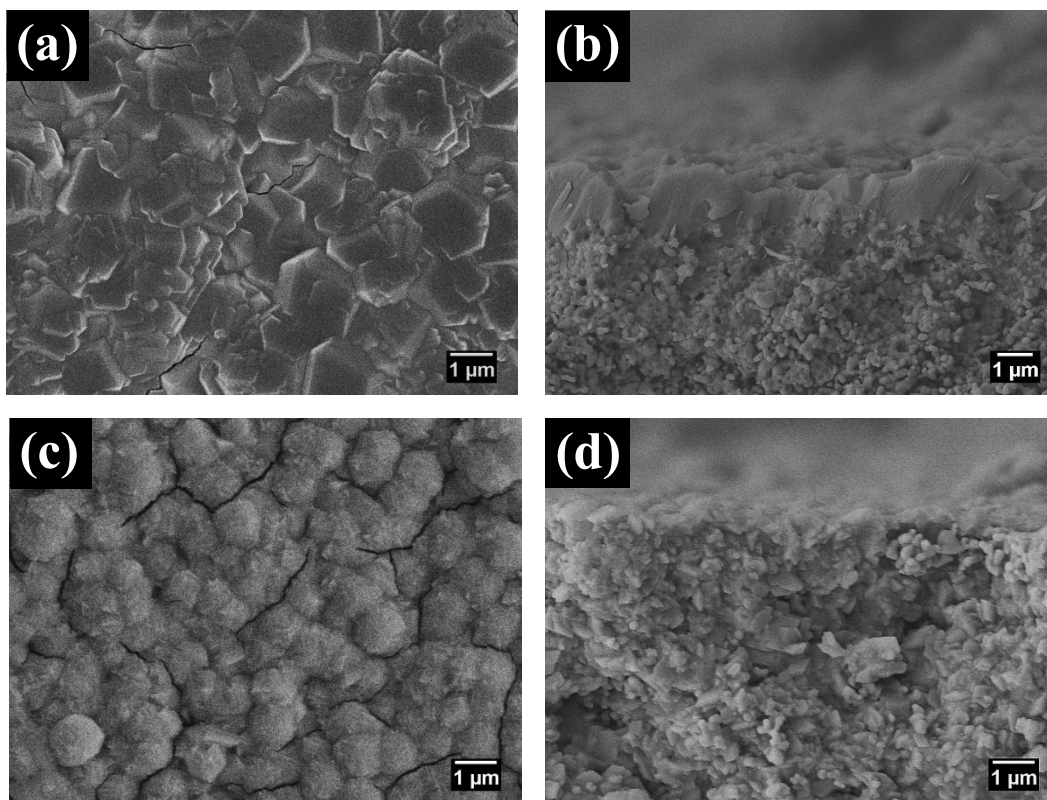
Figure 4.19 SEM images of a SIM-1 membrane (a, b) and a ZIF-7 membrane (c, d).
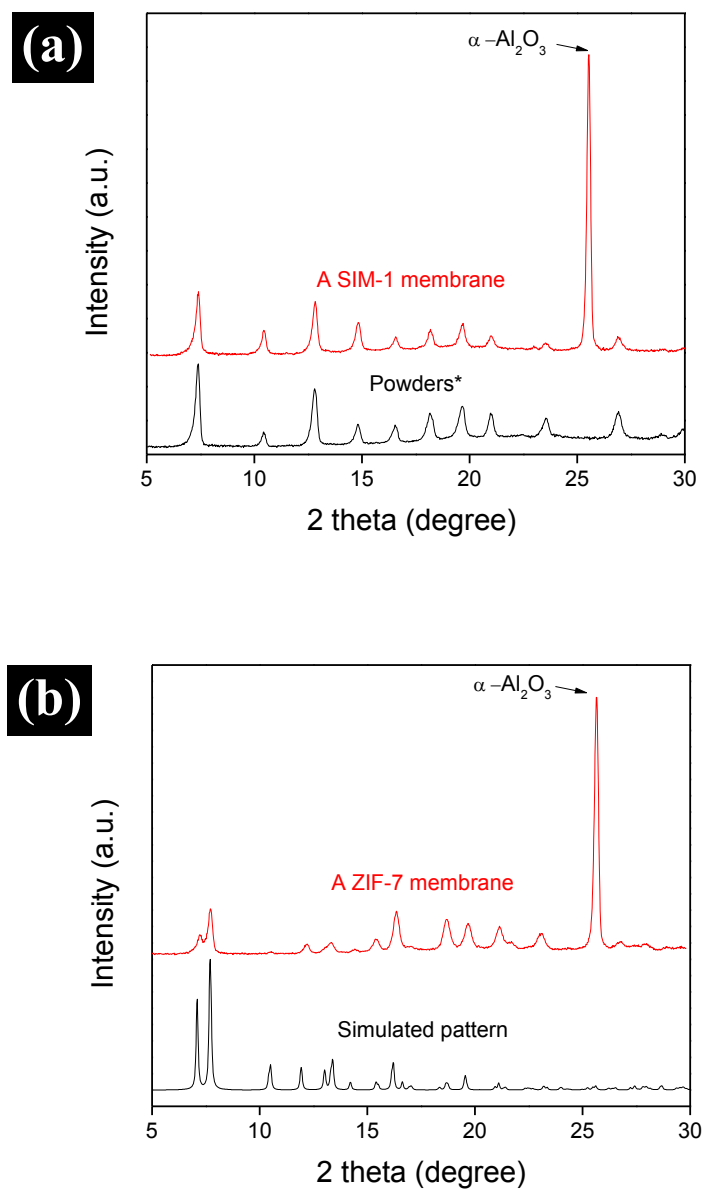
Figure 4.20 XRD patterns of a SIM-1 membrane (a) and a ZIF-7 membrane (b). * Due to the lack of the crystallographic information of SIM-1, SIM-1 powders were synthesized by following the previous report[127] and its XRD pattern is compared to confirm the SIM-1 phase.

solvent molecules (e.g, dimethylforamide) used for ZIF-7 synthesis are included in the framework cages, thereby making activation without crack formation very difficult. Further studies to prevent crack formation are currently under way.

4.4 Conclusions

In conclusion, we have developed a one-step in situ synthesis technique for high-quality MOF membranes based on the concept of counter diffusion. This simple yet highly versatile method enabled the rapid preparation of well-intergrown ZIF-8 membranes with excellent microstructure. The high-quality ZIF-8 membranes showed an excellent separation performance of a propylene/propane (50/50) mixture (selectivity ~55). Furthermore, the ZIF-8 membranes were found to be mechanically very strong with their separation performance maintained high even after 2 h of intensive sonication. The unique feature of the counter-diffusion concept allowed the poorly intergrown membranes to be healed. In addition, the costly precursor solutions can be recycled multiple times for membrane synthesis. Finally, prototypical ZIF-7 and SIM-1 membranes were also successfully synthesized using our method, proving its general applicability. Considering its unique features including postsynthetic healing and reduced precursor consumption, the simple general method reported here enabling the synthesis of high-quality MOF membranes with excellent microstructure offers unique opportunities for potential large-scale practical applications of MOF membranes.

CHAPTER V

IMPROVING PROPYLENE/PROPANE SEPARATION PERFORMANCE OF

ZEOLITIC-IMIDAZOLATE FRAMEWORK ZIF-8 MEMBRANES[*]

5.1 Introduction

Zeolitic-imidazolate frameworks (ZIFs), a sub-class of metal-organic frameworks (MOFs), are hybrid crystalline materials consisting of metallic nodes (usually Zn or Co) and imidazole or its derivative linkers.[15] Due to their unique features such as excellent chemical/thermal stability, molecular-scale pore apertures combined with high microporosity, and structural and chemical diversity,[15,55] ZIFs have been investigated for a variety of applications including gas/liquid separation,[105,143] catalysis,[60,144] drug delivery,[145] and sensing.[126]

In particular, ZIF-8, a prototypical ZIF, consisting of zinc ions interconnected with 2-methylimidazolate ligands forming a SOD zeolite structure, has shown very promising for propylene/propane separations.[128] This is primarily due to the fact that its effective pore aperture size, which is larger than crystallographic aperture diameter of 3.4 Å owing to the flopping motion of the ligands, falls in the range of 4.0 ~ 4.2 Å, allowing to distinguish propylene (~ 4 Å) from propane (~ 4.3 Å) based on the size-exclusion principle.[31]

Efforts have been made to prepare high performance ZIF-8 membranes for effective propylene/propane separation. Pan et. al. prepared ZIF-8 membranes using secondary growth and demonstrated for the first time that the ZIF-8 membranes exhibit propylene/propane separation performance with an average selectivity of ~35.[35] Later, a few research groups have successfully prepared propylene-selective membranes of both polycrystalline ZIF-8[32,34,36,37,146] and composite with polymers.[7] For example, Zhang et. al. fabricated ZIF-8/polyimide mixed matrix membranes, showing their membrane performance for propylene/propane separation falling beyond the upper bound of polymeric membranes.[7] Recently our group reported a counter diffusion-based *in situ* method (hereafter CD method) which resulted in further improvement in the membrane performance with the propylene permeance of ~ 200 x 10^{-10} mol / $m^2 \cdot s \cdot Pa$ and the propylene/propane separation factor of ~ 55.[32] Due to its unique self-limiting nature, the relatively simple CD method enables to prepare rather thin ZIF-8 membranes (~ 1.5 μm thick) with enhanced microstructure and improved reproducibility. Our group also devised an innovative approach called rapid thermal deposition (RTD) technique based on evaporation-induced crystallization to rapidly prepare propylene-selective ZIF-8 membranes (propylene/propane separation factor ~30) under ambient pressure.[146] Lastly, Liu et. al. performed detailed studies on the transport properties and long-term stability of propylene-selective ZIF-8 membranes by a secondary growth method.[36]

Even though the above-mentioned ZIF-8 membranes (in particular those prepared using the CD method) show impressive propylene/propane separation capabilities, for ZIF-8 membranes to be practically applied, however, further

improvement of membrane performances is clearly required. Specifically, improvement in the propylene permeances of ZIF-8 membranes is of critical importance for process economics considering the large amount of propylene to be processed. To further increase the performances of CD-prepared ZIF-8 membranes, here we present our investigation on the effects of sodium formate and zinc salts on the microstructures and thereby the propylene/propane separation performances of ZIF-8 membranes synthesized by the CD method. In addition, activation processes are also studied to improve the membrane microstructures.

5.2 Experimental Section

5.2.1 Chemicals

Zinc chloride ($ZnCl_2$, 99.99%, Alfa Asear), zinc nitrate hexahydrate ($Zn(NO_3)_2 \cdot 6H_2O$, 98%, Sigma-Aldrich), and zinc acetate dehydrate ($Zn(CH_3COO)_2 \cdot 2H_2O$, 98%, Alfa Asear) were used as metal sources. 2-methylimidazole ($C_4H_6N_2$, 99%, Sigma-Aldrich) was an organic ligand and sodium formate (HCOONa, 99%, Sigma-Aldrich) was utilized as a deprotonating agent. Methanol (CH_3OH, > 99%, Alfa Asear) was a solvent. All purchased chemicals were used without further purification.

5.2.2 Preparation of porous α-Al_2O_3 supports

Disk-type α-Al_2O_3 supports (porosity = 46 %, diameter = 22 mm, and thickness = 2 mm) with an average pore size of 200 nm were prepared by moulding α-Al_2O_3 powder

(CR6, Baikowski) and sintering them at 1100 $^{\circ}$C for 2 h. One side of the sintered supports were polished using a sand paper (grid #1200) to minimize the surface roughness of the supports and sonicated in methanol for 1 min. Subsequently the supports were dried in an oven at 120 $^{\circ}$C for 1 h before use.

5.2.3 Synthesis of ZIF-8 membranes by a counter-diffusion-based *in situ* method

Membranes were prepared based on our previously reported recipe, a counter-diffusion-based *in-situ* method with a minor alteration.[32] First, a support was immersed in a 0.18 M zinc precursor solution (7.2 mmol of zinc salts dissolved in 40 ml of methanol, hereafter metal solution) for 1 h to saturate the porous support with the metal solution. Then, the support saturated with zinc ions was vertically loaded on a Teflon holder and placed in an autoclave containing 40 ml of a 1.56 M ligand solution in methanol with a pre-determined amount of sodium formate (hereafter ligand solution). To be consistent for membrane synthesis, sodium formate was dried in a vacuum oven at 100 $^{\circ}$C for 6 h to remove adsorbed water each time before usage. Afterwards the autoclave was kept in an oven at 120 $^{\circ}$C for 4 h, followed by natural cooling to room temperature in the oven. Upon completion, the sample was then washed in methanol under gentle rocking for 12 h to remove impurities and/or unreacted chemicals prior to polishing the film formed on the back side of the support (note that films form on both sides of the support). The membrane was then activated by washing in methanol for 5 days. For comparison, some membranes were further treated solvothermally in methanol at 120 $^{\circ}$C for 4 h after the 5 day washing. The membrane was then dried at room

temperature for 5 h, followed by being dried at 60 $^{\circ}$C for 1 h before characterizations and gas permeation measurements.

5.2.4 Characterization

Crystal phase was identified using a Rigaku Miniflex II powder X-ray diffractometer with Cu-Kα radiation (λ=1.5406Å). JEOL JSM-7500F was employed to obtain electron micrographs of membranes. Membranes were tested for binary propylene/propane separation using the Wicke-Kallenbach technique under atmospheric pressure. An equal molar feed stream was supplied to the membrane side with a flow rate of 100 cc/min while the permeate side was constantly swept by an inert argon gas with a flow rate of 100 cc/min. The composition of the permeate was determined using a gas chromatography (Agilent 7890A).

5.3 Results and Discussion

Detailed descriptions on the CD method are presented in our previous report.[32] Briefly, a porous alumina support is first saturated with a zinc solution and the support saturated with the zinc solution is then exposed to a ligand solution. A reaction interface with relatively high concentrations of both zinc and ligand is established due to the counter diffusion of the two species. The location of this reaction interface depends on the relative rates of two competing kinetic processes, diffusion and reaction (i.e., crystallization). It is important to note that reaction rate must be faster than diffusion rate (i.e., high Thiele modulus) in order to form a continuous film inside and on the support.

As reported earlier,[32,41,75] the presence of sodium formate (deprotonator) enhances the reaction rate, leading to the formation of ZIF-8 films.

The CD method enables films to form inside as well as on supports, resulting in both positive and negative consequences on the properties of membranes. On one hand, growing films inside supports leads to enhanced mechanical strength of the membranes due to the formation of mechanical interlocks between crystals and porous supports as demonstrated in our previous report. On the other hand, too much growth inside supports reduces gas flux through the membranes due to increased effective membrane thickness. It is therefore imperative to find optimal synthesis conditions with respect to the Thiele modulus for the mechanical stability as well as the gas permeation properties of membranes. Since the Thiele modulus is greatly affected by the presence of sodium formate, we decided to further investigate the effect of sodium formate on the membrane microstructure (i.e., fractions of films forming inside vs. on supports).

Figure 5.1 and Figure 5.2 display electron micrographs and XRD patterns of ZIF-8 films prepared using zinc chloride with varying sodium formate to ligand ratios (hereafter SF/L ratio). As shown, with no sodium formate or low SF/L ratios (i.e., slow reaction), ZIF-8 films were poorly intergrown, showing macroscopic voids between grains. However, with relatively high SF/L ratio, continuous and well-intergrown films were formed. As expected, the greater the SF/L ratios were the more the films grown both inside and on supports, resulting in the increases in XRD peak intensity, which is consistent with the reaction/diffusion model described above. When the excessive amount of sodium formate was used, however, a ZIF-8 layer with the thickness of about
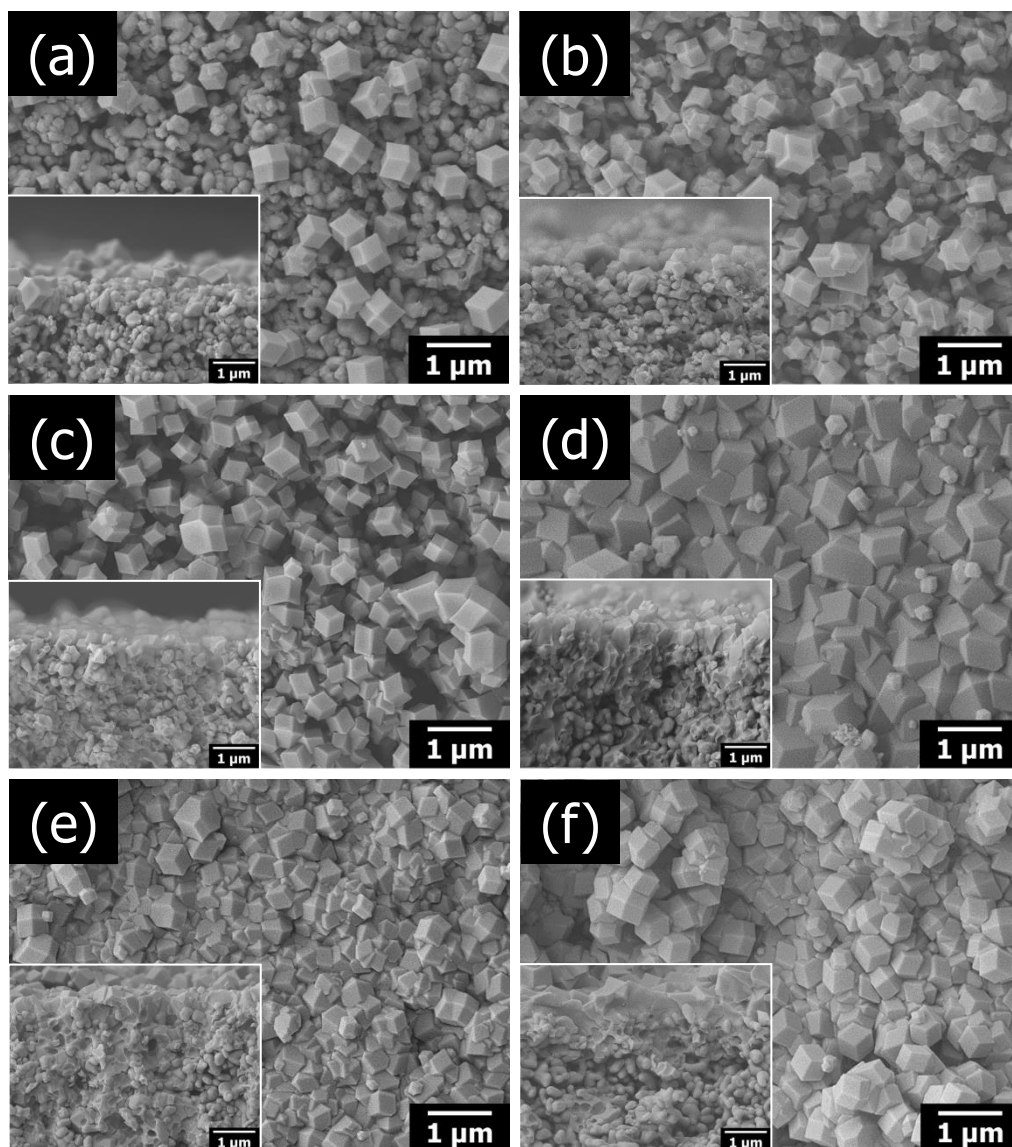
Figure 5.1 Electron micrographs of ZIF-8 membranes prepared with various sodium formate to ligand (SF/L) molar ratios: (a) 0, (b) 0.012, (c) 0.023, (d) 0.058, (e) 0.12, and (f) 0.23. Note that 62.5 mmol of ligand and 7.2 mmol of zinc chloride (both dissolved in 40 ml of methanol) were used to synthesize one ZIF-8 membrane.
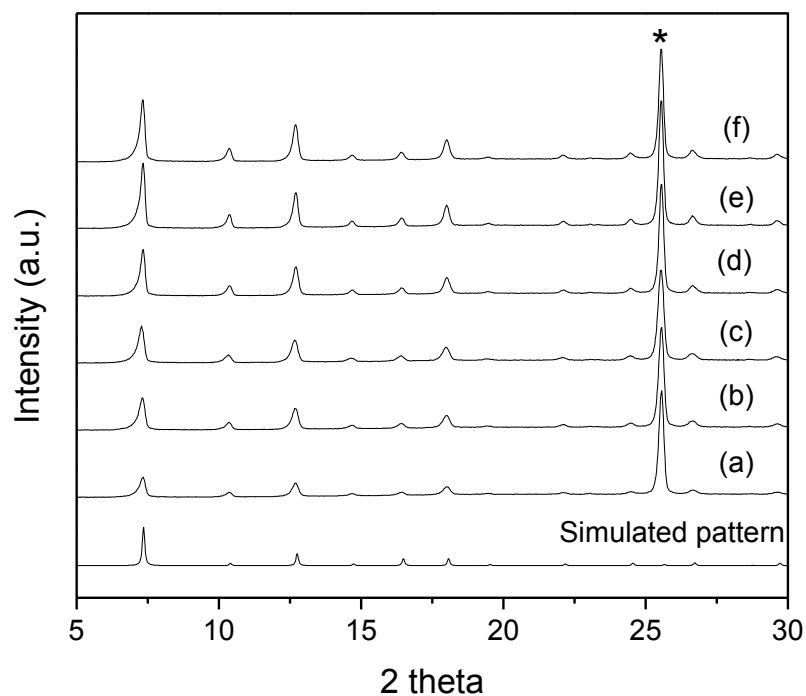
Figure 5.2 XRD patterns of the ZIF-8 membranes presented in Figure 1 that were synthesized with various sodium formate to ligand molar ratios: (a) 0, (b) 0.012, (c) 0.023, (d) 0.058, (e) 0.12, and (f) 0.23.

1 µm was formed with a major fraction of the film on the support surface as shown in Figure 5.1(f). This microstructure is in contrast to the ones prepared with the less amount of sodium formate where a considerable portion of the films formed inside supports (see Figure 5.1(d) and (e) and Figure 5.3). The excess amount of sodium formate leads to the rapid formation of ZIF-8 layer at the support interface, which might hinder counter diffusion of ligands and metal ions.
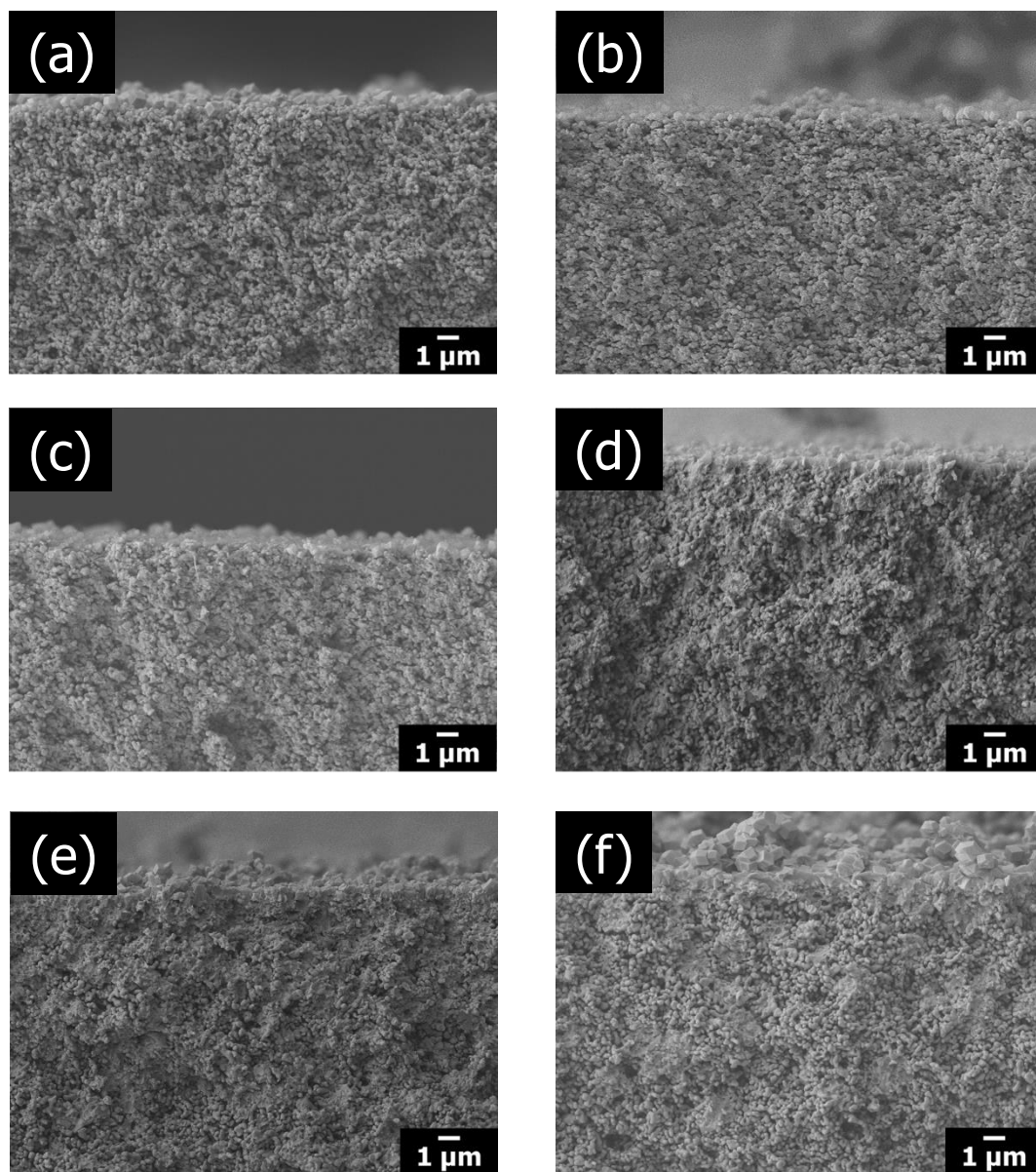
Figure 5.3 Low-magnification electron micrographs of ZIF-8 membranes prepared with sodium formate to ligand (SF/L) molar ratios: (a) 0, (b) 0.012, (c) 0.023, (d) 0.058, (e) 0.12, and (f) 0.23. Note that 62.5 mmol of ligand and 7.2 mmol of zinc chloride.

The performance of ZIF-8 membranes prepared using different amount of sodium formate was examined using room temperature propylene/propane separation test and the results are presented in Table 5.1. As expected, films prepared with insufficient sodium formate (SF/L ratios below 0.023) were non-selective while membranes with too much sodium formate (SF/L ~ 0.23) were barely propylene-selective. On the contrary, membranes synthesized with SF/L ratios of 0.058 and 0.12 showed excellent propylene/propane separation performances. This observation coincides with the membrane microstructures revealed in the electron micrographs (Figure 5.1) and indicates that there is an optimum sodium formate amount (i.e., SF/L ratio) to produce high quality ZIF-8 membranes. With too much sodium formate (e.g., 0.23 of SF/L ratio), though the membranes appear to be well-intergrown, their low propylene/propane separation performances can be attributed to excessively rapid crystal growth, thereby leading to poor grain boundary. On the basis of this observation, all other membranes afterward were synthesized with the SF/L ratio of 0.12.

It has been reported that the microstructures (e.g., size and morphology) of ZIF-8 crystals are affected by the nature of zinc salts.[80,86] We decided to investigate how different zinc salts such as zinc nitrate, zinc acetate, and zinc chloride (hereafter ZnN, ZnAc, and ZnCl, respectively) affect the membrane microstructures. Figure 5.4 shows XRD patterns of ZIF-8 membranes synthesized using three different zinc salts (denoted ZnN, ZnAc, and ZnCl membranes). Although all three membranes are comprised of phase-pure ZIF-8 crystals, their diffraction peak intensities are augmented in the order of ZnN, ZnAc, and ZnCl membranes, likely indicating different film thickness. As shown

Table 5.1 Room temperature binary propylene/propane separation performance of ZIF-8 membranes prepared with various sodium formate to ligand molar ratios that are presented in Figure 5.1 and 5.2. Three membranes were tested to obtain the average values and the corresponding standard deviations.

Sodium formate to ligand molar ratio	Propylene permeance $(x \ 10^{-10} \ mol / m^2 \cdot s \cdot Pa)$	Separation Factor
0	No separation	
0.012	No separation	
0.023	No separation	
0.058	394.5 ± 60.1	28.0 ± 5.8
0.12	267.5 ± 8.9	38.0 ± 1.1
0.23	602.8 ± 211.2	2.5 ± 1.3
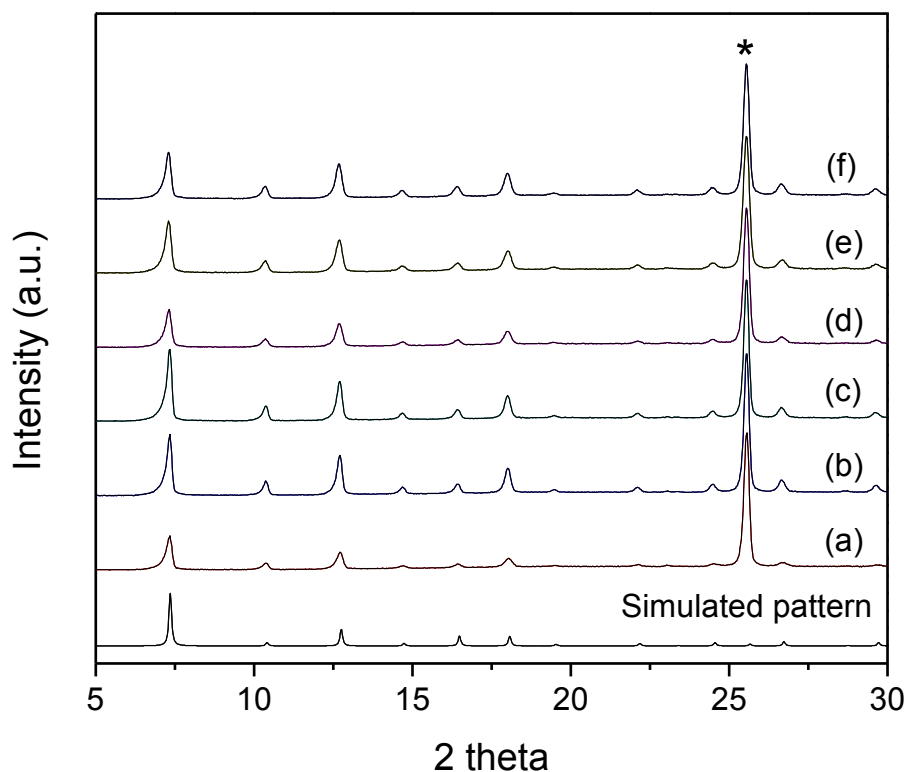
Figure 5.4 XRD patterns of ZIF-8 membranes prepared from different zinc salts and their combinations; (a) ZnN, (b) ZnAc, (c) ZnCl, (d) ZnNAc, (e)ZnNCl, and (f) ZnAcCl. Note that 62.5 mmol of ligand and 7.2 mmol of zinc chloride (both dissolved in 40 ml of methanol, the SF/L ratio of 0.12) were used to synthesize one ZIF-8 membrane and the metal to ligand molar ratio was fixed at ~ 0.11.

in the electron micrographs (Figure 5.5), with ZnN, a ZIF-8 film with the thickness of ca. 500 nm formed predominantly on support surface. On the contrary, with ZnAc and ZnCl, ZIF-8 films were formed both inside and on supports. It is noted that the effective thicknesses of these membranes cannot be readily determined since the membrane

115
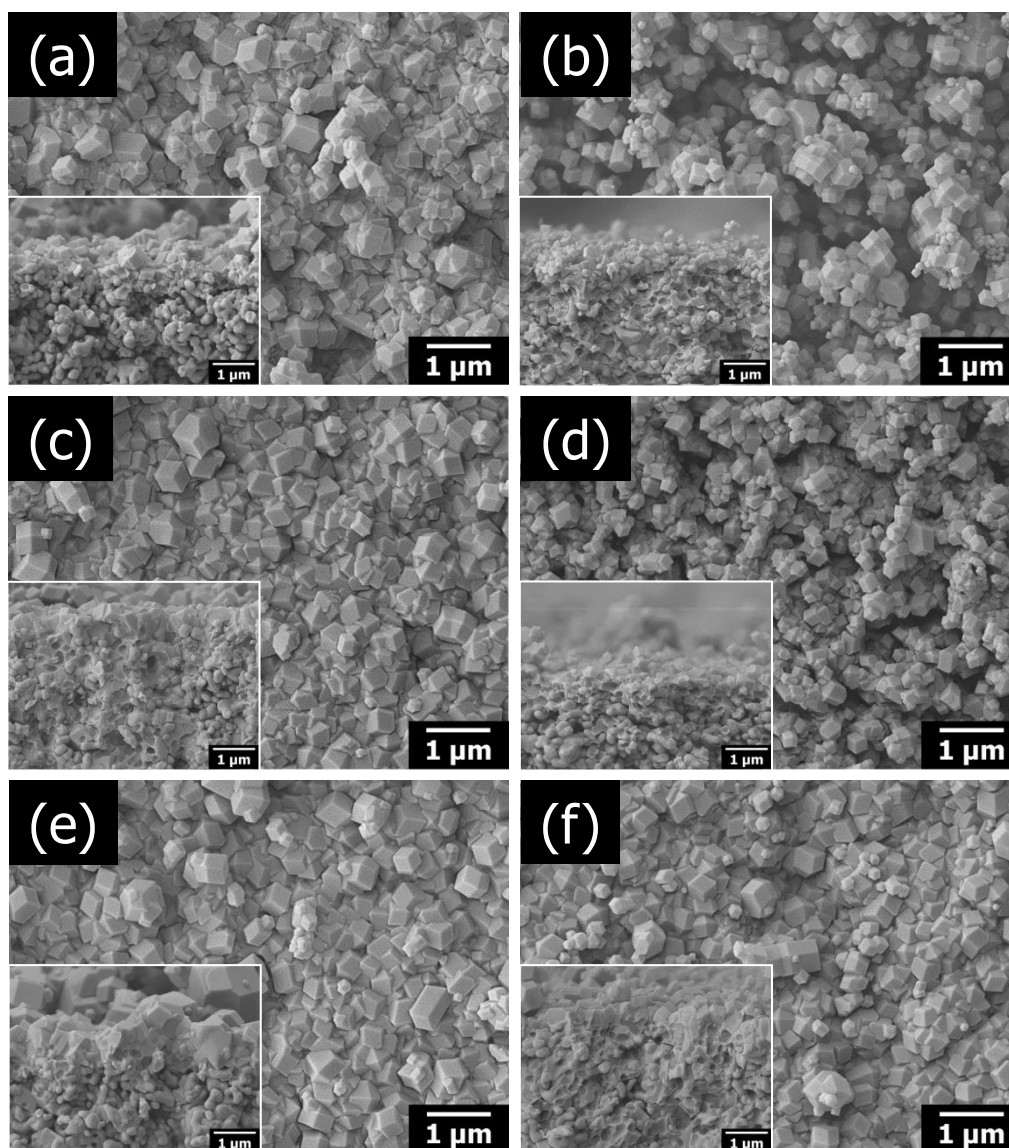
Figure 5.5 Electron micrographs of ZIF-8 membranes presented in Figure 5.4: (a) ZnN, (b) ZnAc, (c) ZnCl, (d) ZnNAc, (e) ZnNCl, and (f) ZnAcCl.

interfaces inside the supports are not uniform (Figure 5.6(b) and (c)). Another observation is that ZnAc and ZnCl membranes exhibit different surface microstructures: while ZnCl membranes show well-intergrown surfaces, ZnAc membranes appear to be poorly-intergrown. One may expect that ZnAc membranes are not desirable for gas separation. The ZnAc membranes, however, exhibit excellent propylene/propane separation performances as presented in Table 5.2, comparable to the ZnCl membranes (propylene/propane separation factors in the range of 37~39). The comparable separation performances of these two membranes with yet different surface microstructure strongly suggest that the separation capability of the membranes may come from films formed inside supports. ZnN membranes with seemly well-intergrown films formed primarily on the supports did not show any appreciable propylene/propane separation affirming the argument above. It is noted that while several ZIF-8 membranes were reported to have molecular sieving capabilities,[18,22,147,148] majority of these ZIF-8 membranes are not known to show any decent propylene/propane separation performances except a few membranes.[32,34-37,146] All of those highly propylene-selective membranes share a common microstructural feature where a portion of films are grown inside porous supports. It is our hypothesis that growing ZIF crystals inside supports reduces grain boundary defects due to the confinement effects of ZIF crystals within porous supports: the expansion of the crystals upon adsorption of gas molecules leads to the closing of the grain boundary between crystals. Further investigations are under way to prove our hypothesis and the results will be reported elsewhere in the future.
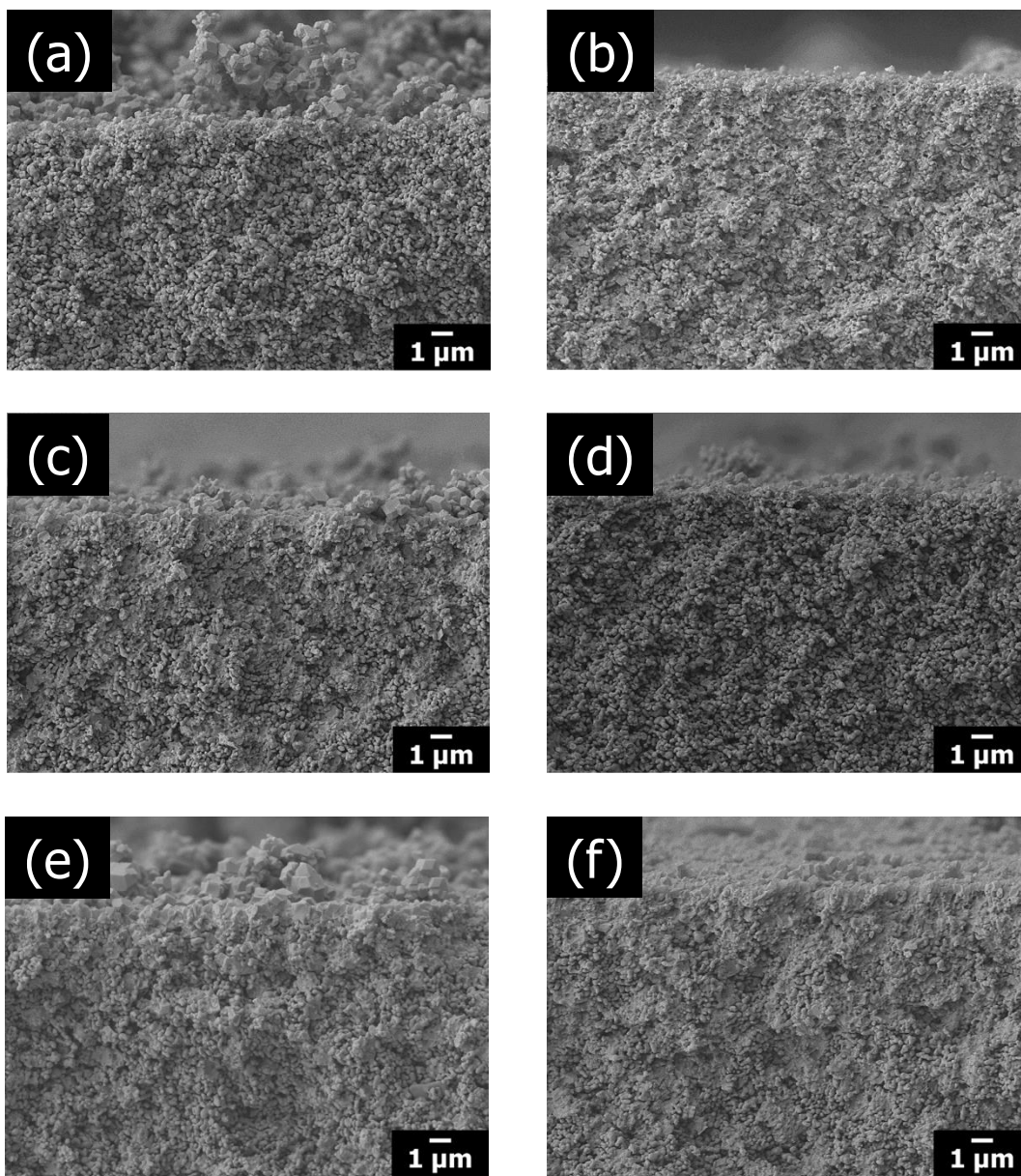
Figure 5.6 Low magnification Electron micrographs of ZIF-8 membranes presented in Figure 5.5; (a) ZnN, (b) ZnAc, (c) ZnCl, (d) ZnNAc, (e) ZnNCl, and (f) ZnAcCl.

Table 5.2 Room temperature propylene/propane separation performance of ZIF-8 membranes prepared from different metal salts and their combinations that are presented in Figure 5.4 and 5.5. Three membranes were tested to obtain the average values and the corresponding standard deviations.

Zinc salts	Propylene permeance (x 10^{-10} mol / m^2·s·Pa)	Separation Factor
ZnN	No separation	
ZnAc	307.7 ± 63.2	33.10 ± 5.2
ZnCl	267.5 ± 8.9	38.0 ± 1.1
ZnNAc	No separation	
ZnNCl	268.5 ± 12.0	70.6 ± 11.1
ZnAcCl	195.0 ± 0.1	39.7 ± 9.3

Motivated by controlling membrane microstructures using different zinc salts, the effect of zinc salt mixtures on the microstructures was also studied. With a fixed zinc ion concentration of 0.18 M in 40 ml methanol, three different combinations of salt mixtures (equal molar mixtures of ZnN/ZnAc, ZnN/ZnCl, and ZnAc/ZnCl) were used for the synthesis of ZIF-8 membranes (hereafter, ZnNAc, ZnNCl, and ZnAcCl membranes). The XRD patterns and electron micrographs of these membranes are

presented in Figure 5.4 and 5.5, respectively. While showing similar XRD peak intensities suggesting the comparable film thicknesses, electron micrographs reveal that the microstructures of these membranes are quite different. A general observation is that the membranes with zinc salt mixtures possess microstructural features that are a combination of the membranes with individual zinc salts. For instance, with a mixture containing ZnN (Figure 5.5(d) and (e)), membranes formed predominantly near the support surface, which is a characteristic of ZnN membranes (Figure 5.5(a)) while their surface microstructure appears halfway between membranes produced with individual zinc salts. In case of ZnAcCl (Figure 5.5(f)), membranes were grown inside supports, which is observed in both ZnAc and ZnCl membranes (Figure 5.5(b) and (c)). Furthermore, the membranes were well-intergrown with a grain size of 300 ~ 500 nm, which is similar to ZnCl membranes (Figure 5.5(c)). ZnNCl membranes showed much improved separation performances (Table 5.2) as compared to any membranes with individual salts. The average propylene/propane separation factor of ZnNCl membranes was almost doubled (~ 70.6) without compromising propylene permeance, indicating synergistic effects of nitrate and chloride salts leading to enhanced membrane grain boundary structure (i.e., smaller non-selective inter-crystalline gap) and likely reduced effective membrane thickness. This decrease in the effective membrane thickness is attributed to the presence of ZnN which suppresses the formation of crystals inside supports as depicted earlier. In contrast, ZnNAc membranes were not propylene-selective (Figure 5.5(d) and Table 5.2). When compared with ZnAc and ZnCl membranes, ZnAcCl membranes showed similar propylene/propane separation factor

120

but less propylene permeance possibly due to their thicker effective thickness (Figure 5.5(f) and Figure 5.6(f)). In comparison with the previously reported ZIF-8 membranes, the membranes in this study (in particular the ZnNCl membranes) exhibit improved propylene/propane separation performances in Table 5.3.

Lastly we investigated the effects of activation processes on the performances of ZIF-8 membranes. ZnNCl membranes with the highest propylene/propane separation factor were further treated under solvothermal conditions in methanol. The propylene permeance of the solvothermally activated membranes increased significantly from ~ 268 to ~ 537 x 10^{-10} mol / m^2·s·Pa (Table 5.4) while the separation factor reduced from ~ 70 to ~ 22, indicating the grain boundary structure of the membranes was compromised. The solvothermal activation process caused some degradation of the membrane surface (Figure 5.7). The degradation was however limited mostly to the membrane surface (Figure 5.7(b)) resulting in still decent propylene/propane separation factor. It is important to note that once membranes meet required minimum separation factors, highly permeable membranes are much more desired than highly selective membranes for practical industrial applications because of the large amount of gases to be processed. In this regard, solvothermal activation processes are expected to be a new strategy to further increase the propylene permeance of ZIF-8 membranes. For comparison, ZIF-8 membranes prepared by a secondary growth method[36] were subjected to the solvothermal activation. Unexpectedly, the membranes were completely peeled off (Figure 5.8). This difference in the mechanical stabilities of the two membranes upon the solvothermal activation can be explained by the fact that as compared with the secondary

Table 5.3 Comparison of binary propylene/propane separation performance with other ZIF-8 membranes.

Preparation method	Zinc salts	Propylene permeance (x 10^{-10} mol/m^2·s·pa)	Propylene/propane separation factor	Reference
CD method	ZnAC	307.7 ± 63.2	33.1 ± 5.2	this work
	ZnCl	267.5 ± 8.9	38.0 ± 1.1	
	ZnNCl	268.5 ± 12.0	76.6 ± 11.1	
	ZnAcCl	195.0 ± 0.1	39.7 ± 9.3	
	ZnN	23.0 ± 1.9*	57.0 ± 6.3*	ref[37]
Secondary growth	ZnN	207.9 ± 6.5	40.4 ± 8.5	ref[34]
		278.2 ± 63.9	34.6 ± 6.4	ref[35]
		122.0 ± 25.5	28.6 ± 2.0	ref[36]
Rapid thermal deposition	ZnAc	73.9 ± 6.1	29.0 ± 12.5	ref[146]

* Data obtained from a single gas permeation test

Table 5.4 Room temperature propylene/propane separation performance of ZnNCl membranes before and after solvothermal activation in methanol at 120 $^\circ$C for 4 h. Note that the membranes were activated by washing in methanol for 5 days prior to the solvothermal activation process.

Solvothermal Activation	Propylene permeance (x 10^{-10} mol / m^2·s·Pa)	Selectivity
Before	268.5 ± 12.0	70.6 ± 11.1
After	537.5 ± 29.2	22.4 ± 1.8
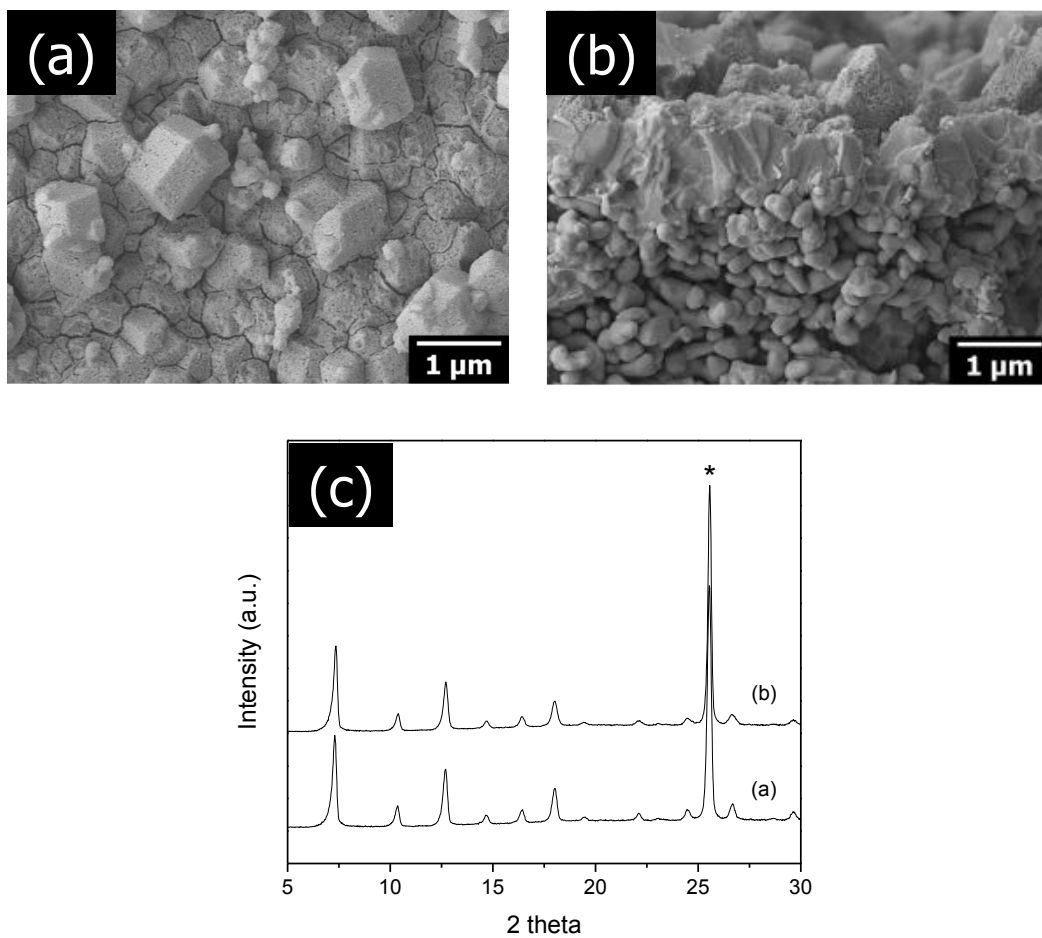
Figure 5.7 Electron micrographs of ZnNCl membranes after solvothermal activation at 120 $^{\circ}$C for 4 h: (a) top view and (b) cross-sectional view and XRD patterns of ZnNCl membranes before and after solvothermal activation (c).
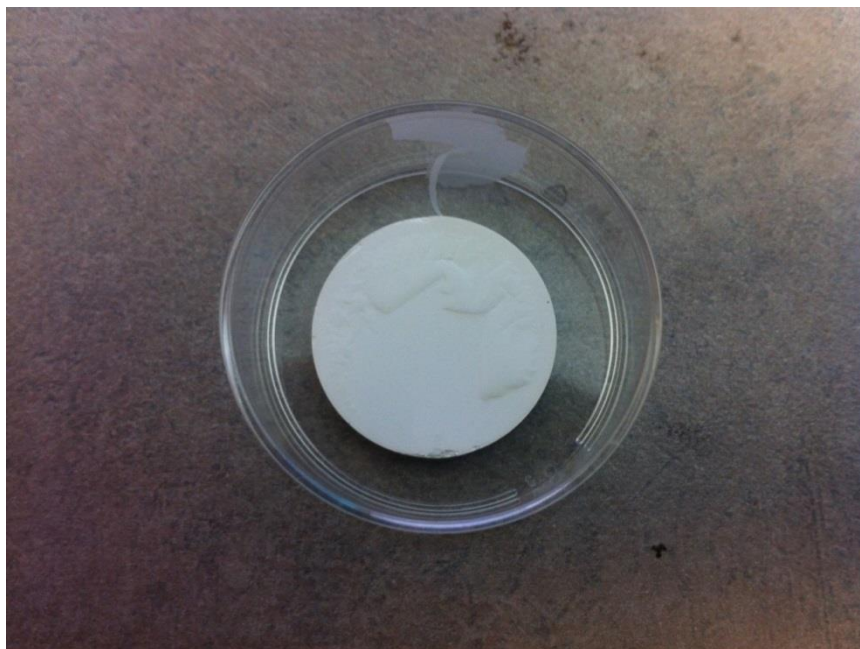
Figure 5.8 Digital photograph of a ZIF-8 membrane prepared by a secondary growth method in an aqueous solution after solvothermal activation.

growth approach, the CD method renders a greater faction of ZIF-8 films to form inside supports, leading to mechanically more stable membranes through the physical interlocks between films and supports.

5.4 Conclusions

In conclusion, we have demonstrated that the microstructures of ZIF-8 membranes by the CD method depend on two important synthesis conditions (sodium formate to ligand ratios and nature of zinc salts) as well as activation processes, thereby affecting their propylene/propane separation performances. It was found that an optimal SF/L ratio is present to produce high quality ZIF-8 membranes. Zinc nitrates resulted in

the formation of films primarily on supports while zinc acetates and zinc chlorides promoted film formation inside supports. Although ZnAc membranes appear to be poorly intergrown, they showed comparable propylene/propane separation performances with well-intergrown ZnCl membranes (propylene/propane separation factors in the range of 37~39), indicating films formed inside supports may determine separation performances of the membranes. When two zinc salts combined, membranes exhibited microstructural features that are combination of those with individual zinc salts. Membranes synthesized by zinc nitrates and chlorides showed outstanding propylene/propane separation performances with the separation factor of ~ 70 and the propylene permeance of ~ 268 x 10^{-10} mol/m^2·s·Pa), strongly suggesting synergistic effects of the two salts. Finally, solvothermal activation processes were found to be effective in significantly increasing the propylene permeances while maintaining decent propylene/propane separation factors. Solvothermal activation processes are expected to be a new strategy to further increase the propylene permeances of ZIF-8 membranes.

CHAPTER VI

HETEROEPITAXIALLY GROWN ZEOLITIC-IMIDAZOLATE FRAMEWORK

MEMBRANES WITH UNPRECEDENTED PROPYLENE/PROPANE SEPARATION

PERFORMANCE[*]

6.1 Introduction

      Propylene is one of the most highly demanded commodity chemicals in chemical and petrochemical industries. When produced by the steam-cracking of hydrocarbon sources such as natural gas, propylene needs to be separated from propane. Currently highly energy-intensive cryogenic distillation is employed due to the similar physical properties (e.g., volatility and size) between propane and propylene. Despite tremendous research interests in more energy-efficient membrane-based separation technologies, there exist no commercial membranes currently available for propylene/propane separation mainly due to the limitations of polymeric membranes (i.e., low separation factor).[2,48] Though molecular sieving materials such as carbon molecular sieves[4-6,149] and zeolites[3,150] are shown to be promising, the majority of these materials fail to meet the performance requirements except a few.[32,48] Facilitated transport membranes[8]

---

exhibit extremely high separation factors but suffer from irreversible degradation due to the impurities in the feed stream.

Due to their well-defined pores and labile surface chemistry, MOFs have drawn tremendous attentions as a new class of membrane materials for gas/liquid separations.[14,121,151] Zeolitic imidazolate frameworks (ZIFs)[15] with zeolite topologies, consisting of transition metals (Zn or Co) and imidazole-based ligands, are of particular interest and most extensively investigated for membrane-based gas separations[30] mainly owing to their ultra-micropores and relatively high thermal/chemical stabilities as compared to other MOFs.[15] To date, several ZIF materials such as ZIF-7,[24] ZIF-8,[18] ZIF-22,[21] ZIF-69,[20] ZIF-71,[25] ZIF-78,[26] ZIF-90,[27] ZIF-95,[28] and SIM-1[29] have been successfully processed into supported polycrystalline and/or mixed matrix membranes and tested for gas separations.[30] Due to the effective aperture of ~ 4.0 Å,[31] ZIF-8 membranes showed a sharp propylene/propane separation based on size exclusion principle.[32,34-40] So far, well-intergrown ZIF-8 membranes were prepared using either *in situ*[18,32,41] or secondary[22,34-36] growth. However, only a few ZIF-8 membranes[32-40] exhibited relatively high propylene/propane separation performances primarily because of the difficulty in controlling the microstructures of polycrystalline membranes (e.g., grain boundary structure). It is noted that the separation performance of well-intergrown polycrystalline ZIF-8 membranes is determined not only by the selective intracrystalline diffusion (i.e., intrinsic material property) but also by the non-selective intercrystalline diffusion (i.e., grain boundary structure). This is equivalent to the resistances-in-parallel model where the overall transport resistance is governed by the relative importance of

the two transport resistances, one through grains and the other through grain boundaries. The microstructures of polycrystalline films are greatly affected by processing techniques. It is, therefore, imperative to develop new processing techniques that may result in the improved microstructures of polycrystalline membranes, thereby leading to the improved separation performances.

Heteroepitaxial growth is an effective strategy to engineer the properties of crystalline materials by combining different crystalline systems via molecular level connections. As opposed to other MOF modification strategies (e.g., metal/ligand exchange and covalent/click chemistry on ligand pendent groups),[152] this molecular-level connection between two different crystalline systems enables the formation of hybrid crystals possessing combined properties without sacrificing the intrinsic features of individual crystals.[153] This unique advantage of heteroepitaxial growth resulted in a battery of hierarchical MOF structures[154-162] which cannot be obtained otherwise. Kitagawa and his coworkers constructed hybrid MOF structures such as heterometallic core-shells,[155] ABA-type blocks[163] and hybrid oriented films,[161] and shed lights on the epitaxial relations via exhaustive surface X-ray diffraction analyses.[155,161,163] Later several groups reported heteroepitaxially-grown hybrid MOFs including IRMOF-1/-3 core-shells,[156,159,160] hybrid SURMOFs using $[Cu_2(bdc)_2(dabco)]$, $[Cu_2(NH_2-bdc)_2(dabco)]$, and $[Cu_2(ndc)_2(dabco)]$,[154] and more recently ZIF-67/-8 Janus crystals.[157] Furthermore, in our previous report,[159] we demonstrated that IRMOF-3/IRMOF-1 hybrid membranes can be prepared by heteroexpitaxially growing IRMOF-3 on IRMOF-1 seed crystal layers. It should be noted that several zeolite films and membranes were also

prepared using the heteroepitaxial growth strategy.[25,164,165] To the best of our knowledge, there have been no reported ZIF membranes prepared by the heteroepitaxial growth.

ZIF-67 is a cobalt-substituted equivalent to ZIF-8 composed of cobalt ions interconnected with 2-methylimidazole ligand, forming a SOD zeolite topology.[17] Since it is iso-structural to ZIF-8, we reckoned ZIF-67 membranes might be promising for propylene/propane separation as with ZIF-8 membranes. In addition, due to the presence of the redox catalytic cobalt centers,[166-171] ZIF-67 membranes have the potential to be effective perm-selective membrane reactors. To the best of our knowledge, however, there has been no report on well-intergrown ZIF-67 membranes.

To this end, we report the first ZIF-67 membranes, exhibiting excellent propylene/propane separation performances. Submicron-thick ZIF-67 membranes were heteroepitaxially grown from ZIF-8 seed layers. The heteroepitaxy between ZIF-8 and ZIF-67 was unambiguously determined by constructing core shells such as ZIF-8@ZIF-67 (ZIF-67 shell on ZIF-8 core) and ZIF-8@ZIF-67@ZIF-8 (ZIF-8 shell on ZIF-8@ZIF-67 core-shell) and observing the growth of shell layers that preserved both in-plane and out-of-plane orientations. Furthermore, a tertiary heteroepitaxial growth of ZIF-8 layers on ZIF-67 membranes turned out to be an effective means to further improve membrane microstructures, leading to significant enhancement in propylene/propane separation factors.

6.2   Experimental Section

6.2.1   Chemicals

To synthesize ZIF-8 and ZIF-67 seed layers and films, zinc nitrate hexahydrate ($Zn(NO_3)_2 \cdot 6H_2O$, 98%, Sigma-Aldrich) and cobalt nitrate hexahydrate ($Co(NO_3)_2 \cdot 6H_2O$, 98%, Sigma-Aldrich) as metal sources , 2-methylimidazole ($C_4H_6N_2$, 99%, Sigma-Aldrich) as an organic linker, sodium formate (HCOONa, 99%, Sigma-Aldrich) as a deprotonating agent, and   methanol (CH_3OH, > 99%, Alfa Asear) as a solvent or co-solvent in tandem with D.I. water were used. For the synthesis of ZIF-8 and ZIF-67 single crystals, methanol (CH3OH, > 99%, Alfa Asear) and dimethylformamide ($HCON(CH_3)_2$, 99.8+%, Alfa Asear) were used as solvents. All chemicals were used as received without further purification.

6.2.2   Preparation of porous α-Al$_2$O$_3$ substrates

Disk-shaped alumina substrates (porosity = ~ 46 %, diameter = 22 mm, and thickness = 2 mm) with an average pore diameter of 200 nm were prepared by a pressing and sintering method slightly modified from a previously reported method.[34] Briefly, α-Al$_2$O$_3$ power (CR6, Baikowski) was molded into a disk shape by uniaxial pressing and was sintered at 1100 ^{o}C for 2 h. Then one side of the sintered disks was polished using a sand paper (grid #1200) to reduce the surface roughness of the substrates, followed by sonication for 1 min in methanol. Subsequently the supports were dried in an oven at 120 ^{o}C for 1 h before usage.

6.2.3   Preparation of ZIF-8 seed layer using a microwave-assisted seeding

Densely-packed ZIF-8 seed layers on α-Al_2O_3 substrates were prepared using our previously reported microwave-assisted seeding method.[34] First, 2.43 g of zinc nitrate hexahydrate was dissolved in 40 ml of methanol (solution A) and 2.59 g of 2-methylimidazole and 0.125 g of sodium formate were dissolved in 30 ml of methanol (solution B). Second, a substrate was immersed in the solution A for 1 h to saturate the substrate with the metal solution. Then the saturated substrate was held vertically using a home-made Teflon holder and immediately inserted into the solution B in a microwave-inert glass tube, followed by microwave irradiation with the power of 100 W for 1.5 min. Finally, the tube was naturally cooled down for 30 min and the prepared seeded support was washed in 30 ml of methanol under gentle rocking for 12 h and dried at room temperature for 24 h.

6.2.4   Secondary growth of ZIF-67 membranes

Continuous ZIF-67 membranes were grown heteroepitaxially on ZIF-8 seed layers under solvothermal conditions. Briefly, 0.11 g of cobalt nitrate hexahydrate and 2.27 g of 2-methylimidazole were dissolved in a mixture of 2.5 ml of methanol and 17.5 ml of D.I. water, respectively. Two solutions were blended for 2 min and poured into a 45 ml autoclave containing a ZIF-8 seeded substrate. The seeded support was held vertically using a home-made Teflon holder. The autoclave was kept in an oven at 120 ^{o}C for 6h. Afterwards, the autoclave was naturally cooled down for 6 h and the as-prepared membrane was washed for 2 days in 30 ml of methanol under gentle rocking.

The sample was replenished with fresh methanol every 12 h before completing the washing step. Finally, the membrane was dried at room temperature for 12 h before characterizations and testing. Importantly, if needed, this whole growth step was repeated to improve membrane quality.

6.2.5 Tertiary growth of a submicron thick ZIF-8 overlayer on ZIF-67 membranes

First, a ZIF-67 membrane was solvothermally treated in an aqueous ligand solution (4.54 g in 40 ml of D.I. water) at 120 ^{o}C for 4 h. Then the treated membrane was washed in 30 ml of methanol for 2 days and dried at room temperature for 12 h before the tertiary growth of a ZIF-8 overlayer. Afterwards, a vertically loaded ZIF-67 membrane in a Teflon holder was inserted in a precursor solution, prepared by dissolving 0.11 g of zinc nitrate hexahydrate and 2.27 g of 2-methylimidazole in 40 ml of D.I. water.[35] Afterwards, the reactor was kept in an oven at 30 ^{o}C. The growth time was varied in the range of 20 ~ 60 min to control the thickness of ZIF-8 overlayers. As-prepared membranes were washed and dried using the identical procedures for the ZIF-67 membranes described above.

6.2.6 Synthesis of ZIF-8 single crystals

ZIF-8 single crystals with size in the range of 100 - 150 μm were obtained by following the recipe reported by Zhang et al.[31] with a minor modification. In a typical synthesis, 1.764g of zinc nitrate hexahydrate, 0.973g of 2-methylimidazole, and 0.404 g of sodium formate were dissolved in 40ml of methanol. Then the mixture was poured

into a 45 ml autoclave containing a glass slide and kept in an oven at 90 ^{o}C for 6 h. After the reaction, the autoclave was naturally cooled down for 2 h under ambient conditions and single crystals formed on the glass slide were removed by gently sonicating in methanol. Finally the single crystals were kept in methanol for 5 days while replenished with fresh methanol every 12 h, followed by vacuum drying at 70 ^{o}C for 24 h. Single crystals with larger size (~500 μm) for a single crystal X-ray analysis were prepared using the recipe reported elsewhere.[60] Briefly, 0.35g of Zinc nitrate hexahydrate and 0.2g of 2-methylimidazole were dissolved in 15 ml of dimethylformamide containing 9 drops of 1M HNO$_3$. Then, the mixture was kept in a 20 ml glass vial and incubated in an oven at 120 ^{o}C for 24 h, followed by natural cooling at ambient conditions. For a single crystal analysis, crystals were quickly rinsed with fresh dimethylformamide and used for the analysis without further.

6.2.7 Synthesis of ZIF-67 single crystals

In a typical synthesis, 1.05 g of cobalt nitrate hexahydrate, and 0.27g of 2-methylimidazole were dissolved in 108 ml of dimethylformamide containing 6 drops of 1M HNO$_3$. Then the mixture was poured into a 250 ml glass vial and kept in an oven at 130 ^{o}C for 72 h. After the reaction, the vial was naturally cooled down and the formed single crystals, primarily at vial bottom, were collected and kept in methanol for 7 days while replenished with fresh methanol every 12 h, followed by vacuum drying at 70 ^{o}C for 24 h.

6.2.8   Synthesis of ZIF-8@ZIF-67 and ZIF-8@ZIF-67@ZIF-8 core-shell structures

To prepare ZIF-8@ZIF-67 core shells, 0.1 g of ZIF-8 single crystals (100 - 150 μm) were put into an autoclave containing 40 ml of the identical precursor solution used for the growth of ZIF-67 membranes. Then the autoclave was incubated in an oven at 120 $^{\circ}$C for 4 h under rotation (10 rpm). After the reaction, the autoclave was naturally cooled down and precipitated core-shell crystals were collected. The samples were immersed in 30 ml of methanol for 3 days while replenished with fresh methanol every 12h, followed by vacuum drying at 70 $^{\circ}$C for 24 h. To synthesize ZIF-8@ZIF-67@ZIF-8 core shells, 0.1g of the ZIF-8@ZIF-67 crystals were solvothermally treated in a ZIF-8 precursor solution under the identical conditions used for the growth of the ZIF-67 shell layers. The ZIF-8 precursor solution was prepared by dissolving 0.11 g of zinc nitrate hexahydrate and 2.27 g of 2-methylimidazole in a mixture of 2.5 ml of methanol and 17.5 ml of D.I. water. Finally, the resulted core shell crystals were immersed in 30 ml of methanol for 3 days while replenished with fresh methanol every 12 h, followed by vacuum drying at 70 $^{\circ}$C for 24 h before characterizations.

6.2.9   Propylene/propane permeation measurements

Binary propylene/propane gas permeation measurements were performed at room temperature under atmospheric pressure using the Wicke-Kallenbach technique. A 50:50 mixture of propylene/propane was supplied to a feed side while argon gas kept sweeping a permeate side. Compositions of the permeated stream were determined using a gas chromatography (Agilent GC 7890A equipped with a HP-PLOT/Q column and a

FID detector). The volumetric flow rate of the feed and sweeping gases was maintained at 100 cc/min using mass flow controllers. The GC was calibrated in 10 ppm concentration range for both propylene and propane using a standard gas. Note that the calibrated concentration range was less than minimum propane concentration observed throughout the measurements.

6.2.10 Characterization

Electron micrographs were collected using JEOL JSM-7500F that was operated with 5 keV of acceleration voltage and 15 mm of working distance. Optical micrographs were taken using a microscope (Axio Imager A1m, Carl Zeiss). X-ray diffraction patterns were recorded using a Rigaku Miniflex II powder diffractometer with Cu-Kα radiation (λ = 1.5406 Å). EDX elemental mapping and line scanning analyses were performed using Tescan Vega 3 that was operated with 20 keV of acceleration voltage and 9 mm of working distance. For crystal structure determination, defect-free single crystals of ZIF-8 and ZIF-67 soaked in dimethylformamide were selected and loaded on a Bruker APEX-II CCD diffractometer with Mo-Kα radiation (λ = 0.71073 Å). The crystals were kept at 110K during data collection. The structures were solved with the SHELXT structure solution program using direct method and refined with the SHELXL refinement package using least squares minimization. Infra-red spectra were collected using a NICOLET IR100 FT-IR spectrometer. Pulverized ZIF-8 and ZIF-67 particles were homogeneously mixed with KBr and pelletized for measurements. A Varian INOVA 400 NMR spectrometer was employed to collect ^{15}N spectra of ZIF-8 and ZIF-

67 with a 7.5 mm CP/MAS probe, which was operated in air at 25 $^{\circ}$C at a ^{15}N resonance frequency of 40.53 MHz. The spinning frequency and a contact time were 10 kHz and 4 ms, respectively. Samples were packed into 7.5 mm zirconia rotors and sealed with Kel-F short caps. All samples were dried at 70 $^{\circ}$C before NMR spectra acquisitions. N_2 adsorption measurements were conducted using an ASAP 2000 (Micrometics).

6.3   Results and Discussion

ZIF-8 and ZIF-67 are iso-structural (i.e., crystallographically same structure) with different metal nodes (Zn in ZIF-8 and Co in ZIF-67). They share the same crystallographic features such as crystal system and space group with similar lattice parameters (cubic, $I\bar{4}3m$, and a = 16.881 Å (ZIF-8)/16.908 Å (ZIF-67) at 110 K (Table 6.1)). It is, therefore, expected to obtain the heteroepitaxial growth of these two iso-structural ZIFs. It should be pointed out that while preparing this manuscript, two independent reports were brought to our attention, showing ZIF-67/-8 Janus crystals[157] and ZIF-8@ZIF-67 core-shell structures,[172] respectively. None of these reports, however, presented unambiguous evidences of heteroepitaxial growth.

To establish the heteroepitaxial relationships between ZIF-8 and ZIF-67, core-shell structures of ZIF-8@ZIF-67 and ZIF-8@ZIF-67@ZIF-8 were prepared solvothermally. Figure 6.1 presents optical and electron micrographs of the core-shell structures. It should be noted that the colors of the samples are different from those under the optical microscope due to an optical filter. ZIF-67 and ZIF-8 powders are in purple and in yellow, respectively, as shown in Figure 6.2. As-synthesized core ZIF-8

Table 6.1 Comparison of structural dimensions between ZIF-8 and ZIF-67 at 110K. D1, D2, and PA denote metal-nitrogen distance, metal-metal distance, and approximated pore aperture, respectively.
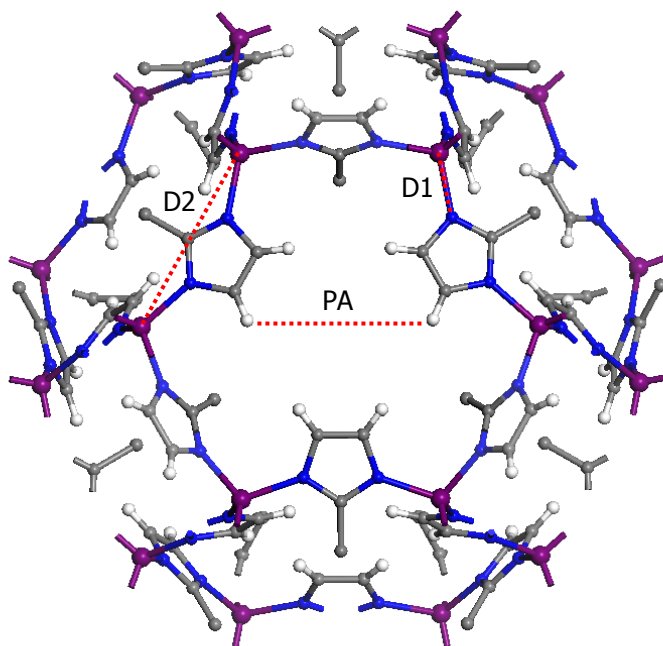
Adsorbent	D1 (Å)	D2 (Å)	PA (Å)	Unit cell (Å)
ZIF-8	1.979	5.969	3.387	16.881
ZIF-67	1.977	5.978	3.401	16.908

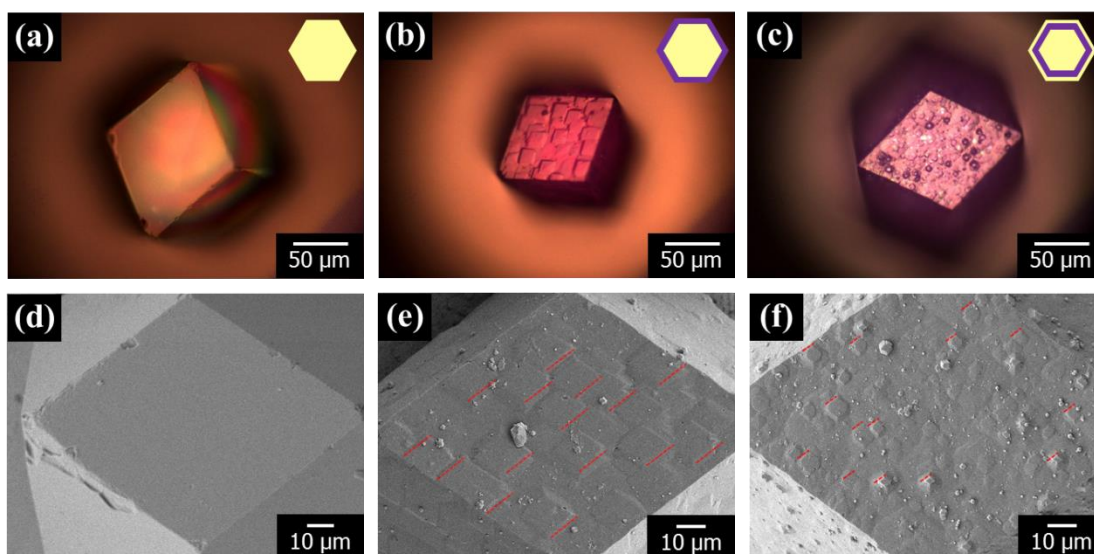Figure 6.1 Optical and electron micrographs of the {110} facets of a ZIF-8 single crystal (a, d), a ZIF-8@ZIF-67 core shell (b, e), and a ZIF-8@ZIF-67@ZIF-8 core shell (c, f). A, B, C in a A@B@C structure indicates that a core crystal, a second subshell and the most outer shell, respectively.
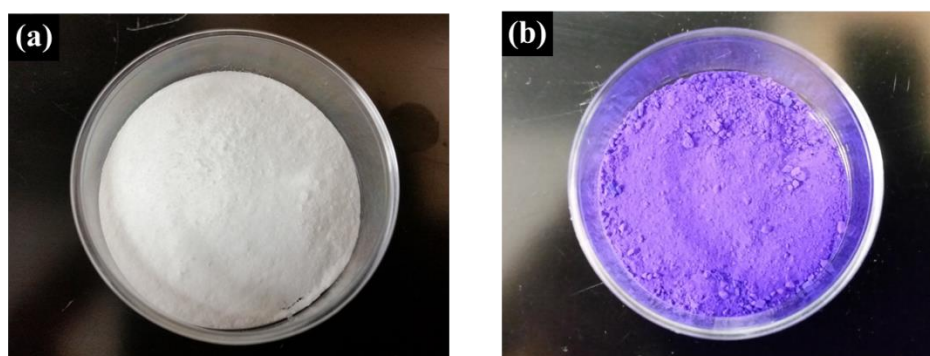
Figure 6.2 Digital photographs of bulk ZIF-8 (a) and ZIF-67 (b) powders.

single crystals have a rhombic dodecahedron shape with 12 of the {110} facets with the size of ca. 150 μm. The ZIF-8 core crystals are transparent with a yellowish tint and have relatively smooth surfaces (Figure 6.1(a) and (d)). Upon growing a ZIF-67 shell, the crystal exhibits purplish red color (Fig. 6.1(b)) and pinkish red color after the subsequent growth of an additional ZIF-8 layer on ZIF-8@ZIF-67 (Fig. 6.1(c)), indicating the growth of overlayers on the core crystals. Powder X-ray diffraction patterns of the core-shell crystals confirmed that the samples were phase-pure (see Figure 6.3(a) and (b)). Fig. 6.1(e) and (f) present the electron micrographs of the core-shell samples. As compared to ZIF-8 core crystals (Figure 6.1(d)), newly grown shell crystal domains are observed on the external surfaces of both core-shell crystals. These domains have a rhombus shape resembling the shape of the {110} facets of ZIF-8 core crystals. As highlighted with red dotted lines marked on the electron micrographs, individual domains are aligned with each other along the in-plane directions as well as with core crystals, explicitly confirming that the shells were grown in an epitaxial manner. Individual shell domains of ZIF-8@ZIF-67 and ZIF-8@ZIF-67@ZIF-8 were compared in Figure 6.4. As shown, domains were different in size as well as in the level of their shape development. Under the same growth conditions, ZIF-8 shell domains (Figure 6.4(c)) were smaller in size and not well developed along the [-110] direction evidenced by the presence of numerous terraces and steps as compared to ZIF-67 shell domains (Figure 6.4(b)). This suggests that under the current synthesis conditions, ZIF-67 shells nucleate and grow faster than ZIF-8 shells and the growth of ZIF-8 shells along the [001] direction is faster than along the [-110] direction. Indeed, ZIF-67 grew faster

140
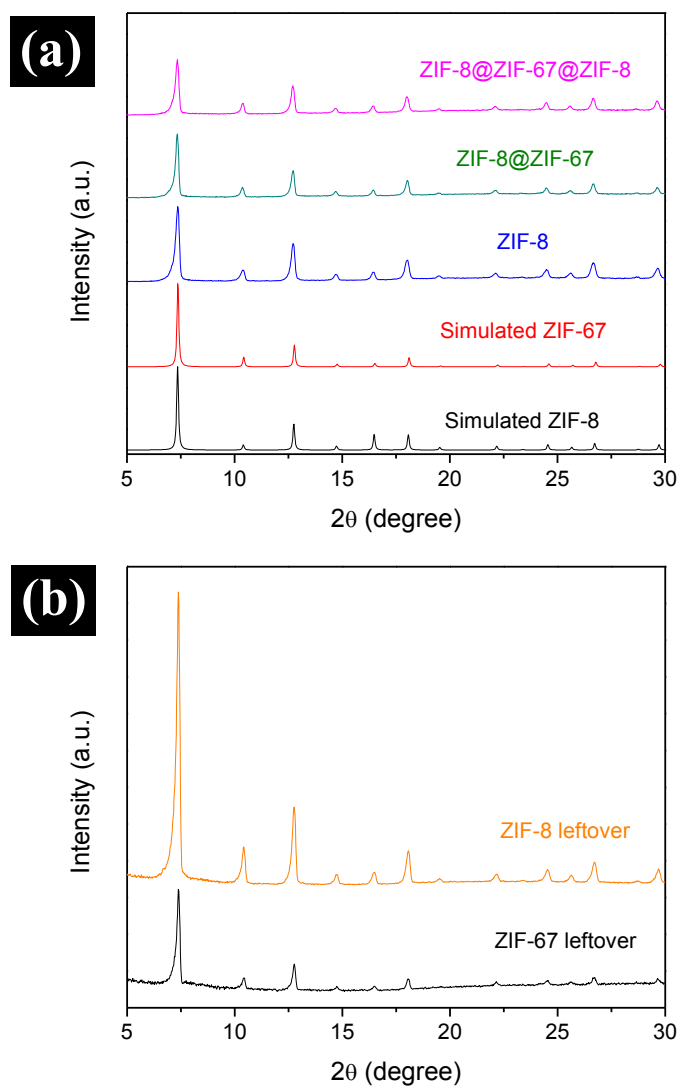
Figure 6.3 Powder X-ray diffraction patterns of core-shell crystals (a) and leftover powders collected after removing the core-shell crystals from corresponding growth solutions (b).
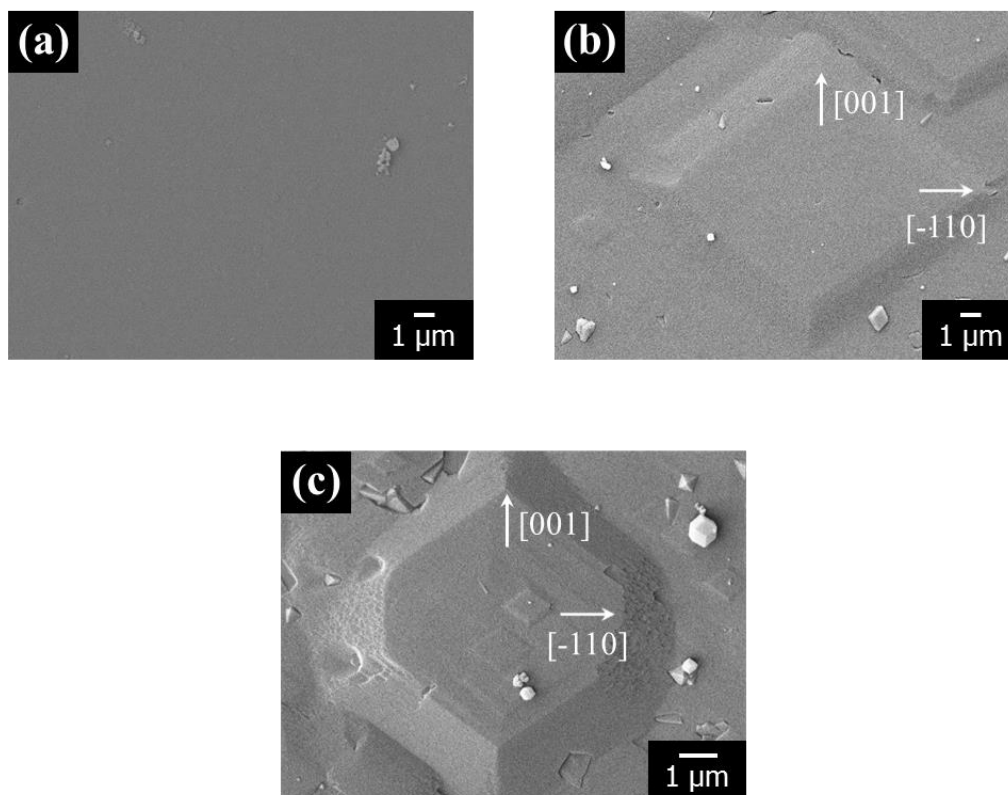
Figure 6.4 Magnified electron micrographs of the {110} facets of a ZIF-8 single crystal (a), a ZIF-8@ZIF-67 core shell (b), and a ZIF-8@ZIF-67@ZIF-8 core shell (c).

than ZIF-8 evidenced by the fact that the average particle size of powders collected from the growth solutions (~ 0.5 µm (ZIF-8) vs. ~ 1 µm (ZIF-67)) as shown in Figure 6.5.

Figure 6.6 illustrates the heteroepitaxial synthesis of ZIF membranes. In order to prepare well-intergrown ZIF-67 membranes using the heteroepitaxial growth, densely-packed ZIF-8 seed crystals were first deposited on α-Al$_2$O$_3$ supports using the microwave-assisted seeding method.[34] Subsequently, ZIF-67 crystals were grown on ZIF-8 seed layers in a heteroepitaxial manner. The microwave-assisted seeding method
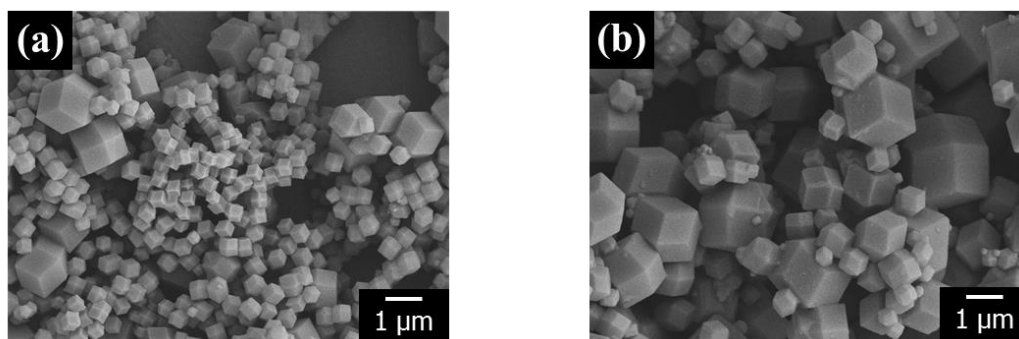
Figure 6.5 Electron micrographs of ZIF-8 (a) and ZIF-67 (b) powders precipitated in the solutions after the core-shell syntheses.
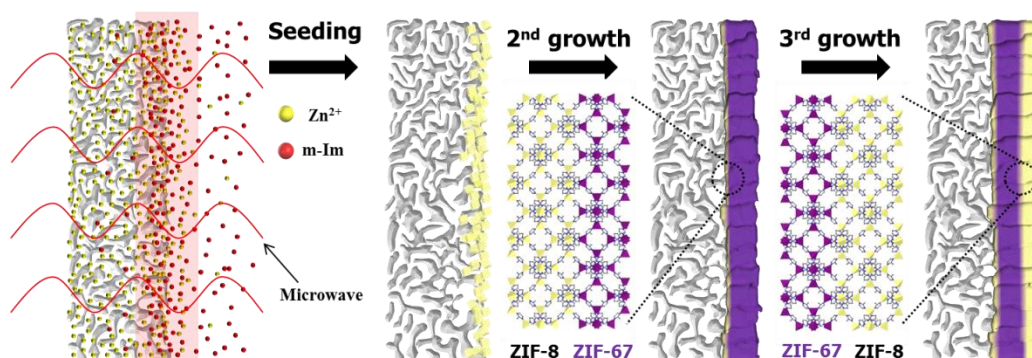
Figure 6.6 Schematic illustration of the membrane synthesis via heteroepitaxial growth.

enables to achieve ZIF-8 seed layers rather strongly attached to supports due to the rapid formation of seed crystals with a majority of crystals formed inside supports as presented in Figure 6.7(a). With strongly-bound ZIF-8 seed crystals, well-intergrown defect-free ZIF-67 membranes (hereafter, ZIF-67 membranes) with a thickness of ca. 700 nm were produced by heteroepitaxially growing ZIF-67 from ZIF-8 seed crystals (see Figure 6.7(b) and(d) and Figure 6.8). Figure 6.7(e) shows an EDX line scan analysis along the

143
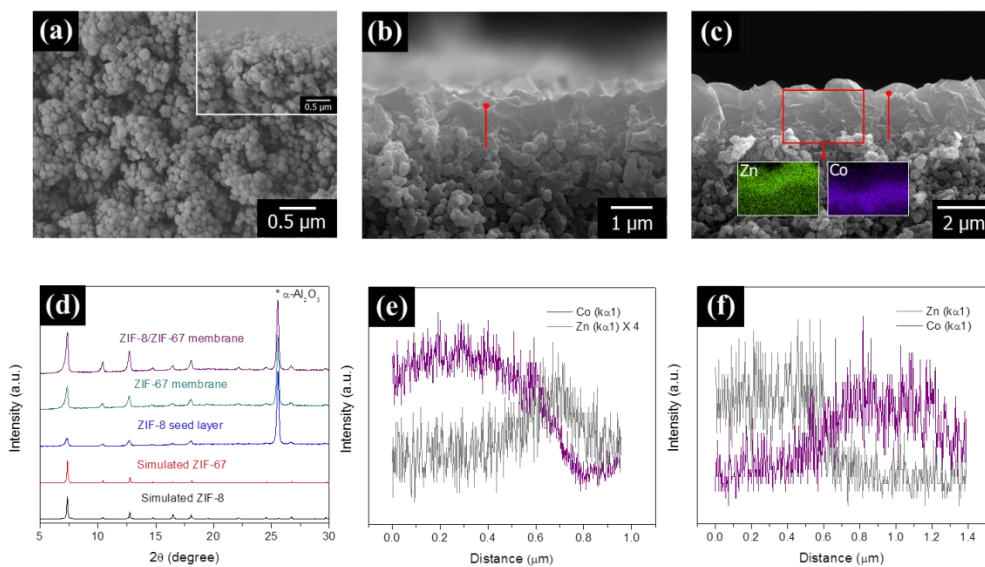
Figure 6.7 Electron micrographs of a ZIF-8 seed layer (a), a ZIF-67 membrane (b), and a ZIF-8/ZIF-67 membrane (c); X-ray diffraction patterns of the ZIF-8 seed layer, ZIF-67, and ZIF-8/ZIF-67 membrane (d); energy-dispersive X-ray elemental profiles of the cross section of the ZIF-67 (e) and ZIF-8/ZIF-67 membranes (f) with the corresponding red solid lines marked on (b) and (c). The inset image in (a) shows the cross-sectional view of the seed layer.
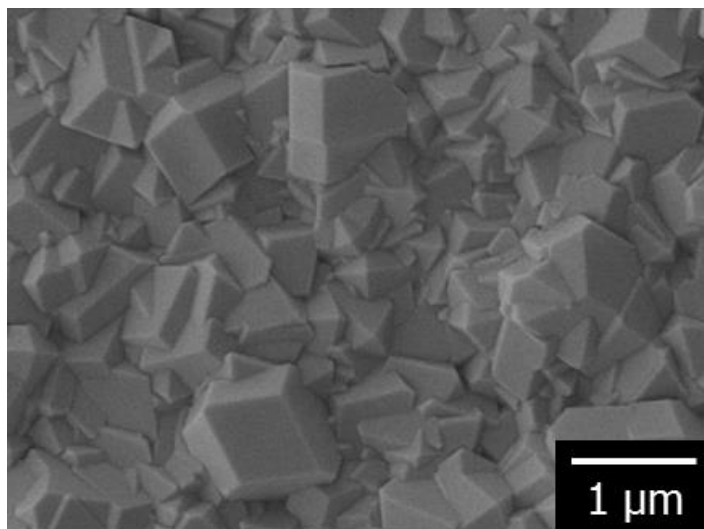
Figure 6.8 An electron micrograph (top view) of a ZIF-67 membrane grown on a ZIF-8 seed layer by the heteroepitaxial secondary growth.

cross-section of ZIF-67 membranes marked with a red solid line. As expected, a zinc-rich region is clearly seen as moving to the bottom of the membranes, ca. 700 nm in depth, demonstrating the presence of ZIF-8 seed crystals embedded in the membrane structure and the continuous growth of the ZIF-67 layer from the ZIF-8 seed crystals. Similarly, when additional ZIF-8 layers (hereafter, ZIF-8 overlayers) were overgrown on ZIF-67 membranes (i.e., tertiary growth), the resulting membranes (hereafter, ZIF-8/ZIF-67 membranes) appear to be well-intergrown and grown seamlessly while the thickness of the membranes increased to ca. 1.4 μm (Figure 6.7(c) and (d)). Elemental maps and profiles confirm the presence of a ZIF-8 layer on top of the ZIF-67 layer as shown in Figure 6.7(c) and (f).

The strong attachment of ZIF-8 seed crystal layers on alumina supports found to be critical to achieve well-intergrown ZIF-67 membranes. With ZIF-8 seed layers prepared by a simple dip-coating method (Figure 6.9(a)), it was not possible to obtain ZIF-67 membranes. Instead, an unknown dense phase with a plate-like morphology was formed on the support (Figure 6.9(b) and (c)). The powder sample precipitated simultaneously in the solution was, however, determined to be phase-pure ZIF-67 (Figure 6.10). The same unknown phase was also formed on unseeded alumina supports (Figure 6.11). Based on these observations, it is presumed that the unknown phase was formed, likely catalyzed by α-Al$_2$O$_3$ supports under the current synthesis conditions. When weakly attached, seed crystals can be easily detached from the supports during the secondary growth step, failing to form ZIF-67 films, instead resulting in the formation of the unknown phase.

It should be noted that our repeated attempts failed to synthesize high-quality ZIF-67 membranes with ZIF-67 seed layers prepared by the microwave-assisted seeding method mainly due to the poor quality of ZIF-67 seed layers as shown in Figure 6.12. This is attributed to the fact that ZIF-67 nucleates and grows faster than ZIF-8 under the current synthesis conditions. When crystals nucleate and grow too fast, homogeneous nucleation/growth can be significant relative to heterogeneous nucleation/growth, leading to the poor quality of seed layers.

Due to the very close structural similarities between ZIF-8 and ZIF-67, one might expect a keen kinetic separation of a propylene/propane mixture from ZIF-67 membranes based on the size-exclusion principle as observed in ZIF-8 membranes.[128] It
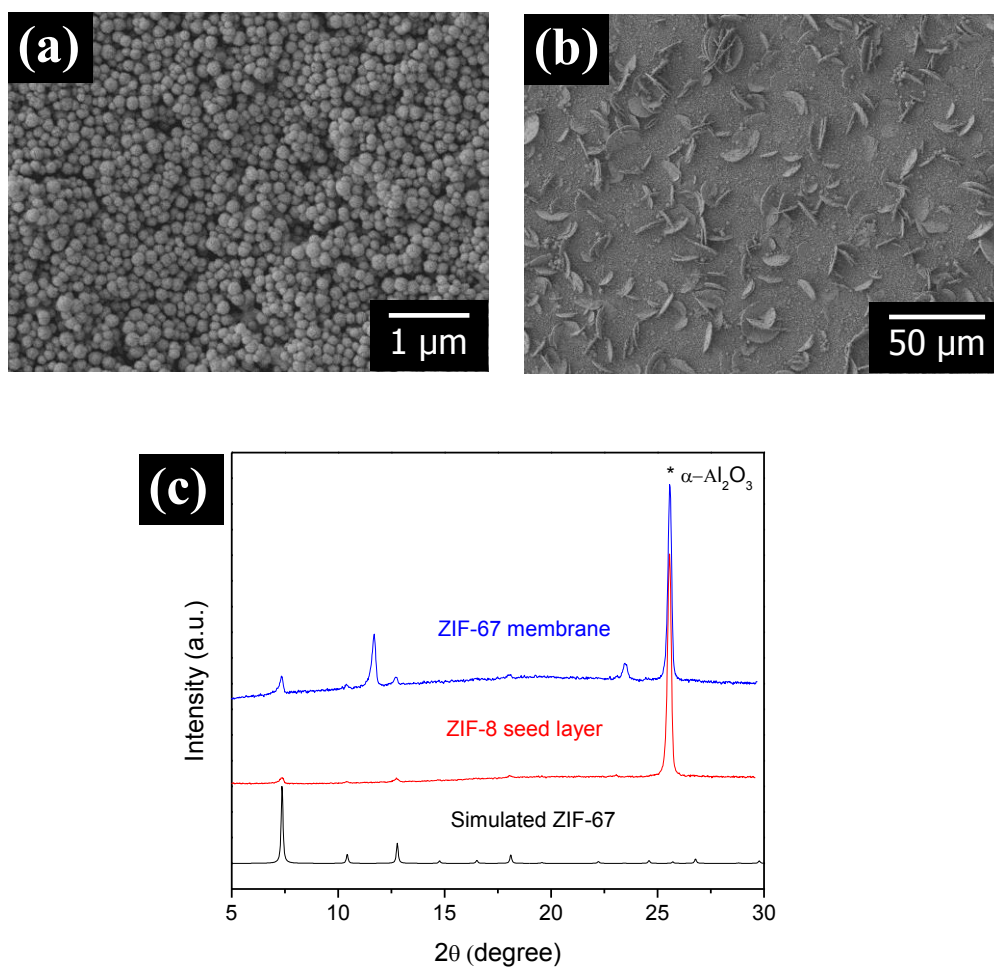
Figure 6.9 Electron micrographs of a ZIF-8 seed layer prepared by a dip coating method (a) and a ZIF-67 membrane grown on the dip-coated seed layer (b); XRD patterns of the dip-coated seed layer and secondarily grown ZIF-67 membrane on it (c).
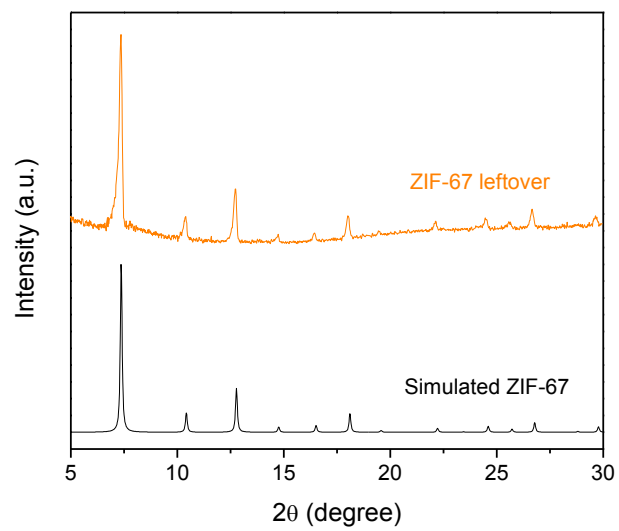
Figure 6.10 PXRD pattern of ZIF-67 leftover powders collected after the synthesis of a ZIF-67 membrane on a dip-coated ZIF-8 seed layer.
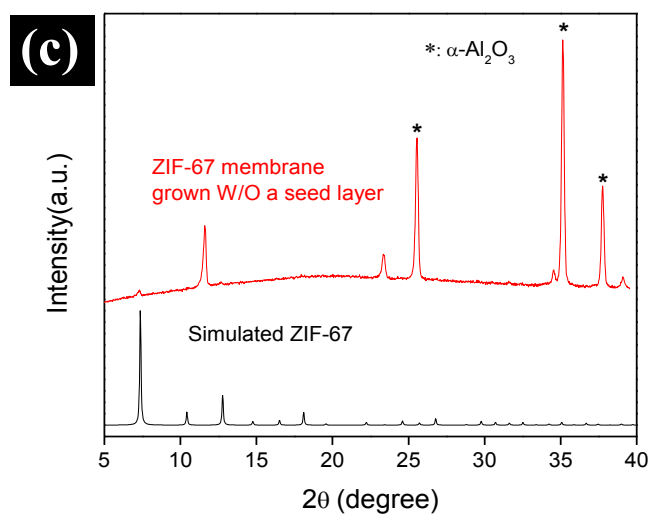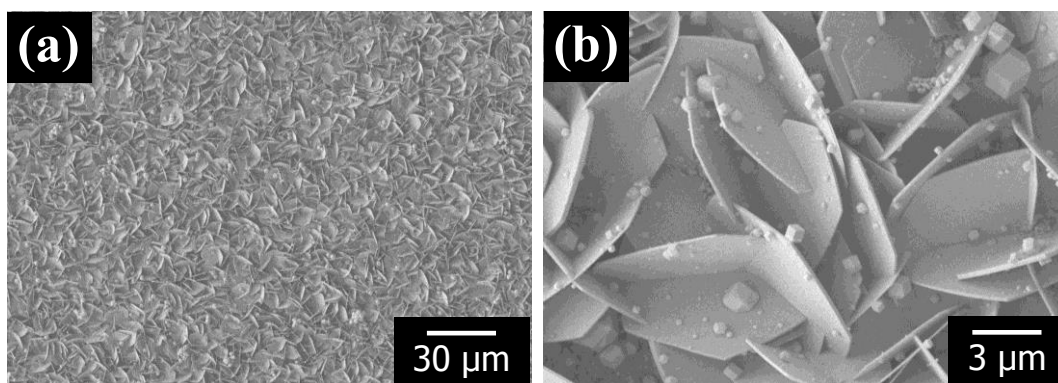
Figure 6.11 Electron micrographs (a, b) and XRD patterns (c) of ZIF-67 membranes grown without a ZIF-8 seed layer.
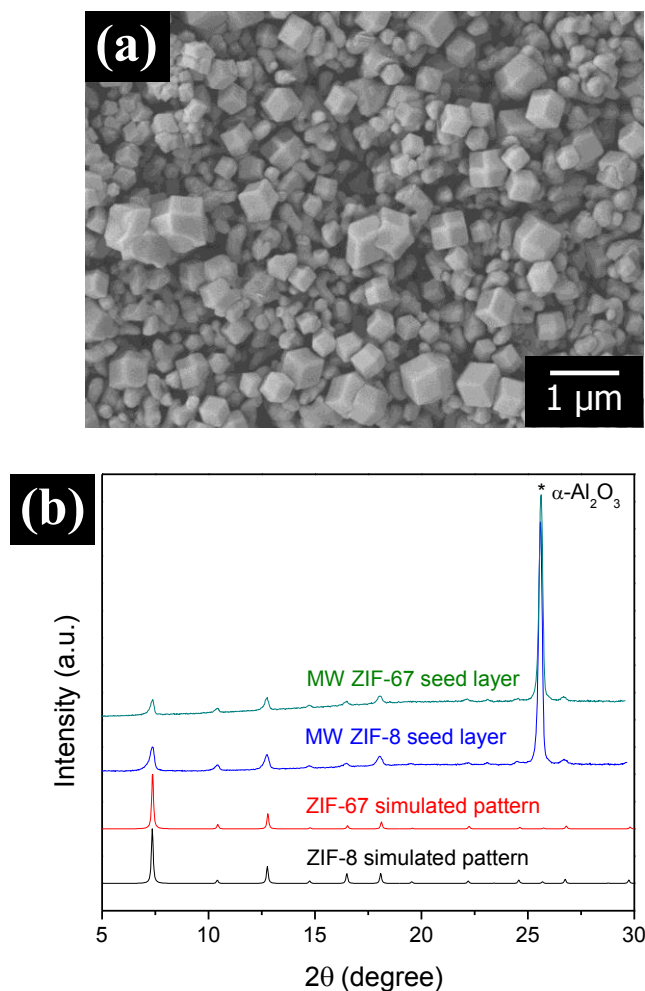
Figure 6.12 An electron micrograph (a) and a XRD pattern (b) of ZIF-67 seed layers prepared using the microwave-assisted seeding method.

is noteworthy that as with ZIF-8, ZIF-67 presented a negligible solubility contribution on propylene/propane separation, evidenced by almost identical propylene/propane adsorption isotherm profiles as shown in Figure 6.13. The separation performances of heteroepitaxially-grown membranes (ZIF-67 and ZIF-8/ZIF-67 membranes) were examined by performing gas separation measurements with a binary (50/50)
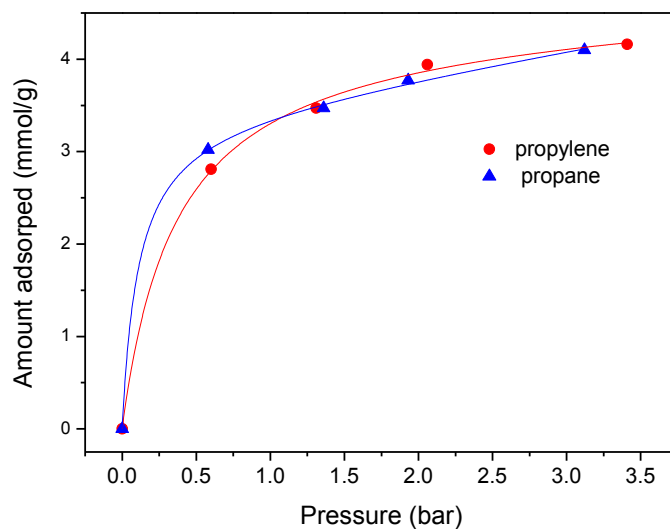
Figure 6.13 Propylene and propane adsorption isotherms on ZIF-67 at 35 $^{\circ}$C.

propylene/propane mixture using a Wicke-Kallenbach set-up (Figure 6.14) under ambient conditions. Table 6.2 summarizes the performance results of all tested membranes. ZIF-67 membranes exhibit the average propylene permeance of ~ 460 ×10^{-10} mol Pa^{-1} m^{-2} s^{-1} and the average propylene/propane separation factor of ~ 85, outperforming almost all of the reported ZIF-8 membranes (Table 6.3). This impressive binary propylene/propane separation performance of ZIF-67 membranes is ascribed to their sub-micron thickness (ca. 700 nm) and improved grain boundary structure. Since the performance of high-quality polycrystalline membranes is determined not only by the quality of grain boundary structure (i.e., non-selective intercrystalline diffusion) but also by the intrinsic transport property of materials (i.e., selective intracrystalline diffusion), however, it is not feasible to exclude the possibility that ZIF-67 might be inherently better than ZIF-8 for propylene/propane separation. While the

151
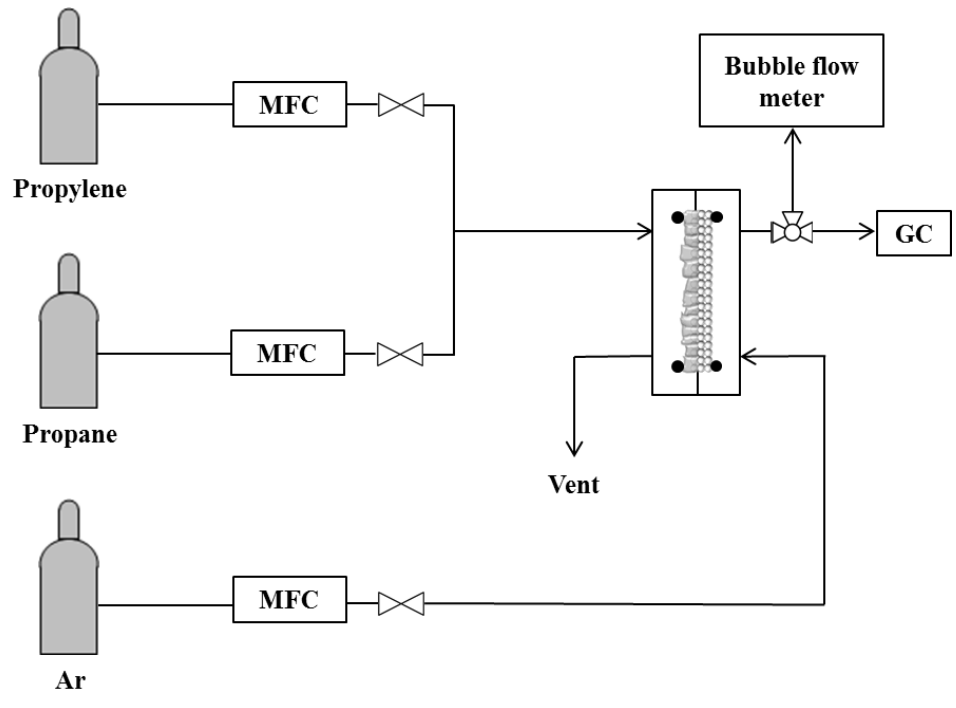
Figure 6.14 Schematic diagram of a gas permeation set-up (Wicke-Kallenbach technique).

Table 6.2 Room temperature binary propylene/propane separation performances of ZIF-67, ZIF-8/ZIF-67, and ZIF-67/ZIF-67 membranes grown on ZIF-8 seed layers. The average and standard deviation values were calculated from the performances of three membranes of each. *: the membranes were prepared with ZIF-67 membranes hydrothermally-treated in an aqueous ligand solution before a tertiary growth of a ZIF-8 layer or a ZIF-67 layer.

Membrane	Thickness (μm)	C_3H_6 permeance ($\times 10^{-10}$ mol Pa^{-1} m^{-2} s^{-1})	C_3H_6/C_3H_8 separation factor
ZIF-67	0.7	460.8 ± 56.1	84.8 ± 6.2
ZIF-8/ZIF-67*	1.0	370.0 ± 33.7	209.1 ± 8.5
ZIF-67/ZIF-67*	1.5	309.0 ± 10.9	163.2 ± 30.9

Table 6.3 Summary on the binary propylene/propane performances of reported ZIF-8 membranes. Asterisks indicate performance data obtained from single gas permeation tests. The thickness of some ZIF-8 membranes could not be defined due to a lack of sharp boundaries between substrates and membranes.

Substrate	Thickness (µm)	C_3H_6 permeance (x 10^{-10} mol/m^2 s Pa)	C_3H_6 permeability (Barrer)	C_3H_6/C_3H_8 separation factor	Reference
α-Al$_2$O$_3$ disk	2.2	278.2 ± 63.9	182.8 ± 42.0	34.6 ± 6.4	Pan et al[35]
	1.5	212.7 ± 29.5	95.2 ± 13.2	50.0 ± 4.6	Kwon et al[32]
	1.5	207.7 ± 6.5	93.1 ± 2.9	40.4 ± 8.4	Kwon et al[34]
	2.5	140.0 ± 5.8	104.5 ± 4.3	32.7 ± 2.4	
	2.5	122 ± 25.5	91.0 ± 19.0	28.6 ± 2.0	Liu et al[36]
α-Al$_2$O$_3$ tube	80	25.0	597.0	59.0	*Hara et al[37]
α-Al$_2$O$_3$ tube	30	11.0	98.5	135.0	*Hara et al[40]
α-Al$_2$O$_3$ disk	0.8	268.5 ± 12.0	64.1 ± 2.9	70.6 ± 11.1	Kwon et al[33]
	0.8	537.6 ± 29.1	128.4 ± 6.9	22.4 ± 1.8	
	X	394.5 ± 60.1	X	28.0 ± 5.8	
	X	267.5 ± 8.9	X	38.0 ± 1.1	
	X	307.7 ± 63.2	X	33.10 ± 5.2	
	X	267.5 ± 8.9	X	38.0 ± 1.1	
	X	195.0 ± 0.1	X	39.7 ± 9.3	
Polymer HF	8.8	90.4 ± 10.0	237.6 ± 26.4	12.0 ± 3.0	Brown et al[38]
α-Al$_2$O$_3$ tube	30	52.0	465.7	7.2	*Hara et al[39]
	20	120.0	716.4	20.0	
	X	390.0	X	6.9	

crystallographically determined pore apertures show negligible difference between ZIF-8 and ZIF-67 (Table 6.1), the IR band corresponding to the metal-nitrogen stretching frequency in ZIF-67 (ν_{Co-N}) is blue-shifted as compared to the one in ZIF-8 (ν_{Zn-N}) (Figure 6.15(a)). This blue shift implies that Co-N bonds are more rigid (i.e., stiffer connectivity) than Zn-N bonds. Figure 6.15(b) and (c) compares the ^{13}C and ^{15}N NMR spectra of ZIF-8 and ZIF-67. The resonance peaks of ZIF-67 are notably downshifted when compared to ZIF-8, which is attributed to the higher electronegativity of cobalt than zinc (1.88 (cobalt) vs 1.65 (zinc)). This implies that Co-N bonds are more ionic than Zn-N bonds, therefore stiffer, consistent with the IR results. Furthermore, both of the ^{13}C and ^{15}N NMR peaks of ZIF-67 are substantially broader than those of ZIF-8 primarily due to the shielding effect of the unpaired electrons of Co^{2+}.[173] Considering the fact that the effective pore aperture of ZIFs depends on the magnitude of ligand flipping motion,[174] it is not unreasonable to surmise that the more rigid the metal-nitrogen connectivity is, the less the degree of the ligand flipping motion is. This restricted motion might lead to the slightly smaller effective pore aperture of ZIF-67 and consequently improved separation factors. At this point, it is worthy of mentioning that our attempts to determine the diffusion coefficients of propylene and propane in ZIF-67 using kinetic sorption measurements failed to lead to any meaningful data (not shown here) mainly owning to 1) the insufficient size of ZIF-67 crystals (short diffusion time scale) and 2) the rather wide size distribution. Further studies on the measurement of diffusion coefficients using PFG-NMR[175] and IR microimaging[176] are, however,
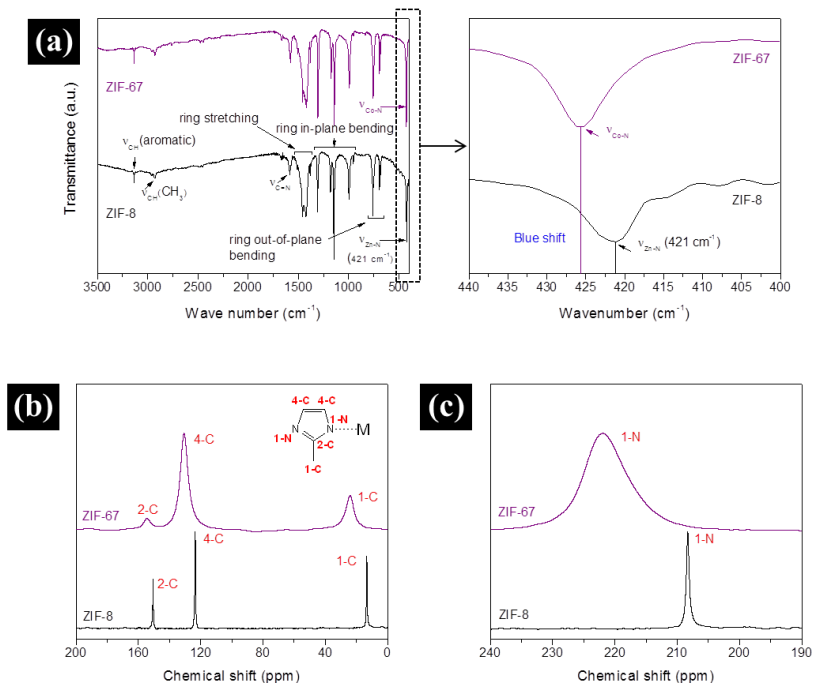
Figure 6.15 FT**-**IR (a) and ^{13}C (b) and ^{15}N (c) NMR spectra of ZIF-8 and ZIF-67 powders.

essential and currently underway in collaborations to elucidate the mechanisms by which ZIF-67 membranes perform better than ZIF-8 membranes.

    The presence of an organic solvent (methanol) in an aqueous precursor solution was found critical to assure the quality and reproducibility of ZIF-67 membranes. In the absence of methanol, the membranes not only grew thicker (1.8 μm) (Figure 6.16) but also formed visible white spots containing pinhole defects in an uncontrolled manner (Figure 6.17). These ZIF-67 membranes show comparatively low permeance and poor reproducibility in general as shown in Table 6.4.
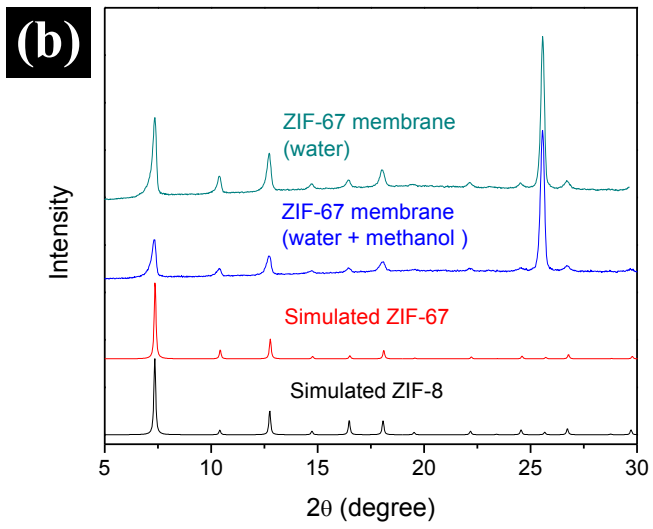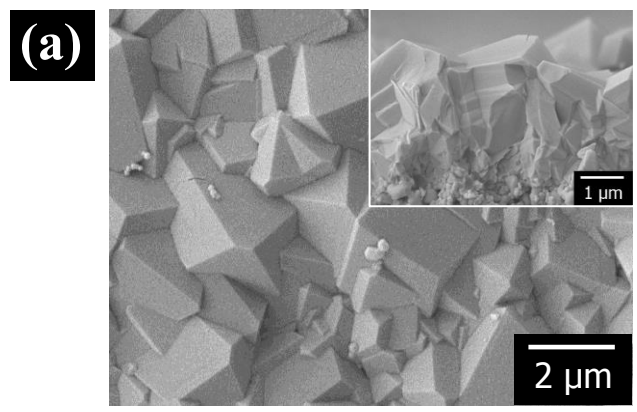
Figure 6.16 An electron micrograph of a ZIF-67 membrane prepared in water alone (a); XRD patterns of ZIF-67 membranes prepared in water alone and water with methanol co-solvent (b).
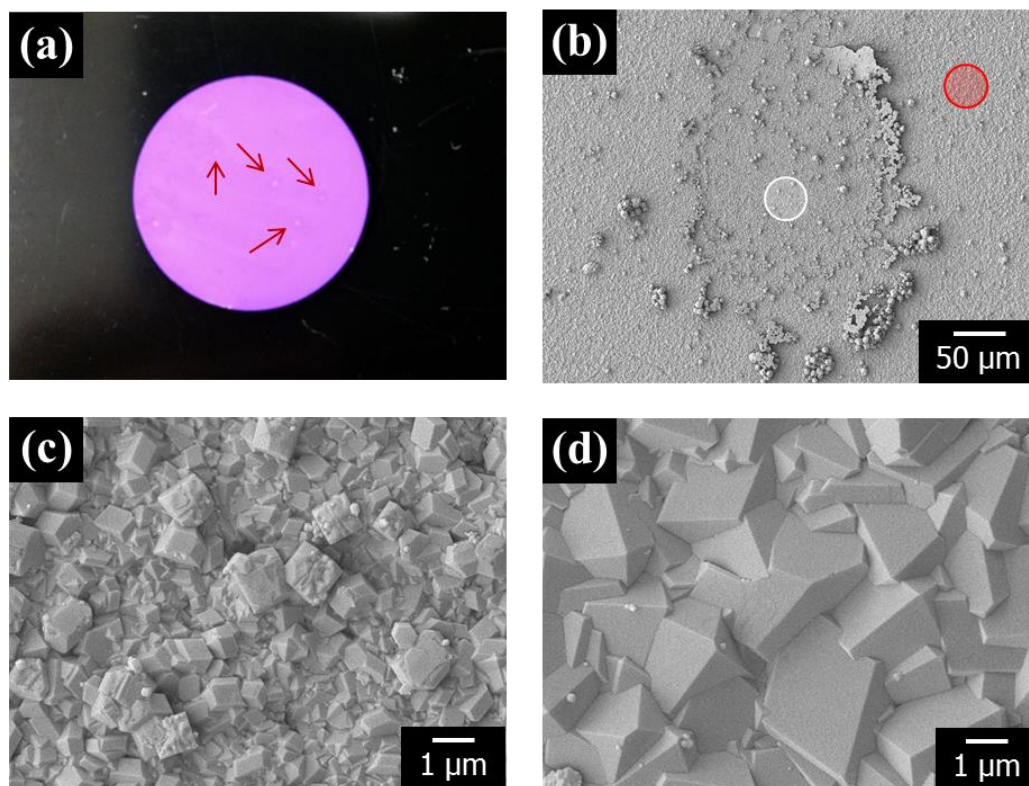
Figure 6.17 An optical micrograph of a ZIF-67 membrane grown in water (a); an electron micrograph of white spots (defects) marked by arrows on (a) (b) and magnified electron micrographs of the areas highlighted with white (c) and red circles (d) on (b).

Table 6.4 Room temperature binary propylene/propane separation performance of ZIF-67 membranes grown in water without methanol co-solvent.

Membrane	C_3H_6 permeance (X 10^{-10} mol/m^2 s Pa)	C_3H_6/C_3H_8 separation factor
M1	406.6	7.9
M2	136.0	80.3
M3	245.2	15.3
M4	174.2	163.7
M5	130.4	65.6
M6	121.3	132.3
M7	127.4	14.2
M8	220.2	19.7

Interestingly, remarkable enhancement in the propylene/propane separation factors was observed upon the addition of a ZIF-8 overlayer (~ 300 nm) on ZIF-67 membranes by a tertiary growth (Table 6.2 and Figure 6.18(a)). The average propylene/propane separation factor of ~ 190 was obtained after 2 h of the measurement. As shown in Figure 6.19(a), however, the propylene permeance gradually decreases as the measurement time increases, consequently resulting in the decrease in propylene/propane separation factors, approximately 36 % and 38 % reduction in the permeance and separation factor, respectively, after 70 h of the on-stream measurement. In contrast, both ZIF-8 and ZIF-67 membranes showed relatively stable performances throughout the measurements (Figure 6.20). X-ray diffraction patterns of the membranes
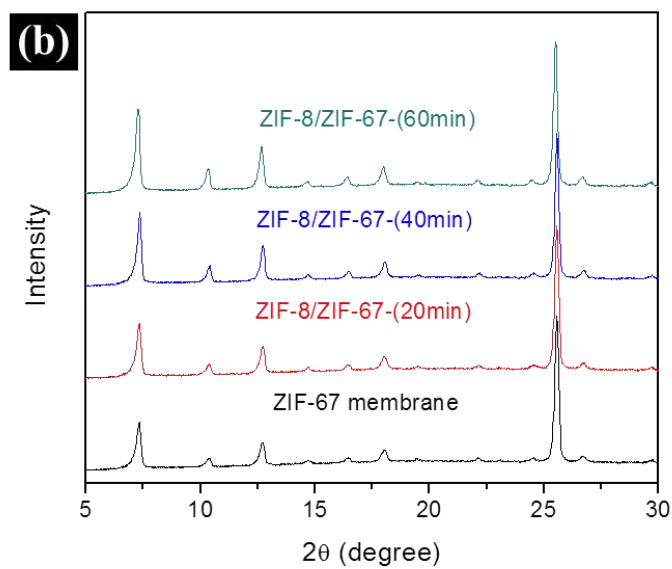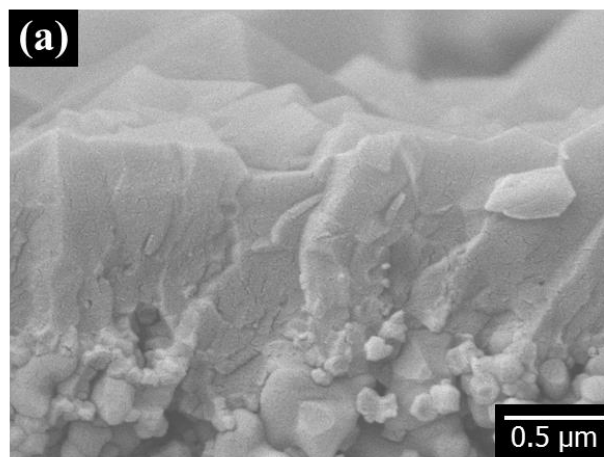
Figure 6.18 An electron micrograph of a ZIF-8/ZIF-67 membrane with a ZIF-8 layer grown for 20 min (a); XRD patterns of ZIF-8/ZIF-67 membranes with ZIF-8 layers grown as a function of time (b).

160
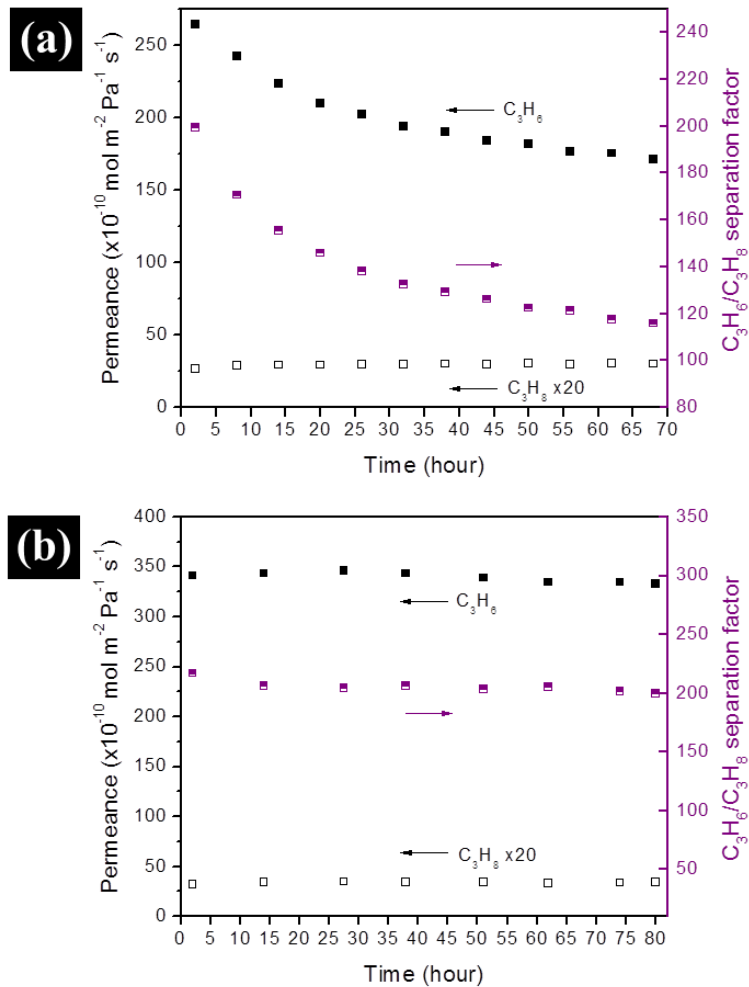
Figure 6.19 On-stream propylene/propane separation performances of ZIF-8/ZIF-67 membranes with ZIF-67 layers (a) before and (b) after hydrothermal ligand treatment prior to the tertiary growth of a ZIF-8 layer.
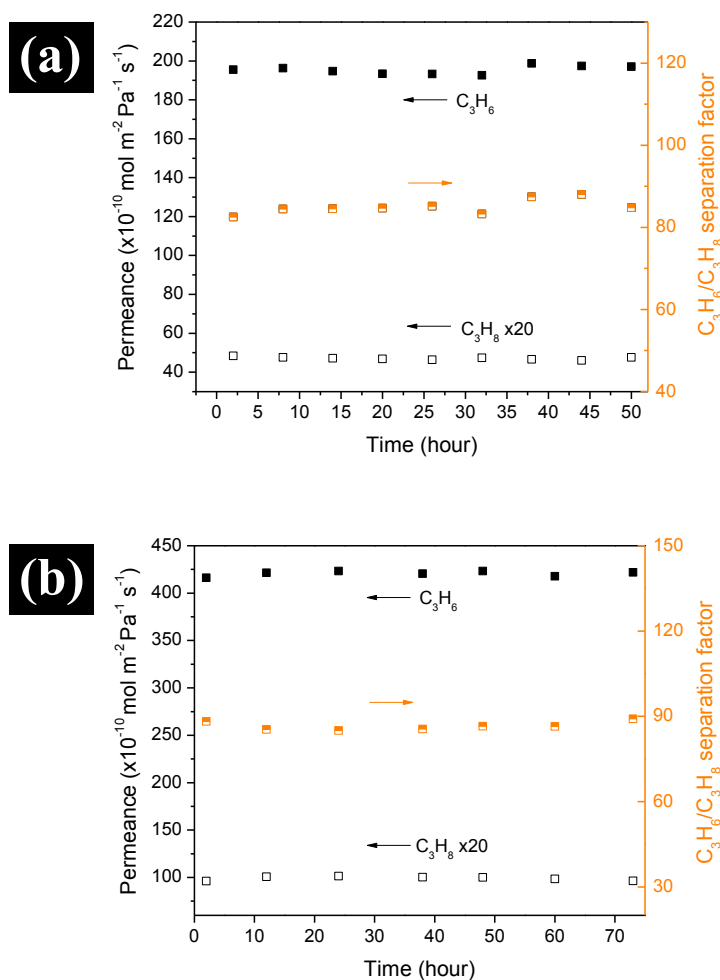
Figure 6.20 On-stream propylene/propane separation performances of ZIF-8 (a) and ZIF-67 (b) membranes under ambient conditions. The ZIF-8 membrane was secondarily grown on a ZIF-8 seed layer prepared by a microwave-seeding. Note that the performances of both membranes are stable unlike tertiarily grown ZIF-67 membranes (i.e., ZIF-8/ZIF-67 and ZIF-67/ZIF-67 membranes), strongly suggesting the unstable permeation behavior stems from the tertiary growth

162

before and after the measurement indicate the overall crystallinity of the samples was preserved (Figure 6.21). Furthermore, N_2 adsorption measurements on ZIF-8 and ZIF-67 powder samples show no appreciable pore structure change after being exposed to the propylene/propane mixture stream over 5 days (Figure 6.22). Since both X-ray diffraction and N_2 adsorption analyses give average structural information, however, it is not possible to rule out the local structure change during the permeation measurements. It is our hypothesis that local defects such as under-saturated metal (Co) sites[177-179] might have been generated during the heteroepitaxial tertiary growth of the ZIF-8 overlayer and the local structure might have been modified during the measurements, causing the performance instability.

By treating a secondarily-grown ZIF-67 layer hydrothermally with an aqueous ligand solution prior to the tertiary growth of a ZIF-8 overlayer, the performance of ZIF-8/ZIF-67 membranes was stabilized (Figure 6.19(b)). Notably, after the ligand treatment, the propylene permeance amounted to $\sim 370 \times 10^{-10}$ mol Pa^{-1} $m^{-2}s^{-1}$ while the propylene/propane separation factors remained high (~ 200). The propylene/propane separation factor of ~ 200 is unprecedented. The ligand treatment neither compromised the crystallinity of the ZIF-67 layer nor changed the thickness of final ZIF-8/ZIF-67 membranes (Figure 6.23). It is hypothesized that the surface defects of ZIF-67 layers were likely healed during the hydrothermal ligand treatment, minimizing defect sites possibly at the interface between ZIF-8 and ZIF-67 layers as well as at the grain boundary, thereby stabilizing the membrane performance. ^{13}C NMR spectra of ZIF-67
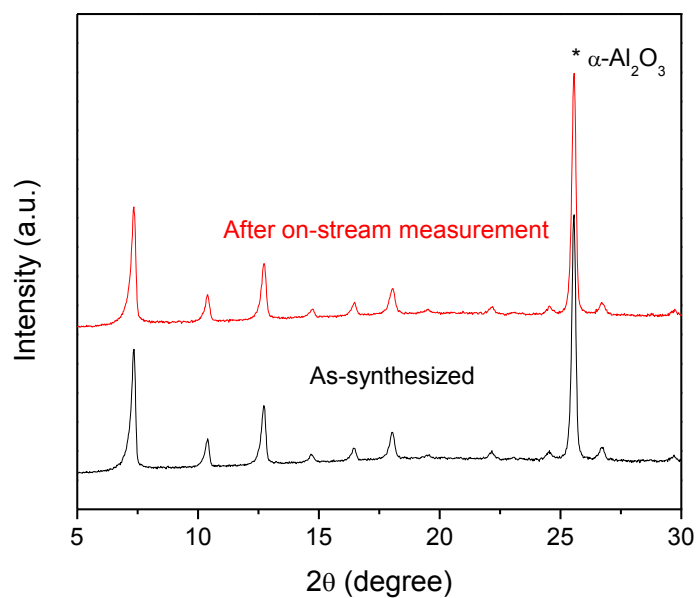
Figure 6.21 XRD patterns of a ZIF-8/ZIF-67 membrane prepared with a ZIF-67 layer which was not treated hydrothermally in an aqueous ligand solution before and after the on-stream measurement.
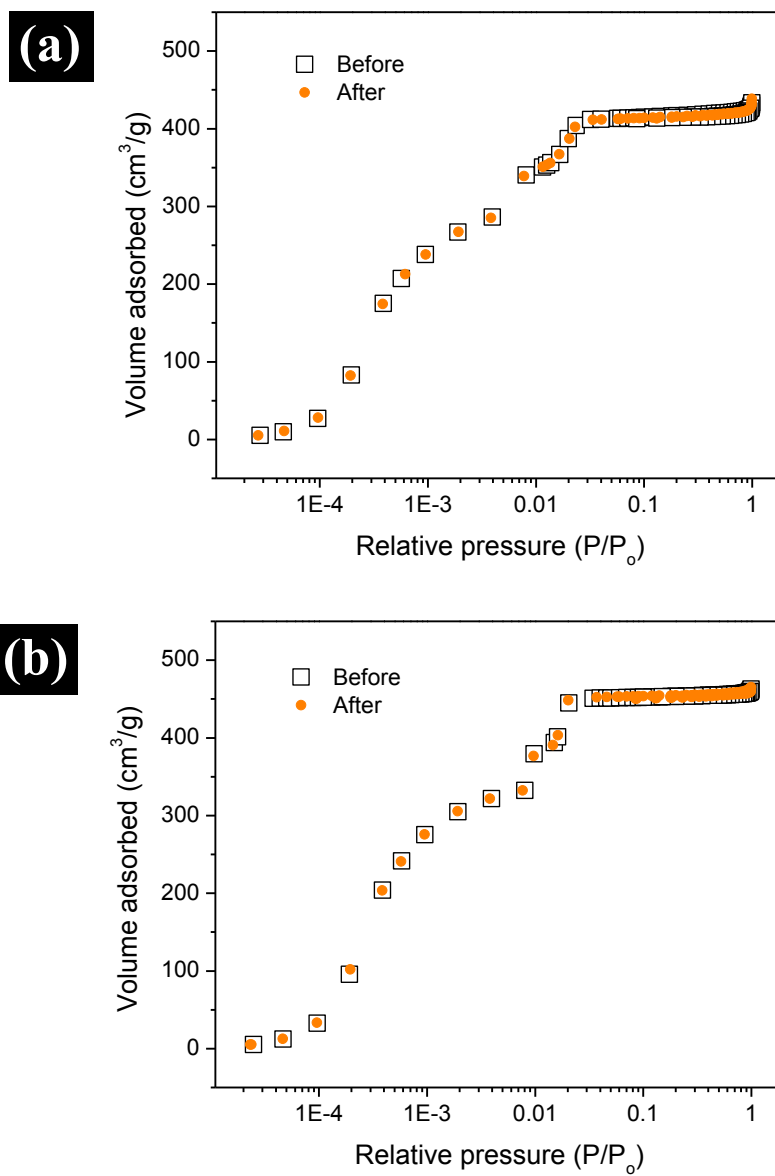
Figure 6.22 N$_2$ adsorption measurements of ZIF-8 (a) and ZIF-67 (b) powders collected from the membrane growth solutions before and after exposed to the binary propylene/propane mixture stream over 5 days.
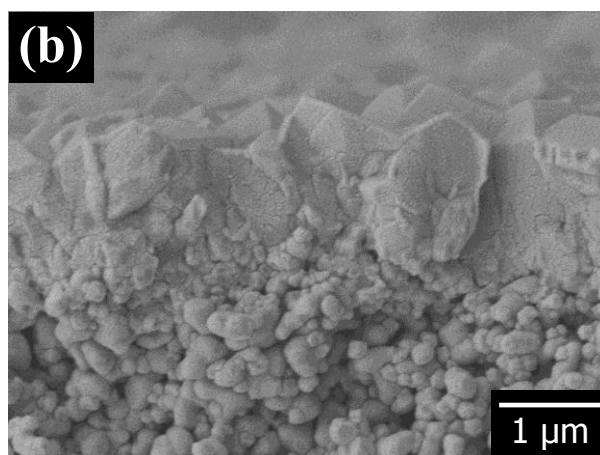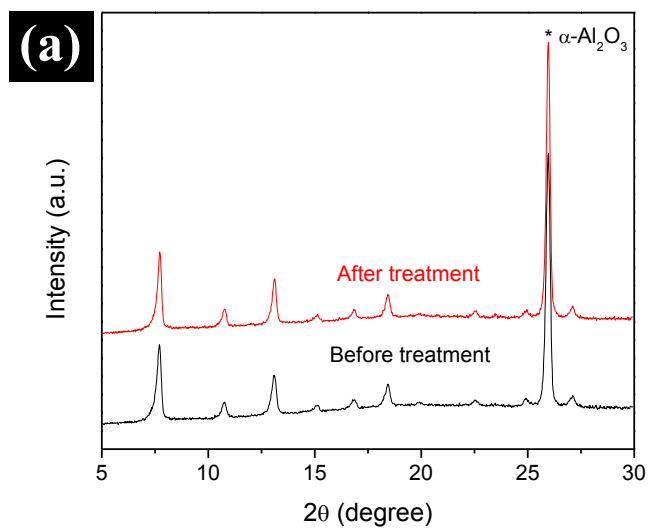
Figure 6.23 XRD patterns of a ZIF-67 membrane before and after the hydrothermal ligand treatment (a); an electron micrograph of a ZIF-8/ZIF-67 membrane with the ligand-treated ZIF-67 layer (b).

166

powders (Figure 6.24) revealed peak sharpening after the ligand treatment, implying the increased uniformity of carbon environments due to reduced defect sites.

Lastly, it was found that this ligand treatment/tertiary growth effect (i.e., enhancing and stabilizing membrane performance) was not specific to ZIF-8 overlayers as verified in that ZIF-67/ZIF-67 membranes (i.e., ZIF-67 membranes with ZIF-67 overlayers)) exhibited not only enhancement in the separation factors but also stabilization in the membrane performance (see Table 6.2 and Figure 6.25). It should be noted that ZIF-67/ZIF-67 membranes showed a much larger sample-to-sample variation than ZIF-8/ZIF-67 membranes. This result implies that the grain boundary structure of ZIF-67 membranes was further improved due to the tertiary growth of overlayers (whether ZIF-8 or ZIF-67). Improved grain boundary structure alone might not account for the significantly enhanced separation performance (from ~ 85 to ~ 200), given the expected propylene/propane diffusion separation factor of 125 ~ 145.[31,128] It is reasonable to expect that the selective intracrystalline transport pathway of ZIF-67, which might be inherently better than that of ZIF-8 as hypothesized and discussed earlier, became more important than the non-selective intercrystalline pathway (i.e., transport through grain boundary), thereby resulting in dramatic increase of propylene/propane separation performance. In other words, as the intercrystalline transport resistance becomes larger, the intracrystalline transport resistance becomes more important for the overall resistance in the resistances-in-parallel model. Furthermore, forming ZIF-8 overlayers on ZIF-8 membranes by the tertiary growth did not result in as much improvement as ZIF-67 membranes (not shown here). These

After ligand treatment

Before ligand treatment

160   120   80   40   0

Chemical shift (ppm)
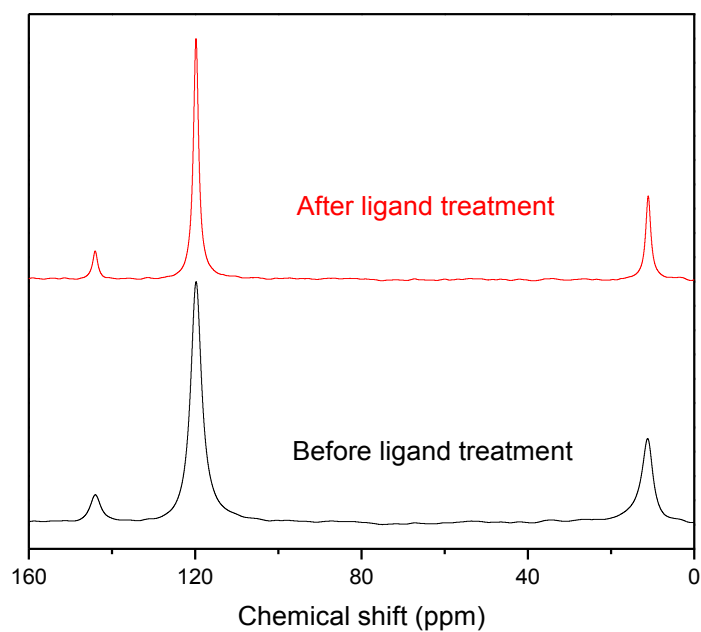
Figure 6.24 ^{13}C NMR spectra of ZIF-67 powder collected from the membrane growth solution before and after being treated hydrothermally with an aqueous ligand solution
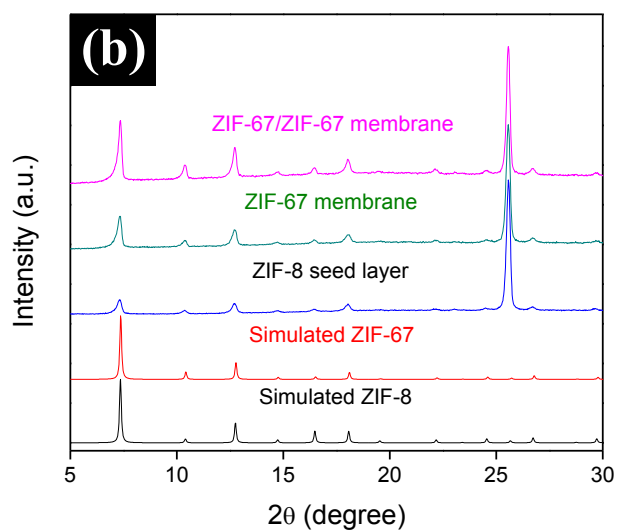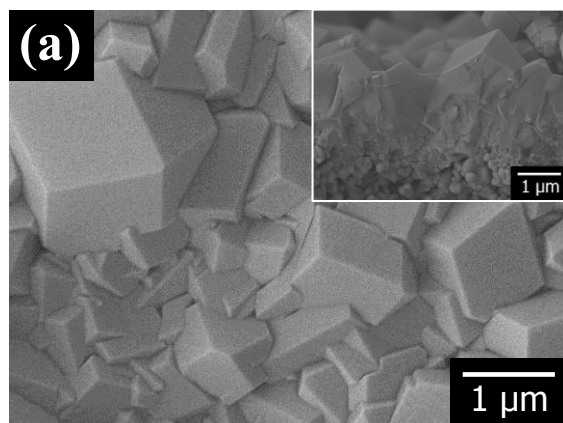
Figure 6.25 Electron micrographs (a) and XRD patterns (b) of a ZIF-67/ZIF-67 membrane. The membrane was prepared by consecutively growing a ZIF-67 layer on a ZIF-67 membrane.

observations strengthen our hypothesis that ZIF-67 might be inherently more propylene-selective than ZIF-8.

Lastly, Figure 6.26 compares the propylene/propane separation performances of our ZIF membranes with those membranes previously reported. As shown in the figure, our membranes satisfy the proposed performance criteria[1] (a minimum permeability of 1 Barrer and selectivity of 35) for commercial applications. More importantly, both of our ZIF-67 and ZIF-8/ZIF-67 membranes significantly outperform polymer and carbon molecular sieve membranes as well as polycrystalline membranes such as zeolite and ZIF-8.
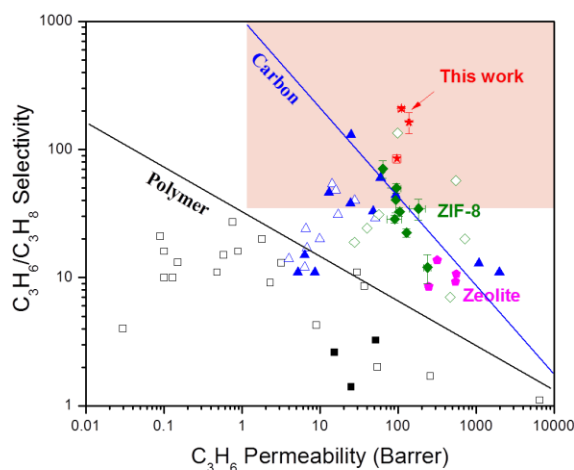
Figure 6.26 Comparison of the propylene/propane separation performances with previously reported membranes. Open and closed symbols denote separation data obtained from single and binary gas permeation tests, respectively. Rectangle: polymer membranes;[2] triangle: carbon membranes;[4-6,149] pentagon: zeolite membranes;[150] rhombus: ZIF-8 membranes;[32-40] star: this work.

170

6.4 Conclusions

Here, for the first time, we have successfully applied the heteroepitaxial growth to prepare well-intergrown ZIF-67 and ZIF-8/ZIF-67 membranes displaying exceptional propylene/propane separation performance. The heteroepitaxial growth between ZIF-8 and ZIF-67 was unambiguously determined. Strongly-attached and densely-packed ZIF-8 seed crystals were found essential to heteroepitaxially prepare ZIF-67 membranes. In addition, the presence of a methanol co-solvent in the ZIF-67 secondary growth solution led to the reduction in the membrane thickness as well as to the enhancement in the reproducibility. The resulted sub-micron thick ZIF-67 membranes displayed an outstanding binary propylene/propane separation performance (average propylene permeance of $\sim$ 460 $\times 10^{-10}$ mol Pa^{-1} m^{-2}s^{-1} and average separation factor of $\sim$ 85), outperforming almost all of the previously reported ZIF-8 membranes. Furthermore, the tertiary heteroepitaxial growth of ZIF-8 layers on ZIF-67 membranes stabilized by hydrothermally treating in a ligand solution resulted in unprecedentedly high propylene/propane separation factor of $\sim$ 200. Heteroepitaxially-grown ZIF membranes with remarkable propylene/propane separation performances are a significant step forward for bringing membrane-based propylene/propane separation close to the commercial applications.

CHAPTER VII

CONCLUSIONS AND FUTURE DIRECTIONS

7.1 Conclusions

In this dissertation, we successfully devised three different synthesis techniques of ZIF membranes which are either secondary or *in situ* growth methods. Two of prototypical ZIFs such as ZIF-8 and ZIF-67, which are capable of separating propylene/propane mixtures based on the molecular sieving effect, were used as material platforms to validate the developed techniques.

The first technique was a new microwave-assisted rapid seeding method that enables rapid formation of nanosized seed crystals strongly attached on porous supports with uniform and high surface coverage in a couple of minutes, which is delineated in Chapter III. The key step in this method is to saturate porous supports with metal ions prior to the microwave irradiation in a ligand solution. The strong absorption of microwave energy by metal ions inside support along with the concentration of microwave energy on the support surface rapidly increase the local temperature of the supports, resulting in the rapid heterogeneous nucleation and growth of ZIF-8 nanocrystals. Subsequent secondary growth of these ZIF-8 seed layers led to well-intergrown ZIF-8 membranes, which have shown an excellent propylene/propane separation performance. Our rapid microwave-assisted seeding in combination with secondary growth led to the successful synthesis of well-intergrown membranes of other

ZIFs including ZIF-7 and SIM-1, suggesting the feasibility of its potentially general applicability.

The second technique was a one-step *in situ* synthesis method for high-quality MOF membranes based on the concept of counter diffusion, which is described in Chapter IV and V. This simple yet highly versatile method enabled the rapid preparation of well-intergrown ZIF-8 membranes with excellent microstructure in a couple of hours. The high-quality ZIF-8 membranes showed an excellent separation performance of a propylene/propane (50/50) mixture (selectivity ~70). Furthermore, the ZIF-8 membranes were found to be mechanically very strong with their separation performance maintained high even after 2 h of intensive sonication. The unique feature of the counter-diffusion concept allowed the poorly intergrown membranes to be healed. In addition, the costly precursor solutions can be recycled multiple times for membrane synthesis. Finally, prototypical ZIF-7 and SIM-1 membranes were also successfully synthesized using our method, proving its general applicability. Considering its unique features including postsynthetic healing and reduced precursor consumption, the simple general method reported here enabling the synthesis of high-quality MOF membranes with excellent microstructure offers unique opportunities for potential large-scale practical applications of MOF membranes.

The last technique was a heteroepitaxial growth method to prepare well-intergrown ZIF-67 and ZIF-8/ZIF-67 membranes displaying exceptional propylene/propane separation performance, which is elucidated in Chapter VI. The heteroepitaxial growth between ZIF-8 and ZIF-67 was unambiguously determined.

173

Strongly-attached and densely-packed ZIF-8 seed crystals were found essential to heteroepitaxially prepare ZIF-67 membranes. In addition, the presence of a methanol co-solvent in the ZIF-67 secondary growth solution led to the reduction in the membrane thickness as well as to the enhancement in the reproducibility. The resulted sub-micron thick ZIF-67 membranes displayed an outstanding binary propylene/propane separation performance (average propylene permeance of $\sim 460 \times 10^{-10}$ mol Pa^{-1} m^{-2}s^{-1} and average separation factor of $\sim$ 85), outperforming almost all of the previously reported ZIF-8 membranes. Furthermore, the tertiary heteroepitaxial growth of ZIF-8 layers on ZIF-67 membranes stabilized by hydrothermally treating in a ligand solution resulted in unprecedentedly high propylene/propane separation factor of $\sim$ 200. Heteroepitaxially-grown ZIF membranes with remarkable propylene/propane separation performances are a significant step forward for bringing membrane-based propylene/propane separation close to the commercial applications.

7.2   Future Directions

7.2.1   Moving toward commercial scale membrane applications

7.2.1.1   Testing the membranes at practical conditions

Although the reported membranes here showed impressive and promising potential for propylene/propane separations (e.g., S $\sim$ 200), the performances were measured somewhat under too ideal conditions (e.g., P $\sim$ 1bar, T $\sim$ room temperature). Therefore, to estimate their realistic potential before considering scale-up, the membranes need to be tested under practical field operating conditions (e.g., high

temperature, transmembrane pressure, and long-term period). As approximately suggested by UOP during the on-site meeting, the membranes needs to steadily operate under P ~ 10 bar and T ~ 90°C. In addition, apart from the operating conditions, since there always exist minor impurities in propylene/propane feed mixtures (e.g., water, and other long and short hydrocarbons), monitoring the membranes' performance and stability in the presence of impurities is also a very important research subject to implement.

7.2.1.2 Replacing ceramic substrates with cheaper polymeric hollow fibers

The expensive ceramic substrates have been one of major hurdles to the commercialization of polycrystalline membranes. If replaced with cheaper and more easily accessible polymeric substrates (e.g., polymer hollow fibers), enormous cost reduction in membrane manufacturing can be envisioned. However, the polymeric substrates have a couple of intrinsic issues hindering the substrate replacement: (1) they are not mechanically and chemically durable to withstand harsh conventional solvothermal/hydrothermal membrane synthesis conditions, and (2) the flexible nature of them can easily generate cracks on the rigid polycrystalline membranes during handling (e.g. modulation). These issues might be able to be circumvented. First, although the recipe is not optimized yet, the counter-diffusion-based *in situ* method can produce ZIF-8 membranes and others even at room temperature (not shown in this dissertation). Therefore the polymeric substrates do not need to endure harsh solvothermal/hydrothermal conditions. Second, if we modulate the polymeric substrates

first, which eliminates later handing issues and further reinforces the mechanical strength of the polymeric substrates, and conduct membrane synthesis, the issue (2) also might be avoidable.

7.2.2 Improving and enhancing membrane performance further

7.2.2.1 Pore engineering

As we observed in Chapter VI, by constructing ZIF-8 with more electronegative cobalt instead of zinc, the resulted membranes displayed dramatic performance enhancement possibly due to reduced pore aperture (more corroboration is required). This implies that if we construct frameworks with the combination of zinc and other divalent metals (e.g., cobalt and cadmium) and vary the composition continuously, it might be possible to obtain ZIF materials with a continuous spectrum of properties (e.g., pore aperture and surface properties), which might enable to customize the framework properties for aimed separations. The same principle also goes to mixed ligand frameworks. However, as briefly reviewed in Chapter II, because the nature of ligand and metal both are important synthesis variables which can alter final framework topology, it is imperative to select metal or ligand pairs which are compatible in a single framework in a wide range.

7.2.2.2 Postsynthetic modifications

Due to the labile nature of coordination chemistry of ZIFs, the properties of ZIFs can be modified in postsynthetic ways (e.g., metal and/or ligand exchange, and covalent

chemistry on organic ligands). Although these postsynthetic modifications have already been proven promising in various MOFs and ZIFs, the majority of the demonstrations were conducted with MOF/ZIF powders and there are negligible cases of them on ZIF membranes. Via the successful demonstration of postsynthetic modifications on ZIF membranes, we might assign new functions or enhance intrinsic properties deficient to parent ZIF membranes (e.g., pore aperture reduction, surface affinity modification, and multifunctional multilayer membranes) which cannot be achieved via direct synthesis. One of successful examples which are an ongoing project in our laboratory is schematically illustrated in Figure 7.1.
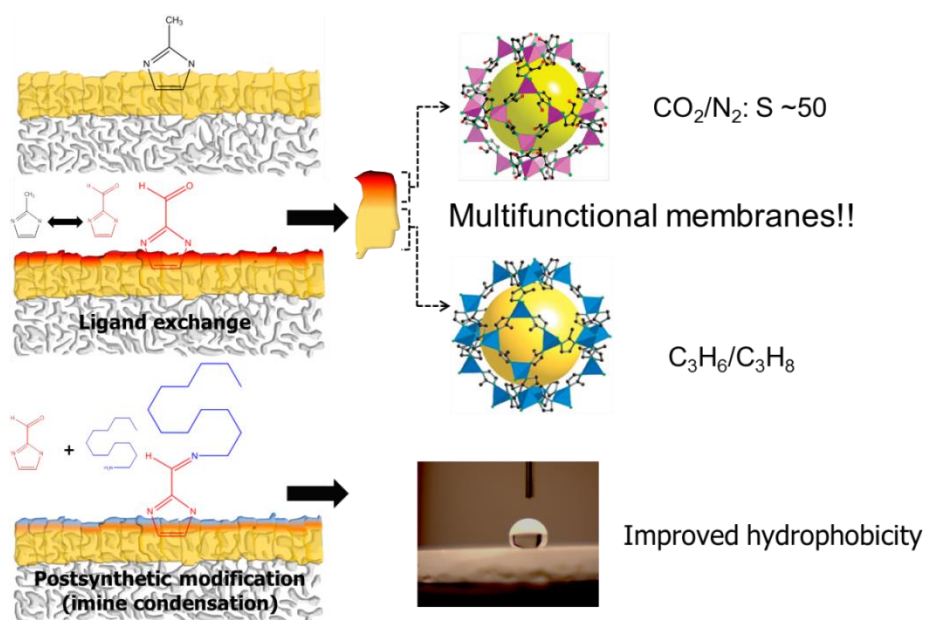
Figure 7.1 An example of postsynthetic modifications on ZIF-8 membranes which are currently underway in our laboratory.

REFERENCES

(1)   Colling, C. W.; Huff, G. A.; Bartels, J. V. *US patent* 20040004040 A1.

(2)   Burns, R. L.; Koros, W. J. *Journal of Membrane Science* 2003, *211*, 299.

(3)   Giannakopoulos, I. G.; Nikolakis, V. *Industrial & Engineering Chemistry Research* 2005, *44*, 226.

(4)   Chng, M. L.; Xiao, Y.; Chung, T.-S.; Toriida, M.; Tamai, S. *Carbon* 2009, *47*, 1857.

(5)   Okamoto, K.-i.; Kawamura, S.; Yoshino, M.; Kita, H.; Hirayama, Y.; Tanihara, N.; Kusuki, Y. *Industrial & Engineering Chemistry Research* 1999, *38*, 4424.

(6)   Hayashi, J.-i.; Mizuta, H.; Yamamoto, M.; Kusakabe, K.; Morooka, S.; Suh, S.-H. *Industrial & Engineering Chemistry Research* 1996, *35*, 4176.

(7)   Zhang, C.; Dai, Y.; Johnson, J. R.; Karvan, O.; Koros, W. J. *Journal of Membrane Science* 2012, *389*, 34.

(8)   Takht Ravanchi, M.; Kaghazchi, T.; Kargari, A. *Desalination* 2009, *235*, 199.

(9)   Ferey, G. *Chemical Society Reviews* 2008, *37*, 191.

(10)   Perry Iv, J. J.; Perman, J. A.; Zaworotko, M. J. *Chemical Society Reviews* 2009, *38*, 1400.

(11)   Rowsell, J. L. C.; Yaghi, O. M. *Microporous and Mesoporous Materials* 2004, *73*, 3.

(12)   Haldoupis, E.; Nair, S.; Sholl, D. S. *Journal of the American Chemical Society* 2010, *132*, 7528.

(13)   Li, J.-R.; Kuppler, R. J.; Zhou, H.-C. *Chemical Society Reviews* 2009, *38*, 1477.

(14)   Shah, M.; McCarthy, M. C.; Sachdeva, S.; Lee, A. K.; Jeong, H.-K. *Industrial & Engineering Chemistry Research* 2012, *51*, 2179.

(15)   Park, K. S.; Ni, Z.; Côté, A. P.; Choi, J. Y.; Huang, R.; Uribe-Romo, F. J.; Chae, H. K.; O'Keeffe, M.; Yaghi, O. M. *Proceedings of the National Academy of Sciences* 2006, *103*, 10186.

(16)   Hayashi, H.; Cote, A. P.; Furukawa, H.; O/'Keeffe, M.; Yaghi, O. M. *Nat Mater* 2007, *6*, 501.

(17)   Banerjee, R.; Phan, A.; Wang, B.; Knobler, C.; Furukawa, H.; O'Keeffe, M.; Yaghi, O. M. *Science* 2008, *319*, 939.

(18)   Bux, H.; Liang, F.; Li, Y.; Cravillon, J.; Wiebcke, M.; Caro, J. *Journal of the American Chemical Society* 2009, *131*, 16000.

(19)   Li, Y.-S.; Bux, H.; Feldhoff, A.; Li, G.-L.; Yang, W.-S.; Caro, J. *Advanced Materials* 2010, *22*, 3322.

(20)   Liu, Y.; Hu, E.; Khan, E. A.; Lai, Z. *Journal of Membrane Science* 2010, *353*, 36.

(21)   Huang, A.; Bux, H.; Steinbach, F.; Caro, J. *Angewandte Chemie International Edition* 2010, *49*, 4958.

(22)   Venna, S. R.; Carreon, M. A. *Journal of the American Chemical Society* 2010, *132*, 76.

(23)   McCarthy, M. C.; Varela-Guerrero, V.; Barnett, G. V.; Jeong, H.-K. *Langmuir* 2010, *26*, 14636.

(24) Li, Y.; Liang, F.; Bux, H.; Yang, W.; Caro, J. *Journal of Membrane Science* 2010, *354*, 48.

(25) Dong, X.; Lin, Y. S. *Chemical Communications* 2013, *49*, 1196.

(26) Dong, X.; Huang, K.; Liu, S.; Ren, R.; Jin, W.; Lin, Y. S. *Journal of Materials Chemistry* 2012, *22*, 19222.

(27) Huang, A.; Dou, W.; Caro, J. *Journal of the American Chemical Society* 2010, *132*, 15562.

(28) Huang, A.; Chen, Y.; Wang, N.; Hu, Z.; Jiang, J.; Caro, J. *Chemical Communications* 2012, *48*, 10981.

(29) Aguado, S.; Nicolas, C.-H.; Moizan-Basle, V.; Nieto, C.; Amrouche, H.; Bats, N.; Audebrand, N.; Farrusseng, D. *New Journal of Chemistry* 2011, *35*, 41.

(30) Yao, J.; Wang, H. *Chemical Society Reviews* 2014, *43*, 4470.

(31) Zhang, C.; Lively, R. P.; Zhang, K.; Johnson, J. R.; Karvan, O.; Koros, W. J. *The Journal of Physical Chemistry Letters* 2012, *3*, 2130.

(32) Kwon, H. T.; Jeong, H.-K. *Journal of the American Chemical Society* 2013, *135*, 10763.

(33) Kwon, H. T.; Jeong, H.-K. *Chemical Engineering Science* 2015, *124*, 20.

(34) Kwon, H. T.; Jeong, H.-K. *Chemical Communications* 2013, *49*, 3854.

(35) Pan, Y.; Li, T.; Lestari, G.; Lai, Z. *Journal of Membrane Science* 2012, *390*, 93.

(36) Liu, D.; Ma, X.; Xi, H.; Lin, Y. S. *Journal of Membrane Science* 2014, *451*, 85.

(37) Hara, N.; Yoshimune, M.; Negishi, H.; Haraya, K.; Hara, S.; Yamaguchi, T. *Journal of Membrane Science* 2014, *450*, 215.

(38)   Brown, A. J.; Brunelli, N. A.; Eum, K.; Rashidi, F.; Johnson, J. R.; Koros, W. J.; Jones, C. W.; Nair, S. *Science* 2014, *345*, 72.

(39)   Hara, N.; Yoshimune, M.; Negishi, H.; Haraya, K.; Hara, S.; Yamaguchi, T. *Microporous and Mesoporous Materials* 2015, *206*, 75.

(40)   Hara, N.; Yoshimune, M.; Negishi, H.; Haraya, K.; Hara, S.; Yamaguchi, T. *Journal of Chemical Engineering of Japan* 2014, *47*, 770.

(41)   Shah, M.; Kwon, H. T.; Tran, V.; Sachdeva, S.; Jeong, H.-K. *Microporous and Mesoporous Materials* 2013, *165*, 63.

(42)   Plotkin, J. S. *Catal. Today* 2005, *106*, 10.

(43)   Nexant *Evolving propylene sources: solution to supply shortages*, 2012, http://thinking.nexant.com/sites/default/files/report/field_attachment_prospectus/201201 /STMC11_Evolving_Propylene_Pros.pdf

(44)   booz&co. *Future of Chemicals: rebalancing global feedstock disruptions with "on-purpose" technologies*, 2012, http://www.strategyand.pwc.com/global/home/what-we-think/reports-white-papers/article-display/rebalancing-global-petrochemicals-markets-purpose

(45)   Zinger, S. In *the CMAI World Petrochemical Conference, Houston* 2005.

(46)   Da Silva, F. A.; Rodrigues, A. E. *Industrial & Engineering Chemistry Research* 1999, *38*, 2051.

(47)   Eldridge, R. B. *Industrial & Engineering Chemistry Research* 1993, *32*, 2208.

(48)   Baker, R. W. *Industrial & Engineering Chemistry Research* 2002, *41*, 1393.

(49)   Rungta, M.; Zhang, C.; Koros, W. J.; Xu, L. *AIChE Journal* 2013, *59*, 3475.

(50)   Dimitrios, P. T. *Extractive and Azeotropic Distillation*; *American Chemical Society*, 1974; Vol. 115.

(51)   Rege, S. U.; Padin, J.; Yang, R. T. *AIChE Journal* 1998, *44*, 799.

(52)   Silva, F. A. D.; Rodrigues, A. E. *AIChE Journal* 2001, *47*, 341.

(53)   Grande, C. A.; Rodrigues, A. E. *Industrial & Engineering Chemistry Research* 2005, *44*, 8815.

(54)   Ferreira, A. F. P.; Santos, J. C.; Plaza, M. G.; Lamia, N.; Loureiro, J. M.; Rodrigues, A. E. *Chemical Engineering Journal* 2011, *167*, 1.

(55)   Phan, A.; Doonan, C. J.; Uribe-Romo, F. J.; Knobler, C. B.; O'Keeffe, M.; Yaghi, O. M. *Accounts of Chemical Research* 2010, *43*, 58.

(56)   Chen, B.; Yang, Z.; Zhu, Y.; Xia, Y. *Journal of Materials Chemistry A* 2014, *2*, 16811.

(57)   Morris, W.; He, N.; Ray, K. G.; Klonowski, P.; Furukawa, H.; Daniels, I. N.; Houndonougbo, Y. A.; Asta, M.; Yaghi, O. M.; Laird, B. B. *The Journal of Physical Chemistry C* 2012, *116*, 24084.

(58)   Babarao, R.; Dai, S.; Jiang, D.-e. *The Journal of Physical Chemistry C* 2011, *115*, 8126.

(59)   Zhang, J.-P.; Zhang, Y.-B.; Lin, J.-B.; Chen, X.-M. *Chemical Reviews* 2012, *112*, 1001.

(60)   Karagiaridi, O.; Lalonde, M. B.; Bury, W.; Sarjeant, A. A.; Farha, O. K.; Hupp, J. T. *Journal of the American Chemical Society* 2012, *134*, 18790.

(61)   Huang, X.-C.; Lin, Y.-Y.; Zhang, J.-P.; Chen, X.-M. *Angewandte Chemie International Edition* 2006, *45*, 1557.

(62)   Morris, W.; Leung, B.; Furukawa, H.; Yaghi, O. K.; He, N.; Hayashi, H.; Houndonougbo, Y.; Asta, M.; Laird, B. B.; Yaghi, O. M. *Journal of the American Chemical Society* 2010, *132*, 11006.

(63)   Park, K. S. *Design, Synthesis and Control of Topology and Properties of Zeolitic Imidazolate Frameworks and Metal-organic Frameworks Based on Pyrazolate*; ProQuest, 2008.

(64)   Wang, B.; Cote, A. P.; Furukawa, H.; O/'Keeffe, M.; Yaghi, O. M. *Nature* 2008, *453*, 207.

(65)   He, M.; Yao, J.; Liu, Q.; Zhong, Z.; Wang, H. *Dalton Transactions* 2013, *42*, 16608.

(66)   Biswal, B. P.; Panda, T.; Banerjee, R. *Chemical Communications* 2012, *48*, 11868.

(67)   Schweinefu; Springer, S.; Baburin, I. A.; Hikov, T.; Huber, K.; Leoni, S.; Wiebcke, M. *Dalton Transactions* 2014, *43*, 3528.

(68)   Tian, Y.-Q.; Cai, C.-X.; Ji, Y.; You, X.-Z.; Peng, S.-M.; Lee, G.-H. *Angewandte Chemie International Edition* 2002, *41*, 1384.

(69)   Liu, Y.; Kravtsov, V. C.; Larsen, R.; Eddaoudi, M. *Chemical Communications* 2006, 1488.

(70)   Cravillon, J.; Münzer, S.; Lohmeier, S.-J.; Feldhoff, A.; Huber, K.; Wiebcke, M. *Chemistry of Materials* 2009, *21*, 1410.

(71)   Pan, Y.; Liu, Y.; Zeng, G.; Zhao, L.; Lai, Z. *Chemical Communications* 2011, *47*, 2071.

(72)   Kida, K.; Okita, M.; Fujita, K.; Tanaka, S.; Miyake, Y. *CrystEngComm* 2013, *15*, 1794.

(73)   Li, Y.-S.; Liang, F.-Y.; Bux, H.; Feldhoff, A.; Yang, W.-S.; Caro, J. *Angewandte Chemie International Edition* 2010, *49*, 548.

(74)   Shieh, F.-K.; Wang, S.-C.; Leo, S.-Y.; Wu, K. C. W. *Chemistry – A European Journal* 2013, *19*, 11139.

(75)   Cravillon, J.; Nayuk, R.; Springer, S.; Feldhoff, A.; Huber, K.; Wiebcke, M. *Chemistry of Materials* 2011, *23*, 2130.

(76)   Gross, A. F.; Sherman, E.; Vajo, J. J. *Dalton Transactions* 2012, *41*, 5458.

(77)   Jian, M.; Liu, B.; Liu, R.; Qu, J.; Wang, H.; Zhang, X. *RSC Advances* 2015, *5*, 48433.

(78)   Diring, S.; Furukawa, S.; Takashima, Y.; Tsuruoka, T.; Kitagawa, S. *Chemistry of Materials* 2010, *22*, 4531.

(79)   Cravillon, J.; Schroder, C. A.; Bux, H.; Rothkirch, A.; Caro, J.; Wiebcke, M. *CrystEngComm* 2012, *14*, 492.

(80)   Schejn, A.; Balan, L.; Falk, V.; Aranda, L.; Medjahdi, G.; Schneider, R. *CrystEngComm* 2014, *16*, 4493.

(81)   Pan, Y.; Heryadi, D.; Zhou, F.; Zhao, L.; Lestari, G.; Su, H.; Lai, Z. *CrystEngComm* 2011, *13*, 6937.

(82)   Seoane, B.; Zamaro, J. M.; Tellez, C.; Coronas, J. *CrystEngComm* 2012, *14*, 3103.

(83)   Cho, H.-Y.; Kim, J.; Kim, S.-N.; Ahn, W.-S. *Microporous and Mesoporous Materials* 2013, *169*, 180.

(84)   Bao, Q.; Lou, Y.; Xing, T.; Chen, J. *Inorganic Chemistry Communications* 2013, *37*, 170.

(85)   Li, Y. S.; Bux, H.; Feldhoff, A.; Li, G. L.; Yang, W. S.; Caro, J. *Advanced Materials* 2010, *22*, 3322.

(86)   Liu, Y.; Zeng, G.; Pan, Y.; Lai, Z. *Journal of Membrane Science* 2011, *379*, 46.

(87)   Ban, Y.; Li, Y.; Liu, X.; Peng, Y.; Yang, W. *Microporous and Mesoporous Materials* 2013, *173*, 29.

(88)   Zhang, J. P.; Zhu, A. X.; Lin, R. B.; Qi, X. L.; Chen, X. M. *Advanced Materials* 2011, *23*, 1268.

(89)   Thompson, J. A.; Blad, C. R.; Brunelli, N. A.; Lydon, M. E.; Lively, R. P.; Jones, C. W.; Nair, S. *Chemistry of Materials* 2012, *24*, 1930.

(90)   Eum, K.; Jayachandrababu, K. C.; Rashidi, F.; Zhang, K.; Leisen, J.; Graham, S.; Lively, R. P.; Chance, R. R.; Sholl, D. S.; Jones, C. W. *Journal of the American Chemical Society* 2015, *137*, 4191.

(91)   Thompson, J. A.; Vaughn, J. T.; Brunelli, N. A.; Koros, W. J.; Jones, C. W.; Nair, S. *Microporous and Mesoporous Materials* 2014, *192*, 43.

(92)   Breck, D. W. *Zeolite molecular sieves*; Krieger, 1984.

(93)   Zhang, H.-X.; Liu, M.; Wen, T.; Zhang, J. *Coordination Chemistry Reviews* 2015.

(94)   Zhang, H.-X.; Wang, F.; Yang, H.; Tan, Y.-X.; Zhang, J.; Bu, X. *Journal of the American Chemical Society* 2011, *133*, 11884.

(95)   Wu, T.; Zhang, J.; Zhou, C.; Wang, L.; Bu, X.; Feng, P. *Journal of the American Chemical Society* 2009, *131*, 6111.

(96)   Wang, F.; Shu, Y. B.; Bu, X.; Zhang, J. *Chemistry-A European Journal* 2012, *18*, 11876.

(97)   Zhang, J.; Wu, T.; Zhou, C.; Chen, S.; Feng, P.; Bu, X. *Angewandte Chemie* 2009, *121*, 2580.

(98)   Kim, M.; Cahill, J. F.; Su, Y.; Prather, K. A.; Cohen, S. M. *Chemical Science* 2012, *3*, 126.

(99)   Karagiaridi, O.; Bury, W.; Sarjeant, A. A.; Stern, C. L.; Farha, O. K.; Hupp, J. T. *Chemical Science* 2012, *3*, 3256.

(100)   Liu, X.; Li, Y.; Ban, Y.; Peng, Y.; Jin, H.; Bux, H.; Xu, L.; Caro, J.; Yang, W. *Chemical Communications* 2013, *49*, 9140.

(101)   Fei, H.; Cahill, J. F.; Prather, K. A.; Cohen, S. M. *Inorganic chemistry* 2013, *52*, 4011.

(102)   Jiang, J.-Q.; Yang, C.-X.; Yan, X.-P. *Chemical Communications* 2015, *51*, 6540.

(103)   Lalonde, M. B.; Mondloch, J. E.; Deria, P.; Sarjeant, A. A.; Al-Juaid, S. S.; Osman, O. I.; Farha, O. K.; Hupp, J. T. *Inorganic chemistry* 2015, *54*, 7142.

(104)   Karagiaridi, O.; Bury, W.; Mondloch, J. E.; Hupp, J. T.; Farha, O. K. *Angewandte Chemie International Edition* 2014, *53*, 4530.

(105)   Morris, W.; Doonan, C. J.; Furukawa, H.; Banerjee, R.; Yaghi, O. M. *Journal of the American Chemical Society* 2008, *130*, 12626.

(106)   Huang, A.; Caro, J. *Angewandte Chemie International Edition* 2011, *50*, 4979.

(107)   Huang, A.; Wang, N.; Kong, C.; Caro, J. *Angewandte Chemie International Edition* 2012, *51*, 10551.

(108)   Aguado, S.; Canivet, J.; Farrusseng, D. *Journal of Materials Chemistry* 2011, *21*, 7582.

(109)   Aguado, S.; Canivet, J.; Schuurman, Y.; Farrusseng, D. *Journal of Catalysis* 2011, *284*, 207.

(110)   Jose, T.; Hwang, Y.; Kim, D.-W.; Kim, M.-I.; Park, D.-W. *Catal. Today* 2015, *245*, 61.

(111)   Bhattacharjee, S.; Lee, Y.-R.; Ahn, W.-S. *CrystEngComm* 2015, *17*, 2575.

(112)   Li, H.; Feng, X.; Guo, Y.; Chen, D.; Li, R.; Ren, X.; Jiang, X.; Dong, Y.; Wang, B. *Scientific reports* 2014, *4*.

(113)   Barrer, R. M. *J. Chem. Soc., Faraday Trans.* 1990, *86*, 1123.

(114)   De Lange, R.; Keizer, K.; Burggraaf, A. *Journal of membrane science* 1995, *104*, 81.

(115)   Kärger, J.; Ruthven, D. M.; Theodorou, D. N. *Diffusion in nanoporous materials*; John Wiley & Sons, 2012.

(116)   Burggraaf, A. *Journal of membrane science* 1999, *155*, 45.

(117)   Satterfield, C. N. *Heterogeneous catalysis in industrial practice*; McGraw Hill Book Co.,1991.

(118)   Everett, D. H.; Powl, J. C. *Journal of the Chemical Society, Faraday Transactions 1: Physical Chemistry in Condensed Phases* 1976, *72*, 619.

(119)   Xiao, J.; Wei, J. *Chemical Engineering Science* 1992, *47*, 1123.

(120)   Carne, A.; Carbonell, C.; Imaz, I.; Maspoch, D. *Chemical Society Reviews* 2011, *40*, 291.

(121)   Shekhah, O.; Liu, J.; Fischer, R. A.; Woll, C. *Chemical Society Reviews* 2011, *40*, 1081.

(122)   Czaja, A. U.; Trukhan, N.; Muller, U. *Chemical Society Reviews* 2009, *38*, 1284.

(123)   Long, J. R.; Yaghi, O. M. *Chemical Society Reviews* 2009, *38*, 1213.

(124)   Li, J.-R.; Ma, Y.; McCarthy, M. C.; Sculley, J.; Yu, J.; Jeong, H.-K.; Balbuena, P. B.; Zhou, H.-C. *Coordination Chemistry Reviews* 2011, *255*, 1791.

(125)   Kitagawa, S.; Kitaura, R.; Noro, S.-i. *Angewandte Chemie International Edition* 2004, *43*, 2334.

(126)   Lu, G.; Hupp, J. T. *Journal of the American Chemical Society* 2010, *132*, 7832.

(127)   Aguado, S.; Canivet, J.; Farrusseng, D. *Chemical Communications* 2010, *46*, 7999.

(128)   Li, K.; Olson, D. H.; Seidel, J.; Emge, T. J.; Gong, H.; Zeng, H.; Li, J. *Journal of the American Chemical Society* 2009, *131*, 10368.

(129)   Bux, H.; Feldhoff, A.; Cravillon, J.; Wiebcke, M.; Li, Y.-S.; Caro, J. *Chemistry of Materials* 2011, *23*, 2262.

(130)   Pan, Y.; Lai, Z. *Chemical Communications* 2011, *47*, 10275.

(131)   Yoon, K. B. *Accounts of Chemical Research* 2007, *40*, 29.

(132)   Yoo, Y.; Jeong, H.-K. *Chemical Communications* 2008, 2441.

(133)   Yoo, Y.; Lai, Z.; Jeong, H.-K. *Microporous and Mesoporous Materials* 2009, *123*, 100.

(134)   Ranjan, R.; Tsapatsis, M. *Chemistry of Materials* 2009, *21*, 4920.

(135)   Peralta, D.; Chaplais, G.; Simon-Masseron, A.; Barthelet, K.; Chizallet, C.; Quoineaud, A.-A.; Pirngruber, G. D. *Journal of the American Chemical Society* 2012, *134*, 8115.

(136)   Ken-ichi, O.; Makoto, Y.; Kenji, N.; Hiroshi, M.; Kazuhiro, T.; Hidetoshi, K. In *Membrane Formation and Modification*; American Chemical Society: 1999; Vol. 744, p 314.

(137)   Staudt-Bickel, C.; Koros, W. J. *Journal of Membrane Science* 2000, *170*, 205.

(138)   Yao, J.; Dong, D.; Li, D.; He, L.; Xu, G.; Wang, H. *Chemical Communications* 2011, *47*, 2559.

(139)   Ameloot, R.; Vermoortele, F.; Vanhove, W.; Roeffaers, M. B.; Sels, B. F.; De Vos, D. E. *Nature chemistry* 2011, *3*, 382.

(140)   Ge, L.; Zhou, W.; Du, A.; Zhu, Z. *The Journal of Physical Chemistry C* 2012, *116*, 13264.

(141)   Bakker, W. J. W.; Van Den Broeke, L. J. P.; Kapteijn, F.; Moulijn, J. A. *AIChE Journal* 1997, *43*, 2203.

(142)   Bernal, M. P.; Coronas, J.; Menéndez, M.; Santamaría, J. *Journal of Membrane Science* 2002, *195*, 125.

(143)   Chang, N.; Gu, Z.-Y.; Yan, X.-P. *Journal of the American Chemical Society* 2010, *132*, 13645.

(144)   Wang, F.; Liu, Z.-S.; Yang, H.; Tan, Y.-X.; Zhang, J. *Angewandte Chemie International Edition* 2011, *50*, 450.

(145)   Sun, C.-Y.; Qin, C.; Wang, X.-L.; Yang, G.-S.; Shao, K.-Z.; Lan, Y.-Q.; Su, Z.-M.; Huang, P.; Wang, C.-G.; Wang, E.-B. *Dalton Transactions* 2012, *41*, 6906.

(146)   Shah, M. N.; Gonzalez, M. A.; McCarthy, M. C.; Jeong, H.-K. *Langmuir* 2013, *29*, 7896.

(147)   Hertäg, L.; Bux, H.; Caro, J.; Chmelik, C.; Remsungnen, T.; Knauth, M.; Fritzsche, S. *Journal of Membrane Science* 2011, *377*, 36.

(148)   Xie, Z.; Yang, J.; Wang, J.; Bai, J.; Yin, H.; Yuan, B.; Lu, J.; Zhang, Y.; Zhou, L.; Duan, C. *Chemical Communications* 2012, *48*, 5977.

(149)   Ma, X.; Lin, B. K.; Wei, X.; Kniep, J.; Lin, Y. S. *Industrial & Engineering Chemistry Research* 2013, *52*, 4297.

(150)   Nikolakis, V.; Xomeritakis, G.; Abibi, A.; Dickson, M.; Tsapatsis, M.; Vlachos, D. G. *Journal of Membrane Science* 2001, *184*, 209.

(151)   Qiu, S.; Xue, M.; Zhu, G. *Chemical Society Reviews* 2014, *43*, 6116.

(152)   Wang, Z.; Cohen, S. M. *Chemical Society Reviews* 2009, *38*, 1315.

(153)   Burrows, A. D. *CrystEngComm* 2011, *13*, 3623.

(154)   Liu, B.; Tu, M.; Zacher, D.; Fischer, R. A. *Advanced Functional Materials* 2013, *23*, 3790.

(155)   Furukawa, S.; Hirai, K.; Nakagawa, K.; Takashima, Y.; Matsuda, R.; Tsuruoka, T.; Kondo, M.; Haruki, R.; Tanaka, D.; Sakamoto, H.; Shimomura, S.; Sakata, O.; Kitagawa, S. *Angewandte Chemie International Edition* 2009, *48*, 1766.

(156)   Koh, K.; Wong-Foy, A. G.; Matzger, A. J. *Chemical Communications* 2009, 6162.

(157)   Tan, T. T. Y.; Cham, J. T. M.; Reithofer, M. R.; Andy Hor, T. S.; Chin, J. M. *Chemical Communications* 2014, *50*, 15175.

(158)   Cubillas, P.; Anderson, M. W.; Attfield, M. P. *Chemistry – A European Journal* 2013, *19*, 8236.

(159)   Yoo, Y.; Jeong, H.-K. *Crystal Growth & Design* 2010, *10*, 1283.

(160)   Szilagyi, P. A.; Lutz, M.; Gascon, J.; Juan-Alcaniz, J.; van Esch, J.; Kapteijn, F.; Geerlings, H.; Dam, B.; van de Krol, R. *CrystEngComm* 2013, *15*, 6003.

(161)   Shekhah, O.; Hirai, K.; Wang, H.; Uehara, H.; Kondo, M.; Diring, S.; Zacher, D.; Fischer, R. A.; Sakata, O.; Kitagawa, S.; Furukawa, S.; Woll, C. *Dalton Transactions* 2011, *40*, 4954.

(162)   Tu, M.; Fischer, R. A. *Journal of Materials Chemistry A* 2014, *2*, 2018.

(163)   Furukawa, S.; Hirai, K.; Takashima, Y.; Nakagawa, K.; Kondo, M.; Tsuruoka, T.; Sakata, O.; Kitagawa, S. *Chemical Communications* 2009, 5097.

(164)   Jeong, H.-K.; Krohn, J.; Sujaoti, K.; Tsapatsis, M. *Journal of the American Chemical Society* 2002, *124*, 12966.

(165) Wakihara, T.; Yamakita, S.; Iezumi, K.; Okubo, T. *Journal of the American Chemical Society* 2003, *125*, 12388.

(166) Tonigold, M.; Lu, Y.; Bredenkötter, B.; Rieger, B.; Bahnmüller, S.; Hitzbleck, J.; Langstein, G.; Volkmer, D. *Angewandte Chemie International Edition* 2009, *48*, 7546.

(167) Zakzeski, J.; Dębczak, A.; Bruijnincx, P. C. A.; Weckhuysen, B. M. *Applied Catalysis A: General* 2011, *394*, 79.

(168) Beier, M. J.; Kleist, W.; Wharmby, M. T.; Kissner, R.; Kimmerle, B.; Wright, P. A.; Grunwaldt, J.-D.; Baiker, A. *Chemistry – A European Journal* 2012, *18*, 887.

(169) Tian, Y.-Q.; Cai, C.-X.; Ren, X.-M.; Duan, C.-Y.; Xu, Y.; Gao, S.; You, X.-Z. *Chemistry – A European Journal* 2003, *9*, 5673.

(170) Llabrés i Xamena, F. X.; Casanova, O.; Galiasso Tailleur, R.; Garcia, H.; Corma, A. *Journal of Catalysis* 2008, *255*, 220.

(171) Lu, Y.; Tonigold, M.; Bredenkötter, B.; Volkmer, D.; Hitzbleck, J.; Langstein, G. *Zeitschrift für anorganische und allgemeine Chemie* 2008, *634*, 2411.

(172) Tang, J.; Salunkhe, R. R.; Liu, J.; Torad, N. L.; Imura, M.; Furukawa, S.; Yamauchi, Y. *Journal of the American Chemical Society* 2015, *137*, 1572.

(173) Kuttatheyil, A. V.; Lässig, D.; Lincke, J.; Kobalz, M.; Baias, M.; König, K.; Hofmann, J.; Krautscheid, H.; Pickard, C. J.; Haase, J.; Bertmer, M. *Inorganic Chemistry* 2013, *52*, 4431.

(174) Zheng, B.; Pan, Y.; Lai, Z.; Huang, K.-W. *Langmuir* 2013, *29*, 8865.

(175) Mueller, R.; Kanungo, R.; Kiyono-Shimobe, M.; Koros, W. J.; Vasenkov, S. *Langmuir* 2012, *28*, 10296.

(176) Chmelik, C. *Microporous and Mesoporous Materials* 2015, *216*, 138.

(177) Tian, F.; Cerro, A. M.; Mosier, A. M.; Wayment-Steele, H. K.; Shine, R. S.; Park, A.; Webster, E. R.; Johnson, L. E.; Johal, M. S.; Benz, L. *The Journal of Physical Chemistry C* 2014, *118*, 14449.

(178) Chizallet, C.; Bats, N. *The Journal of Physical Chemistry Letters* 2010, *1*, 349.

(179) Chizallet, C.; Lazare, S.; Bazer-Bachi, D.; Bonnier, F.; Lecocq, V.; Soyer, E.; Quoineaud, A.-A.; Bats, N. *Journal of the American Chemical Society* 2010, *132*, 12365.